Identification of the epigenetic mechanisms underlying the sensitization of chronic pruritus in atopic dermatitis

Kim, Su Min

Department of Medicine
Graduate School
Yonsei University

Identification of the epigenetic mechanisms underlying the sensitization of chronic pruritus in atopic dermatitis

Advisor Kim, Lark Kyun

A Dissertation Submitted
to the Department of Medicine
and the Committee on Graduate School
of Yonsei University in Partial Fulfillment of the
Requirements for the Degree of
Doctor of Philosophy in Medical Science

Kim, Su Min

June 2025

Identification of the epigenetic mechanisms underlying the sensitization of chronic pruritus in atopic dermatitis

This Certifies that the Dissertation of Kim, Su Min is Approved

Committee Chair	**Park, Chang Ook**
Committee Member	**Kim, Lark Kyun**
Committee Member	**Park, Kyung Min**
Committee Member	**Choi, Jungmin**
Committee Member	**Kim, Tae-Gyun**

Department of Medicine
Graduate School
Yonsei University
June 2025

ACKNOWLEDGEMENTS

I would like to extend my heartfelt gratitude to my thesis supervisor, Professor Lark Kyun Kim, whose unwavering support and insightful guidance have been pivotal in shaping my growth as a researcher. Beyond academic mentorship, he has always provided thoughtful counsel on personal matters, reminding me that patience and perseverance can be just as vital as creativity in the pursuit of research. Professor Kim has been not only an academic mentor but also a lifelong teacher whose wisdom extends far beyond the scope of this degree. I am equally indebted to my esteemed committee members, Professors Chang Ook Park, Kyung Min Park, Jungmin Choi, and Tae-Gyun Kim, for their invaluable advice and constructive feedback, which significantly enriched the quality of this thesis.

My sincere appreciation goes to my lab members—So Hee Dho, Ji Young Kim, Minjeong Cho, Yeongun Lee, Jiyeon Lee, Wonjin Woo, Jina Lee, Eunji Lee, Seolhee Jeong, and Jun Lee—for their warm support and generous assistance. I would like to extend special thanks to Jina Lee and Eunji Lee for their exceptional dedication. Jina Lee stood by me through the challenges of optimizing DRG preparation, facing every obstacle with determination. Both Jina and Eunji have shown remarkable commitment in handling demanding mouse experiments, and their hard work has been invaluable to my research. It has been a privilege to be part of the Lab of ImmunoGenomics.

I would like to express my deepest appreciation to Professor Chang Ook Park, whose mentorship has been particularly influential throughout my academic journey. His guidance during my residency in dermatology laid the foundation for my research career, and his continued support has been a constant source of inspiration. I am also sincerely grateful to his lab members—Kelun Zhang, Hye Li Kim, Reo Won Kim, Wan Jin Kim, Yeon Woo Jung, Young Eun Jung, Alina Tyo, and Gyung Do Moon—for their generous assistance and encouragement. I am especially thankful to Hye Li Kim and Kelun Zhang, with whom I have had the privilege of working since my residency. Their guidance helped me grasp the

fundamentals of research, and their unwavering support has been invaluable whenever I faced challenges.

I am profoundly grateful to my family. To my parents, your unwavering love and encouragement have been the bedrock of my achievements. I am especially thankful to my mother, whose wise guidance and values have shaped the person I am today—without her teachings, I would not have come this far. To my father, your steadfast support and belief in me have been a constant source of motivation throughout my journey. To my sister in San Francisco, your support and encouragement, even from afar, have always been a source of strength and comfort. My accomplishments are deeply rooted in the love and lessons I have received from all of you.

Most of all, I am deeply thankful to my beloved wife, Hyo Jin Park, whose love, patience, and companionship have been my greatest support. Your unwavering encouragement has given me strength during the most challenging times, and your presence has brought comfort and joy to both my personal life and academic journey. Sharing not only our lives but also the lab has been an extraordinary blessing, allowing us to grow together both as partners and as colleagues. Your dedication, understanding, and belief in me have been invaluable, and I am endlessly grateful to have you by my side through every step of this journey.

This thesis is dedicated to all of you, with my deepest appreciation for the love and guidance that have sustained me every step of the way.

Su Min Kim

TABLE OF CONTENTS

LIST OF FIGURES

ABSTRACT

Identification of the epigenetic mechanisms underlying the sensitization of chronic pruritus in atopic dermatitis

Chronic pruritus significantly diminishes the quality of life in individuals with pruritic skin diseases, including atopic dermatitis (AD). Despite advancements in understanding the immunopathogenesis of AD, the transcriptomic alterations within neurons at the single-cell level and the epigenomic regulatory landscape remain largely unexplored in the context of chronic itch in AD. In this context, we utilized single-cell RNA sequencing (scRNA-seq) with ATAC and CUT&RUN multi-omic profiling to elucidate the molecular landscape of sensory neurons in response to chronic pruritic stimulation.

Using murine models of chronic inflammatory skin diseases, including AD and psoriasis, we conducted comprehensive scRNA-seq of dorsal root ganglion (DRG) neurons and skin tissues. This high-resolution approach uncovered distinct neuronal subpopulations with inflammation-specific transcriptional signatures, revealing key pathways involved in neuronal excitability, synaptic plasticity, and neuroimmune interactions. Notably, these transcriptional changes suggested that chronic pruritic stimuli induce adaptive responses in sensory neurons, contributing to persistent itch. Comparative analyses between different disease models highlighted both shared and unique neuronal signatures, providing insights into the differential regulation of pruritus across inflammatory contexts.

Epigenomic profiling through chromatin accessibility analyses, including ATAC-seq and CUT&RUN, revealed dynamic regulatory changes associated with chronic itch. These analyses identified differentially accessible regions linked to genes implicated in sensory neuron function, synaptic modulation. Integrative multi-omic analysis highlighted critical transcriptional regulators orchestrating pruritogenic gene expression programs. Functional validation through conditional knock out mouse model demonstrated that targeted

disruption of these regulatory pathways in sensory neurons significantly reduced spontaneous scratching behaviors, alleviated epidermal hyperplasia in murine models of chronic itch.

Further analysis uncovered an upstream neuroimmune signaling axis that drives persistent neuronal sensitization through transcriptional reprogramming. This axis is mediated by immune-derived signals that activate specific neuronal pathways, forming a feedback loop that connects peripheral inflammation to sustained neuronal plasticity. Comprehensive cell-cell interaction analyses identified critical ligand-receptor pairs facilitating this neuroimmune crosstalk, highlighting the role of inflammatory signals in maintaining neuronal hyperresponsiveness. By reinforcing neuronal hyperexcitability and reshaping gene regulatory networks over time, this neuroimmune feedback loop plays a central role in the chronicity of pruritus.

Together, this study defines novel regulatory networks, offering critical insights into the molecular mechanisms driving chronic itch. By integrating single-cell transcriptomics with epigenomic profiling, our findings deepen the understanding of neuroimmune interactions in pruritus. These insights provide a foundation for developing targeted therapies aimed at alleviating chronic itch and improving patient outcomes in pruritic disorders.

Key words: Chronic pruritus, atopic dermatitis, epigenetics, single cell omics, DRG neuron

1. Introduction

Chronic pruritus is a debilitating symptom that profoundly impacts the quality of life in individuals with atopic dermatitis (AD) and other inflammatory skin disorders(Butler et al., 2024; Labib et al., 2023). Unlike acute itch, which serves as a transient protective mechanism, chronic pruritus persists long after the initial triggers have resolved, evolving into a maladaptive state refractory to conventional treatments(Zeidler et al., 2023). This transition reflects a complex interplay between immune signaling and peripheral sensory neurons, yet the precise molecular and cellular mechanisms that sustain chronic itch remain poorly defined.

Recent advances in neuroimmunology have underscored the critical role of bidirectional communication between sensory neurons and immune cells in perpetuating chronic itch(Deng et al., 2023; Kim et al., 2024; Lu et al., 2023; Trier et al., 2022; Trier et al., 2024; Voisin et al., 2021; Wang & Kim, 2020; F. Wang et al., 2021). Beyond their classical role in itch signal transmission, sensory neurons actively respond to inflammatory cytokines, chemokines, and growth factors, driving neuronal sensitization—a hallmark of chronic pruritus(Steinhoff et al., 2022). Key immune mediators such as IL-31, TSLP, and OSM directly modulate neuronal excitability(Datsi et al., 2021; Tseng & Hoon, 2021; Wilson et al., 2013), yet the transcriptional and epigenetic programs within pruriceptive neurons that maintain this hyperresponsiveness remain largely unexplored.

Single-cell transcriptomics has transformed our understanding of sensory neuron diversity, revealing distinct subsets specialized in pain, itch, and thermal sensation(Chiu et al., 2014; Nguyen et al., 2021; Qi et al., 2024; Yu et al., 2024; Zheng et al., 2019). While transcriptomic changes in neuropathic pain have been characterized(Renthal et al., 2020), preclinical mouse models capturing the neuronal adaptations associated with chronic itch across various dermatologic conditions remain lacking. Moreover, ATAC-seq data in DRG has been largely confined to studies on axonal regeneration(Palmisano et al., 2019; Perry

et al., 2018), and even these have been conducted on whole DRG tissue rather than isolated neurons. Given that neurons constitute only ~10% of the DRG cellular population, this approach presents significant limitations in precisely defining the neuronal epigenomic landscape. Furthermore, CUT&RUN profiling for histone modifications in DRG neurons has yet to be properly established, leaving a major gap in understanding the chromatin dynamics that regulate sensory neuron function in chronic itch.

To address this, we employed a multi-omics approach to dissect the molecular underpinnings of chronic itch in AD and psoriasis. Using murine models of AD (MC903, SAV8, and HDM-induced dermatitis) and an imiquimod-induced psoriasis model, we performed single-cell RNA sequencing (scRNA-seq) of DRG neurons and skin tissues, identifying inflammation-induced neuronal subsets characterized by transcriptional reprogramming towards heightened pruritogenic responses (e.g. Inflammation-specific neurons ; Inf-specific neurons). Comparative analyses revealed distinct transcriptional signatures and pathway activation patterns between AD and psoriasis, delineating disease-specific mechanisms of neuronal sensitization.

Integrative epigenomic profiling via bulk ATAC-seq, scRNA-seq, and CUT&RUN for histone modifications uncovered dynamic chromatin remodeling at distal enhancer regions associated with chronic pruritus. Transcription factor activity analysis revealed that Inf-specific neurons exhibited elevated activity of several immune/neurodevelopment-related transcription factor families, including Interferon regulatory factor (IRF), Signal transducer and activator of transcription (STAT), and Regulatory Factor binding to the X-box (RFX) family transcription factors, implicating these factors in coordinating the transcriptional response to chronic inflammation. While *Ebf1* emerged as a central regulatory hub, motif enrichment and regulon activity scores also pointed to potential roles for RFX family members in histone modification and chromatin remodelling function. Among the transcriptional regulators identified, *Ebf1* emerged as a key driver orchestrating pruriceptive neuronal responses. Functional validation in Nav1.8-Cre x *Ebf1* floxed mice demonstrated that sensory neuron-specific deletion of Ebf1 significantly reduced

spontaneous scratching behavior and suppressed the expression of pruritus-associated genes, including *Il31ra*, *F2rl1* (PAR2), *Lifr*, *Camk2a*, *Scn7a*, and *Smarca5*. Further mechanistic analysis identified a neuroimmune regulatory axis involving Osm-Lifr-STAT3/Ebf1 signaling, where immune-derived *Osm* drives Lifr-mediated activation of *Stat3* and *Ebf1* in sensory neurons, forming a feedback loop that sustains chronic itch.

Collectively, this study establishes the first integrated transcriptomic and epigenomic framework for understanding chronic pruritus. By elucidating the Osm-Lifr-STAT3-Ebf1 signaling axis, we define a previously unrecognized mechanism by which chronic inflammation perpetuates neuronal sensitization. These findings provide new molecular insights into the neuroimmune regulation of chronic itch and identify promising therapeutic targets for pruritic skin disorders, paving the way for precision medicine approaches in chronic pruritus.

2. Materials and methods

2.1. Mice

This study was conducted in strict accordance with the *Guidelines for the Care and Use of Laboratory Animals* established by the Ministry of Food and Drug Safety (MFDS), as well as ethical guidelines established by the Institutional Animal Care and Use Committee (IACUC) at Yonsei University College of Medicine (IACUC Approval No. [2023-0240]).

Mice were housed under standard conditions at the Gangnam Severance Hospital Biomedical Research Center, maintaining a 12-hour light-dark cycle, a controlled temperature of 23°C, and unrestricted access to food and water. C57BL/6 mice were sourced from Orient Bio, while Ebf1-floxed mice were obtained from The Jackson Laboratory. Nav1.8-Cre mice were kindly provided by Dr. Chang Ook Park (Yonsei University, Department of Dermatology). Nav1.8 reporter mice () were generated by breeding Nav1.8-Cre^{+} mice with Ebf1-floxed mice. Male mice aged 5 to 10 weeks were used in all experiments. Mice were either randomly assigned to experimental groups or stratified based on genotype. Genotyping was performed using standard PCR techniques. Sex-based differences were not analyzed.

2.2. Induction of atopic dermatitis & psoriasis mouse model

2.2.1. MC903-Induced AD Model

Atopic dermatitis was induced by topical application of MC903 (calcipotriol, Tocris) to the dorsal skin. Briefly, mice were shaved two days before the experiment, and MC903 (2 nmol in 25 μL ethanol) was applied daily for eight consecutive days. Control mice received vehicle (ethanol) only.

2.2.2. House Dust Mite (HDM) Cream Model

For the HDM-induced AD model, Dermatophagoides farinae (HDM) ointment (Biostir-AD, Biostir Inc., Kobe, Japan) was applied three times per week (Monday, Wednesday, and Friday) for three weeks. Before application, 4% SDS (200 μL) was applied to the back skin to enhance permeability. After 1–2 hours of drying, HDM cream (~100 mg) was applied to the upper back skin using a sterile spoon.

2.2.3. SAV8/HDM Mouse Model

Mice were sensitized by epicutaneous application of HDM extract and the SAV8 adjuvant three times per week for three weeks. HDM extract (GREER LABORATORIES INC) was prepared as a 100 μg/mL solution in PBS. SAV8 (Thermo Scientific) was reconstituted in PBS at 3 mg/mL and stored in light-protected amber tubes at 4°C. To facilitate epicutaneous application, Tegaderm film with gauze were applied to the back of the mouse. A 1.5 cm × 1.5 cm piece of sterile gauze was placed on the larger Tegaderm segment, onto which HDM extract (150 μL, 15 μg) and SAV8 (150 μL, 4.5 μg) were evenly applied. The patch was then affixed to the dorsal skin.

2.2.4. Imiquimod (IMQ)-Induced Psoriasis Model

Psoriasiform dermatitis was induced by topical application of 5% imiquimod cream (Aldara, MEDA Pharmaceuticals) on the shaved dorsal skin for six consecutive days. Mice were monitored for erythema, scaling, and thickening of the skin.

2.3. Dissociation of DRG tissue for single cell RNA sequencing

DRGs were harvested from adult mice (six mice per group) following euthanasia and rapid dissection under a stereomicroscope. The isolated DRGs were transferred to HBSS and enzymatically digested in Collagenase-Dispase solution (3 mg/mL Dispase II and 1 mg/mL Collagenase A) at 37°C for 30 minutes. To further facilitate dissociation, DNase I (2500 U/mL) was added, and the cell suspension was triturated sequentially using 18G,

21G, and 26G syringe needles attached to a 1 mL syringe, with five repetitions per gauge to achieve progressive dissociation. The resulting cell suspension was filtered through a 70-μm cell strainer and purified via density gradient centrifugation using 30% fatty-acid-free BSA. Neurons were then washed six to eight times with cold Ca^{2+}/Mg^{2+}-free 0.04% BSA/PBS by centrifugation at 300g for 5 minutes at 4°C. The purified suspension was passed through a 40-μm Flowmi Cell Strainer (SP Bel-Art) to remove debris. Neuronal yield and viability were assessed using a LUNA-FX7™ Automated Fluorescence Cell Counter (Logos Biosystems), with acridine orange (AO) and propidium iodide (PI) staining to differentiate live and dead cells.

2.4. Dissociation of skin tissue for single cell RNA sequencing

Freshly isolated skin specimens were immediately stored in Tissue Storage Solution (Miltenyi Biotec) at 4°C. Prior to dissociation, tissues were washed with phosphate-buffered saline (PBS) and mechanically minced into ~4 mm pieces. Tissue dissociation was performed using the Whole Skin Dissociation Kit, human (Miltenyi Biotec) in combination with the gentleMACS™ Dissociator (Miltenyi Biotec), following the manufacturer's instructions. After enzymatic digestion, cell suspensions were sequentially filtered through 70 μm and 30 μm strainers to remove debris and undigested tissue fragments. Cells were pelleted by centrifugation at 300 × g, 4°C, for 5 min, and erythrocytes were lysed using Red Blood Cell Lysis Solution (Miltenyi Biotec) at 25°C for 1 min. The samples were subsequently washed twice in calcium- and magnesium-free PBS containing 0.04% bovine serum albumin (BSA) at 300 × g, 4°C, for 5 min. For single-cell viability assessment, cells were resuspended in cold 0.04% BSA/PBS and counted using a LUNA-FX7™ Automated Fluorescence Cell Counter (Logos Biosystems) with acridine orange (AO) and propidium iodide (PI) staining (Logos Biosystems). Dead cells were further removed using the Dead Cell Removal Kit (Miltenyi Biotec) and MS columns (Miltenyi Biotec) following the manufacturer's protocol.

2.5. Single cell RNA library preparation and sequencing

Single-cell RNA sequencing libraries were prepared using the 10x Chromium iX and Next GEM Single Cell 3' GEM Kit v3.1 (10x Genomics, PN-1000268) according to the manufacturer's protocol (10x Chromium Next GEM Single Cell 3' v3.1 User Guide, document no. CG000315). Briefly, a cell suspension (target recovery: 20,000 cells) was combined with the reverse transcription master mix and loaded into a Next GEM Chip G (10x Genomics, PN-1000120) along with Single Cell 3′ Gel Beads and Partitioning Oil to generate single-cell Gel Beads-in-Emulsion (GEMs). Within GEMs, polyadenylated mRNA from individual cells was uniquely barcoded and reverse-transcribed. The resulting barcoded full-length cDNA was amplified by PCR, followed by sequential enzymatic fragmentation, end-repair, A-tailing, adaptor ligation, and index PCR to construct 3′ gene expression libraries. For Nav1.8-Cre × Ebf1 floxed (neuron-specific Ebf1 KO) mice, single-cell RNA sequencing libraries were prepared using the 10x Chromium iX and GEM-X Single Cell 3' Kit v4 (10x Genomics, PN-1000691) and the GEM-X Single Cell 3' Chip Kit v4 (10x Genomics, PN-1000690), following the 10x Chromium GEM-X Single Cell 3' Reagent Kits v4 protocol (document no. CG000731). All purified libraries were quantified using qPCR (KAPA Biosystems) and assessed for quality using the Agilent 4200 TapeStation (Agilent Technologies). Sequencing was performed on an Illumina NovaSeq 6000 platform.

2.6. DRG Single cell RNA sequencing data processing

Raw gene expression matrices were obtained from 10x Genomics Chromium runs and processed using the Seurat package in R. Gene-barcode matrices were loaded using Read10X, and each sample was converted into a Seurat object. Cells were filtered based on quality control metrics, retaining only those with nFeature_RNA > 500, nCount_RNA

> 1000, and percent.mt < 10% to eliminate low-quality cells and mitochondrial contamination. Doublets were identified and removed using DoubletFinder, where the expected doublet rate was dynamically calculated based on the number of detected cells. Optimal pK values were determined using paramSweep() and find.pK(), and homotypic doublet proportions were modeled based on cluster annotations. After filtering, individual datasets were merged and evaluated for possible batch effect. There was no substantial batch effect across experimental groups, individual seurat object were merged to create a combined Seurat object for downstream analysis.

Following data integration, highly variable genes were identified using FindVariableFeatures(), and principal component analysis (PCA) was performed. The optimal number of principal components was determined using ElbowPlot (PCA 20), and clustering was performed using FindNeighbors and FindClusters function at a resolution of 1.5. Dimensionality reduction was applied using UMAP, and clusters were annotated based on known neuronal and non-neuronal marker genes. Neuronal clusters were identified by expression of Rbfox3, Avil, and Pou4f1, while non-neuronal clusters were classified based on glial (Sparc, Mpz, Mbp) and immune/endothelial (Cd74, Cldn5, Mgp) markers. Clusters classified as non-neuronal were excluded from further analysis. To refine neuronal classification, neuronal clusters were subsetted and re-clustered using PCA (20 principal components), UMAP, and FindClusters at resolution = 2.0. Marker genes for neuronal subclusters were identified using FindAllMarkers and filtered to retain only genes with avg_log2FC > 0.5 and adjusted p-value < 0.05. These filtered markers were used for neuronal subtype annotation. Cluster-specific marker genes were further compared with publicly available DRG datasets(Qi et al., 2024; Renthal et al., 2020; Sharma et al., 2020) (GSE139088, GSE154659, GSE254789) to assess the overlap between experimental clusters and known DRG neuronal subtypes. This approach allowed for higher-resolution identification of neuronal subpopulations for subsequent functional and transcriptional analyses.

2.7. Skin Single cell RNA sequencing data processing

Raw gene expression matrices were obtained from 10x Genomics Chromium runs and processed using the Seurat package in R. Gene-barcode matrices were loaded using Read10X, and each sample was converted into a Seurat object. Cells were filtered based on quality control metrics, retaining only those with nFeature_RNA > 200, nCount_RNA > 1000, and percent.mt < 10% to eliminate low-quality cells and mitochondrial contamination. Doublets were identified and removed using DoubletFinder. After filtering, individual datasets were batch-corrected and merged by Harmony with default parameters. The dataset included MC903-treated atopic dermatitis (AD) mouse skin samples and untreated control skin samples generated in-house, while psoriasis-like skin samples were obtained from publicly available scRNA-seq datasets (GSE159704, GSE165021, GSE193350, GSE230512). These publicly sourced datasets were harmonized with in-house samples for integrated analysis. Following data integration, highly variable genes were identified using FindVariableFeatures(), and principal component analysis (PCA) was performed. The optimal number of principal components was determined using ElbowPlot() (PCA 30), and clustering was conducted using FindNeighbors() and FindClusters() at resolution = 1.5. Dimensionality reduction was applied using UMAP, and clusters were annotated based on known skin cell-type markers. Keratinocytes were identified by expression of Krt14, Krt15, Krt10, and Krt1, fibroblasts by Col1a1, Col1a2, Pdgfra, and Dcn, endothelial cells by Pecam1, Cdh5, Vwf, and Eng, while immune cells were classified based on expression of Ptprc, Cd3e (T cells), Cd19 (B cells), Cd68 (macrophages), and Itgax (dendritic cells). Clusters classified as erythrocytes (RBCs) were excluded from further analysis. To refine immune cell classification, immune clusters were subsetted and re-clustered using PCA (30 principal components), UMAP, and FindClusters() at resolution = 1.0. Marker genes for immune subclusters were identified using FindAllMarkers(), filtered for avg_log2FC > 0.5 and adjusted p-value < 0.05, and used for subtype annotation. Finally, cell type annotation was performed using GPT-4-based classification (GPTCelltype) (Hou & Ji, 2024) and validated against known marker genes. This approach

enabled high-resolution characterization of skin epithelial, stromal, immune subpopulations for downstream cell to cell interaction analysis with DRG scRNA-seq dataset.

2.8. Comparison with publicly available DRG single cell RNA sequencing data

To validate neuronal annotations, we integrated our dataset with three public mouse DRG scRNA-seq datasets (GSE154659, GSE254789, GSE139088) using Seurat. Each public dataset was processed differently based on its data format and annotation availability. For GSE154659 and GSE139088, raw count matrices were loaded as Seurat objects and annotated using metadata-provided subtype information. GSE254789 lacked explicit annotations, so neuronal clusters were classified according to methodologies described in the original study. Each dataset was quality-filtered (nFeature_RNA > 500, nCount_RNA > 1000, percent.mt < 10%), normalized with SCTransform, and subjected to PCA. Integration was performed using FindTransferAnchors and MapQuery, aligning our neuronal dataset with each public dataset in PCA space, followed by UMAP projection for visualization. Alluvial plots (ggalluvial) illustrated cluster correspondence across datasets. To check the inflammation-specific-neuron subtypes correspond to the nerve-injury neuron subtypes, injury-associated transcriptional signatures were assessed using AddModuleScore , with common injury-induced genes derived from the original study(Renthal et al., 2020).

2.9. Pathway Activity Inference with decoupleR

To infer regulatory pathway activity, we applied the decoupleR package(Badia et al., 2022) using AUCell-based scoring. Pathway gene sets were obtained from MSigDB(Castanza et al., 2023), including Gene Ontology Biological Process (GOBP),

Molecular Function (GOMF), Cellular Component (GOCC), KEGG, Reactome, WikiPathways (WP), BioCarta, and PID. The computed decoupleR pathway activity scores were imported into the Seurat object as separate assays. Pathway-specific score matrices were extracted from the results, transposed, and integrated into the Seurat object, enabling downstream visualization and comparative analysis. Differential pathway activities were evaluated using the MAST framework. Pathways were ranked based on logFC values, and significantly enriched pathways (adjusted p-value < 0.05) were selected for further analysis and visualization.

2.10. Regulon analysis with pySCENIC

To investigate transcription factor (TF) activity at the single-cell level, regulon analysis was conducted using pySCENIC(Aibar et al., 2017; Van de Sande et al., 2020), a computational framework for gene regulatory network (GRN) inference and regulon activity quantification. The workflow comprised three main steps: GRN inference, regulon definition, and regulon activity scoring, followed by integration into the Seurat object for downstream analysis. First, raw count matrix was extracted from seurat object and exported to Loom format using SCopeLoomR. Mitochondrial genes were excluded to prevent bias. The Loom file was then processed in pySCENIC (version 0.12.1) for GRN inference using GENIE3(Huynh-Thu et al., 2010), which identifies putative TF-target interactions based on expression co-variation. The resulting GRN adjacency matrix captured regulatory relationships between transcription factors and their predicted target genes. Putative regulons were refined using cis-regulatory motif enrichment analysis via the RcisTarget database. This step validated TF-target interactions by identifying enriched DNA motifs within promoter and enhancer regions. The resulting context-specific regulons represented TFs and their high-confidence target genes, forming a refined gene regulatory network. Regulon activity was quantified using AUCell scoring, which measures the enrichment of regulon target genes within each cell's transcriptome. This generated a regulon activity

matrix, which was integrated into the Seurat object as an independent assay. For downstream analysis, regulon activity scores were compared across experimental conditions. Feature plots and violin plots were used to visualize transcription factor activity within neuronal subclusters.

2.11. Pseudotime analysis with Monocle3

Single-cell trajectory inference was performed using Monocle3 to reconstruct the pseudotemporal progression of dorsal root ganglion (DRG) sensory neurons. A preprocessed and annotated Seurat object containing single-cell RNA sequencing (scRNA-seq) data from mouse DRG neurons across different conditions was used as input. The raw count matrix, metadata, and gene annotation were extracted from the Seurat object and used to construct a Monocle3 cell dataset (CDS) via the new_cell_data_set function. Cell identities and gene expression features were validated to ensure consistency between the expression matrix and metadata.

To preserve the original Seurat embeddings and cluster annotations, principal component analysis (PCA) embeddings and the associated variance explained were directly transferred to the Monocle3 object. Uniform manifold approximation and projection (UMAP) coordinates were also retained from the Seurat object, ensuring that the same low-dimensional representation was used for trajectory inference. Cells were clustered using cluster_cells, applying a resolution parameter optimized to capture biologically relevant neuronal subpopulations. The resulting clusters were visualized and annotated according to previously defined neuronal subsets.

Graph-based trajectory learning was conducted using learn_graph, incorporating cell partitions to infer differentiation trajectories. The constructed trajectory was visualized with plot_cells, displaying inferred developmental paths overlaid with cluster identities. To order cells along the pseudotime trajectory, root nodes were manually assigned based on known neuronal subtypes, and pseudotemporal ordering was performed using order_cells. Multiple trajectories were examined by selecting different root nodes corresponding to

major neuronal populations, including non-peptidergic nociceptors (NP1, NP2, NP3) and c-LTMRs.

Differential gene expression along pseudotime was assessed using graph_test, which identified genes exhibiting significant expression dynamics along the principal trajectory. To focus on biologically relevant genes, only those expressed in at least 10% of cells were retained for downstream analysis. DEGs were identified separately for each neuronal partition, and statistical significance was determined based on a false discovery rate (FDR) threshold of 0.05.

2.12. Differential abundance (DA) analysis with miloR

To assess differential abundance across experimental conditions, we employed MiloR(Dann et al., 2022), a graph-based statistical framework designed for neighborhood-level differential testing in single-cell datasets. First, the merged seurat object with multiple conditions were converted to a SingleCellExperiment object. Subsequently, a Milo object was generated to capture neighborhood structures.

Neighborhood graphs were constructed using principal component analysis (PCA)-derived embeddings (d = 20, k = 20), followed by neighborhood refinement to enhance local connectivity. Cell abundance was quantified per neighborhood, and differential testing was performed using graph-overlap-aware multiple hypothesis correction, modeling sample conditions as covariates in a linear design matrix. Contrasts were specified to compare AD and PsO conditions against controls, as well as between AD and PSO groups.

For visualization, DA results were overlaid onto a UMAP embedding and neighborhood graphs, with significant neighborhoods (Spatial FDR < 0.1) highlighted. Additionally, beeswarm plots were generated to illustrate log-fold change distributions across cell subsets,

and post-hoc marker gene analysis was conducted using findNhoodGroupMarkers to identify differentially enriched genes within significant neighborhoods.

2.13. DRG neuron ATAC-seq library preparation

ATAC-seq was performed on DRG neurons using an optimized Omni-ATAC protocol based on the method described by Corces et al., with modifications for neuronal samples(Corces et al., 2017; Grandi et al., 2022). DRG tissues were dissected from six mice per replicate, pooled, and enzymatically dissociated to obtain a single-cell suspension. Each pooled sample contained approximately 50,000 DRG neurons. Two biological replicates were prepared per condition. Dissociated DRG neurons were purified using the MACS Neuron Isolation Kit (Miltenyi Biotec, 130-115-390) according to the manufacturer's protocol to enrich for neuronal populations while minimizing contamination from non-neuronal cells. Purified neurons were resuspended in Bambanker cryopreservation medium (Nippon Genetics, BBF01) and stored at −80°C before processing to minimize batch effects. Cells were thawed rapidly at 37°C, washed in ice-cold 1× PBS, and centrifuged at 500 × g for 5 minutes at 4°C, followed by careful removal of the supernatant to minimize cell loss.

For nuclear extraction, cells were resuspended in ice-cold lysis buffer containing 10 mM Tris-HCl (pH 7.5), 10 mM NaCl, 3 mM $MgCl_2$, 0.1% Tween-20, 0.1% NP-40, and 0.01% digitonin. Lysis was carried out on ice for 3 minutes, followed by quenching with 1 mL of wash buffer (lysis buffer without NP-40 and digitonin). Nuclei were pelleted at 500 × g for 10 minutes at 4°C and resuspended in transposition reaction buffer containing 2× TD buffer, 100 nM Tn5 transposase (Illumina), and 0.1% Tween-20. The transposition reaction was incubated at 37°C for 30 minutes with gentle mixing. Following transposition, samples were purified using the MinElute Reaction Cleanup Kit (Qiagen, 28204) according to the manufacturer's instructions.

For library amplification, transposed DNA was pre-amplified using NEBNext High-Fidelity 2× PCR Master Mix (New England Biolabs, M0541) with custom barcoded primers. The optimal number of PCR cycles was determined by a qPCR side reaction using SYBR Green to monitor amplification kinetics. The final library was amplified for an appropriate number of cycles to minimize PCR bias, followed by purification with Agencourt AMPure XP beads (Beckman Coulter, A63881) at a 1.8× bead-to-DNA ratio.

Library quality and fragment distribution were assessed using an Agilent Bioanalyzer High Sensitivity DNA kit (Agilent, 5067-4626) and quantified with a Qubit 4 fluorometer (Thermo Fisher Scientific). Sequencing libraries were pooled and sequenced on an Illumina NovaSeq 6000 platform with paired-end 151 bp reads, targeting a minimum depth of 50 million reads per sample.

2.14. DRG neuron CUT&RUN-seq library preparation

Cleavage Under Target and Release Using Nuclease (CUT&RUN) was performed following the EpiCypher CUTANA CUT&RUN protocol(Skene et al., 2018), with modifications to optimize nuclei isolation and minimize batch effects. DRG tissues were dissected from 12 mice per replicate, pooled, and subjected to enzymatic dissociation to obtain a single-cell suspension. Neuronal nuclei were extracted and preserved according to the EpiCypher CUTANA™ CUT&RUN kit recommendations. To minimize batch effects, nuclei from all DRG samples were pooled prior to library preparation and processed simultaneously. Rapidly thawed nuclei were bound to magnetic beads, pelleted using a magnetic stand, and the supernatant was discarded. The beads were resuspended in 200 µL of wash buffer containing 20 mM HEPES (pH 7.5), 150 mM NaCl, 0.5 mM spermidine, and a protease inhibitor cocktail (Complete, EDTA-free, Roche). The beads were washed with 100 µL of wash buffer, incubated at room temperature for 10 minutes, and then pelleted again on a magnetic stand. After discarding the supernatant, beads were resuspended in 50 µL of ice-cold antibody buffer composed of 20 mM HEPES (pH 7.5),

150 mM NaCl, 0.5 mM spermidine, 0.001 mM digitonin, 2 mM EDTA, and protease inhibitors. Antibodies for H3K4Me3 (Epicypher, 13-0060), H3K4Me1 (Epicypher, 13-0057) and H3K27Ac (Epicypher, 13-0059) were added (0.5 µL per sample), and samples were gently mixed before overnight incubation at 4°C with constant rotation.

On the following day, beads were recovered using a magnetic stand, washed twice with 250 µL of ice-cold wash buffer supplemented with 0.001% digitonin, and resuspended in 50 µL of the same buffer. Next, 2.5 µL of CUTANA pAG-MNase was added, and samples were gently mixed before a 10-minute incubation at room temperature. Beads were washed twice in 250 µL of wash buffer containing 0.001% digitonin and resuspended in 50 µL of the same buffer. Chromatin digestion was initiated by adding 1 µL of 100 mM $CaCl_2$ to each sample, followed by gentle mixing and a 2-hour incubation at 4°C with constant rotation. Enzymatic cleavage was halted by adding 33 µL of stop buffer (340 mM NaCl, 20 mM EDTA, 4 mM EGTA, 50 µg/mL RNase A, and 50 µg/mL glycogen) and 1.65 µL of Spike-In DNA (Epicypher , 18-1401). Samples were then incubated at 37°C for 10 minutes in a thermocycler, transferred to new tubes, and immediately processed for DNA purification.

DNA was purified using the CUTANA CUT&RUN Library Prep Kit (Epicypher , 14-1001) according to the manufacturer's instructions. The resulting libraries were quantified using a Qubit dsDNA High Sensitivity assay and assessed for quality using an Agilent Bioanalyzer DNA High Sensitivity assay. Sequencing was performed on an Illumina NovaSeq 6000 platform using 151 bp paired-end reads, with a minimum sequencing depth of 50 million reads per sample.

2.15. ATAC-seq data pre-processing

ATAC-seq data processing and genome alignment were performed using PEPATAC (version 1.0.11)(Grandi et al., 2022; Smith et al., 2021), an automated pipeline designed

for ATAC-seq data analysis. Adapter sequences were trimmed from raw sequencing reads using skewer (version 0.2.2) with the parameters -f sanger -t 8 -m pe. Trimmed reads were then aligned to the mm10 reference genome using Bowtie2 with the --very-sensitive parameter to maximize alignment specificity. Mitochondrial reads and duplicate fragments were removed using SAMtools and Picard to retain high-quality nuclear reads.

To adjust for Tn5 transposase insertion bias, fragment ends were shifted by +4 bp on the positive strand and −5 bp on the negative strand. Properly paired reads within a fragment size range of 50–2,000 bp were retained for downstream analysis. Peaks of open chromatin were called using MACS2 with the parameters -q 0.01 --shift 0 --nomodel, ensuring robust identification of accessible regions. Identified peaks were filtered against ENCODE blacklist regions to remove potential artifacts.

Quality control metrics, including fragment size distribution and transposase cut site enrichment at transcription start sites (TSS), were assessed using deepTools. ATAC-seq signal tracks were generated as bigWig files for visualization in IGV (Integrative Genomics Viewer). Peak annotation and functional enrichment analysis were performed using bedtools, HOMER, and ChIPseeker, mapping peaks to genomic regulatory elements such as promoters and enhancers.

All computational analyses were executed in a Singularity container environment to ensure reproducibility, using PEPATAC default settings with custom parameter adjustments for optimized peak calling and read normalization.

2.16. CUT&RUN-seq data pre-processing

CUT&RUN sequencing data were processed using nf-core/cutandrun (version 3.2.2), an automated bioinformatics pipeline designed for reproducible and scalable CUT&RUN analysis(Ewels et al., 2020). The pipeline was executed with Nextflow using the docker profile to ensure containerized and dependency-controlled execution.

Adapter trimming and quality filtering were performed before read alignment to the GRCm38 (mm10) reference genome using Bowtie2. Blacklist filtering was applied using the ENCODE mm10 blacklist (v2) to remove potential sequencing artifacts. Peak calling was conducted with both MACS2, with MACS2 parameters adjusted to a genome size of 1.87×10^9 bp and broad peak calling enabled (--macs2_narrow_peak FALSE). CUT&RUN signal normalization was performed using CPM (Counts Per Million) with a bin size of 1 bp to improve consistency across samples. Gene annotations were assigned using GENCODE vM23.

2.17. Transcription factor motif analysis and footprinting

To assess TF motif accessibility and activity, ATAC-seq data were analyzed using chromVAR, TOBIAS, and diffTF, which provide complementary insights into motif enrichment, footprinting, and differential TF binding.

2.17.1. Motif accessibility analysis with chromVAR

TF motif deviation analysis was conducted using chromVAR(Schep et al., 2017) to quantify chromatin accessibility changes across conditions. Processed ATAC-seq BAM files were used to generate fragment count matrices for fixed-width, non-overlapping peaks. GC bias correction was applied using BSgenome.Mmusculus.UCSC.mm10 to normalize accessibility differences. Motif annotations were obtained from JASPAR2022(Castro-Mondragon et al., 2022), HOCOMOCOv12(Vorontsov et al., 2024), and ENCODE databases(Kheradpour & Kellis, 2014), and motif occurrences were mapped to peaks using motifmatchr. Deviations in motif accessibility were computed and z-scored to quantify TF activity. Highly variable TF motifs were identified, and motif enrichment differences were visualized using heatmaps and PCA.

2.17.2. Transcription factor footprinting with TOBIAS

To infer TF occupancy, TOBIAS(Bentsen et al., 2020) was applied to ATAC-seq footprints using a Snakemake-based workflow. The TOBIAS pipeline included ATACorrect to normalize Tn5 insertion bias and BINDetect to identify differential TF binding between conditions. Motif information was retrieved from JASPAR2022, and peaks were annotated using GENCODE vM23. Differential footprinting analysis was performed on merged peak regions, with blacklisted regions removed. TF binding scores were computed and visualized as coverage profiles, Venn diagrams, and differential binding heatmaps.

2.17.3. Differential TF activity with diffTF

Differential TF binding activity was assessed using diffTF(Berest et al., 2019), leveraging permutations and bootstrap sampling to identify TFs exhibiting significant binding changes. Consensus peaks were obtained from an iterative peak-calling strategy, and motif instances were mapped using HOCOMOCOv10(Kulakovskiy et al., 2018) PWMScan results. diffTF was configured to compare MC903-treated, imiquimod-treated, SAV8-treated, and HDM-treated conditions against control, with 1,000 bootstrap iterations to ensure statistical robustness. TF binding differences were ranked based on log-fold changes in motif accessibility, and visualized with ggplot2.

2.18. CUT&RUN-seq downstream analysis to identify enhancer landscape in DRG neurons

To characterize the enhancer landscape in dorsal root ganglion (DRG) neurons, CUT&RUN-seq data were processed through a series of downstream analyses, including differential binding analysis, enhancer classification, and TF activity assessment.

2.18.1. Differential chromatin accessibility analysis

Differentially enriched CUT&RUN peaks were identified using DiffBind, comparing histone modifications across experimental conditions. Peaks were called using MACS2

with a broad peak cutoff (--broad) for H3K4me1 and H3K27ac, while H3K4me3 peaks were identified with a narrow peak approach. Peak counts were normalized using spike-in controls and FRiP (Fraction of Reads in Peaks) normalization, and differential accessibility was computed using DESeq2 and EdgeR, with statistical significance assessed at FDR < 0.05. Peaks with reproducible differential enrichment were selected for downstream enhancer classification.

2.18.2. Identification of primed and active enhancers

Enhancers were classified into primed and active states based on histone modification signatures. Putative enhancers were first identified by intersecting H3K4me1-marked regions with open chromatin peaks from ATAC-seq, requiring a ≥20% overlap. Enhancers co-marked by H3K27ac were defined as active enhancers, whereas enhancers enriched only for H3K4me1 were classified as primed enhancers. To refine enhancer sets, peaks were merged using bedtools (-d 1000) with a 1-kb extension, ensuring that redundant peaks were collapsed into consensus enhancer regions.

2.18.3. Enhancer-promoter interaction mapping with Activity-by-Contact (ABC) modeling

To predict enhancer-gene interactions, the Activity-by-Contact (ABC) model(Fulco et al., 2019) was applied, integrating CUT&RUN enhancer signal with chromatin conformation constraints. Enhancer activity was inferred from H3K27ac and H3K4me1 CUT&RUN data, and enhancer-promoter interactions were prioritized based on Hi-C-derived distance constraints (500 kb window). Differentially active enhancers were linked to target genes using compareCluster (GO:BP, GO:MF, KEGG), identifying regulatory pathways associated with sensory neuron activity and disease models.

2.19. Cell-to-cell interaction analysis between DRG and skin

Intercellular interactions between dorsal root ganglion (DRG) neurons and skin cells were analyzed using a multi-framework approach incorporating DominoSignal(Cherry et al., 2021), CellComm(Lummertz da Rocha et al., 2022), and curated ligand-receptor interaction databases. The DominoSignal R package (version 0.99.2) was employed to infer receptor-ligand signaling networks and downstream TF regulation, while CellComm (version 1.3.1) was used to assess intercellular communication patterns through network modeling and pathway enrichment. Ligand-receptor interactions were curated from CellPhoneDB(Efremova et al., 2020) (version 5.0.0) and CellTalkDB(Shao et al., 2021) (version 1.0), filtered for experimentally validated mouse-specific interactions.

scRNA-seq datasets from DRG neurons and skin were preprocessed using Seurat. Log-normalized expression values were extracted, and ligand-receptor interactions were inferred by computing mean expression levels per cell cluster. Interactions were retained if both ligand and receptor expression exceeded a ≥ 0.25 normalized count threshold. Statistical significance was assessed using a permutation-based framework with 1,000 iterations, retaining interactions with $p < 0.01$.

Receptor-ligand networks were computed using Domino, integrating transcription factor activity derived from pySCENIC (version 0.12.1), using lists of transcription factors, motif annotations, and cisTarget motifs from the GRCm38 (mm10) reference genome. The analysis focused on Inflammatory-specific neuronal subsets, where TF regulons were reconstructed based on motif enrichment and co-expression patterns. Regulatory networks linking ligand-receptor interactions to TF activation were computed, and statistical significance was assessed using permutation-based enrichment testing, adjusting for background variability.

In parallel, CellComm was used to model intercellular communication based on ligand-receptor connectivity and signaling pathway enrichment. The CellComm framework computed cell-to-cell interaction probabilities using a graph-based approach,

integrating pathway activity scores and differential network analysis across experimental conditions.

2.20. Behavioral study for spontaneous itching

To assess spontaneous itch behavior, mice underwent a habituation process in the recording environment (e.g. infrared behavioral observation box : iBOB) for two consecutive days prior to the experiment (day -2 and day -1). On the day of behavioral assessment, mice were individually placed in a transparent recording chamber, and scratching behavior was continuously recorded for 30 minutes using an infrared camera. Behavioral scoring was performed manually by three independent observers blinded to the experimental conditions. A scratch was defined as a rapid back-and-forth movement of the hind paw directed toward the affected area.

2.21. MC903-induced dermatitis severity scoring

Dermatitis severity was evaluated using a modified version of the SCORAD (SCORing Atopic Dermatitis) system, originally developed for human assessment and adapted for mice(Yamamura et al., 2017). The evaluation included four clinical parameters: erythema, edema, dryness/scarring, and excoriation/erosion, each rated on a scale from 0 (none) to 3 (severe). The total dermatitis score, derived from the sum of individual symptom scores, was assessed and recorded by three independent researchers.

2.22. Histological evaluation of mouse skin

Mouse skin tissues were fixed in 4% (w/v) paraformaldehyde, embedded in paraffin blocks, and sectioned for histological analysis. The sections were stained with hematoxylin

and eosin (H&E) and imaged using a Zeiss Axioscan slide scanner (Carl Zeiss Microscopy GmbH, Jena, Germany). Full-slide scan images were saved in .czi format and analyzed using ZEN Blue software. Epidermal thickness was measured as the distance from the basal layer to the top of the granular layer. Dermal thickness was quantified as the distance from the epidermal-dermal junction to the dermal-subcutaneous interface. For quantification, ten randomized measurements were taken per sample, and the data were used for graphical representation.

2.23. Statistical Analysis

All data were presented as the mean ± standard deviation (SD). Statistical analyses were performed using GraphPad Prism 8 (GraphPad Software, Inc., San Diego, CA, USA). Differences between two groups were assessed using either a two-tailed Student's *t*-test or a Wilcoxon rank-sum test, depending on data distribution followed by Bonferroni post hoc testing to adjust for multiple comparisons. Comparisons involving more than two groups were analyzed using one-way ANOVA followed by Tukey-Kramer post hoc testing. Statistical significance was defined as $P < 0.05$, with significance levels indicated in figures as follows: $*P < 0.05$, $**P < 0.01$, or $***P < 0.001$, $****P < 0.0001$.

3. Results

3.1. scRNA-seq reveals transcriptional reprogramming of DRG neurons in chronic inflammatory skin disease models

Peripheral sensory neurons in the dorsal root ganglion (DRG) serve as primary relays for somatosensory signals, including pain, mechanosensation, and itch. Single-cell RNA sequencing (scRNA-seq) studies have extensively characterized the molecular diversity of DRG neuron subtypes under homeostatic conditions in various species including rodent(Qi et al., 2024; Sharma et al., 2020; Zeisel et al., 2018), primates(Jung et al., 2023) and human(Nguyen et al., 2021; Yang et al., 2022). However, these studies primarily focus on defining neuronal subtypes and their baseline transcriptional profiles, while the extent of transcriptional plasticity in DRG neurons under pathological conditions remains less understood. Recent single-cell and single-nucleus transcriptomic analyses have demonstrated dynamic gene expression and chromatin accessibility changes in DRG neurons following peripheral nerve injury(Renthal et al., 2020) and neuropathic pain states(K. Wang et al., 2021), suggesting that distinct molecular programs are activated in response to nerve injury, which could predispose DRG neurons to a heightened state of vulnerability, potentially contributing to the development of chronic pain. Building upon this framework, we sought to investigate whether distinct transcriptional reprogramming occurs in DRG neurons during the development of chronic pruritus in the context of chronic inflammatory skin diseases. Chronic pruritus is a hallmark symptom of conditions such as atopic dermatitis (AD) and psoriasis, yet the molecular mechanisms driving sensory neuron sensitization and persistent itch remain poorly understood.

To investigate the transcriptional reprogramming of DRG neurons underlying chronic pruritus in chronic inflammatory skin diseases, we utilized well-established mouse models of AD and psoriasis (Figure 1A, 1B, 1C). Among these, the MC903 model is the most widely used and well-characterized model for studying chronic pruritus(Oetjen et al., 2017),

as it reliably induces persistent itch and skin inflammation resembling human AD(Li et al., 2006; Xu et al., 2024). In addition to MC903, we employed supplementary AD models, including SAV8 + HDM (house dust mite) (SAV8)(Deng et al., 2023) and HDM cream models(Shiratori-Hayashi et al., 2015), which incorporate the most common environmental allergen implicated in human AD pathogenesis, to capture the diversity of allergic skin inflammation and pruritus mechanisms. These supplementary models allow us to investigate whether different allergic triggers converge on shared neuronal sensitization pathways in chronic pruritus.

Given that chronic pruritus is not exclusive to AD but also occurs in psoriasis, we further included the imiquimod (IMQ) model(Flutter & Nestle, 2013; Sakai et al., 2016), a well-established murine model of psoriasis. While psoriasis is primarily classified as an inflammatory skin disorder driven by dysregulated immune responses, a subset of patients frequently report pruritus as a major symptom. Increasing evidence suggests that psoriasis-associated itch shares mechanistic similarities with chronic pruritus in AD(Nattkemper et al., 2018), with both conditions involving neuroimmune interactions within the skin and peripheral nervous system(Tseng & Hoon, 2021). Therefore, we incorporated the IMQ model to explore potential shared or disease-specific mechanisms underlying chronic pruritus.

After initial clustering and merging the individual dataset, Unsupervised clustering of single-cell transcriptomes distinguished neuronal from non-neuronal populations, capturing a total of 121,396 cells, of which 37,001 were classified as neurons (control ; 6,650, MC903 ; 8,886, SAV8 ; 5,492, IMQ ; 10,674) and 84,395 as non-neuronal cells (control ; 14,060, MC903 ; 17,665, SAV8 ; 11,318, IMQ ; 12,562) (Figure 2A). This distribution aligns with the known cellular composition of the DRG, where neurons represent a minority population surrounded by glial and immune cells that modulate neuronal function(Yu et al., 2020). The clustering approach further segregated neurons into 11 distinct subtypes, corresponding to known DRG sensory neuron classes, including peptidergic and non-peptidergic nociceptors, C-low-threshold mechanoreceptors (C-

LTMRs), proprioceptors, and large-diameter mechanoreceptors(Nguyen et al., 2017; Usoskin et al., 2015; Zeisel et al., 2018; Zheng et al., 2019) (Figure 2B).

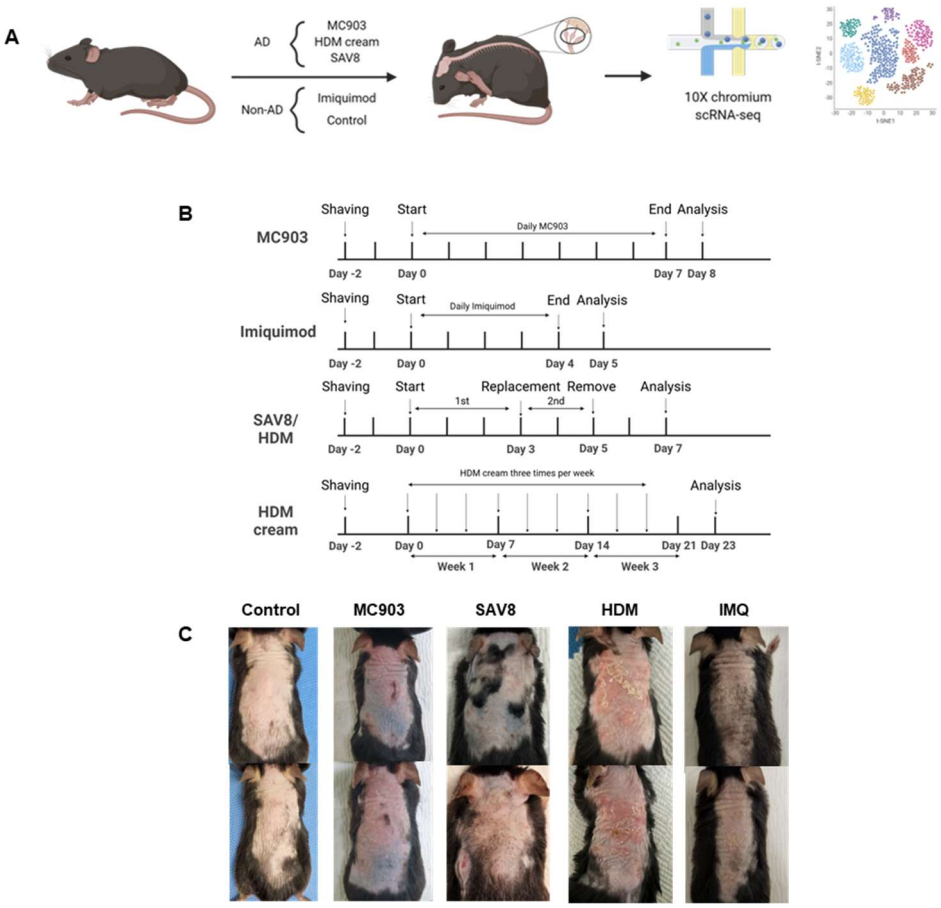

Figure 1. Experimental Workflow and Timeline for Induction of Chronic Inflammatory Skin Disease Models in Mice. (A) Schematic representation of the experimental workflow. Mice were subjected to different skin disease models, followed by sample collection and single-cell RNA sequencing (scRNA-seq) analysis. (B) Timeline of different murine models for AD and psoriasis. (C) Representative images of mouse skin lesions over time for each model. From left to right: Control, MC903, SAV8 + HDM, HDM

cream IMQ models.

Within the neuronal compartment, we identified new neuronal subclusters emerging from NP1, NP2, NP3, CGRP-alpha, CGRP-epsilon, and C-LTMR neurons under chronic inflammatory skin disease conditions, collectively referred to as inflammation-specific clusters (Inf-specific clusters) (Figure 2C, 2D), which suggest functional diversification from origin of newly formed clusters.

Specifically, NP1, NP2, and NP3 neurons are non-peptidergic C-fiber nociceptors linked to distinct sensory modalities. NP1 (MrgprD+) mediates mechanical hypersensitivity(Cavanaugh et al., 2009), NP2 (MrgprA3+) bridges pain and itch(Xing et al., 2020), while NP3 (Nppb+/Sst+) is a key player in inflammatory itch and the itch-scratch cycle(Kupari & Ernfors, 2023). Peptidergic nociceptors, including CGRP-alpha and CGRP-epsilon neurons, also showed transcriptional changes under inflammatory conditions. CGRP-alpha, a key driver of neurogenic inflammation, displayed functional adaptations, suggesting a role in shaping immune responses and sensitization pathways(Powell et al., 2021). CGRP-epsilon, a recently identified subset, likely participates in pain and itch modulation through kappa-opioid receptors(Qi et al., 2024). Their diversification suggests adaptive neuropeptide regulation reinforcing chronic pruritus. C-LTMR neurons, traditionally associated with mechanosensation and affective touch, also showed inflammatory adaptations, possibly contributing to alloknesis. The transcriptional diversification among these subsets highlights the plasticity of DRG neurons in response to chronic inflammation, highlighting potential mechanisms driving persistent sensory dysfunction in inflammatory skin diseases.

In contrast, large-diameter neurons, including CGRP-gamma, CGRP-eta, and CGRP-zeta, did not exhibit the emergence of new subclusters. This suggests that while smaller peptidergic and non-peptidergic C-fiber nociceptors undergo significant molecular changes

to support chronic pruritus and inflammation, these larger-diameter neurons may be functionally distinct, primarily engaging in other sensory modalities or acute nociceptive responses rather than persistent inflammatory conditions.

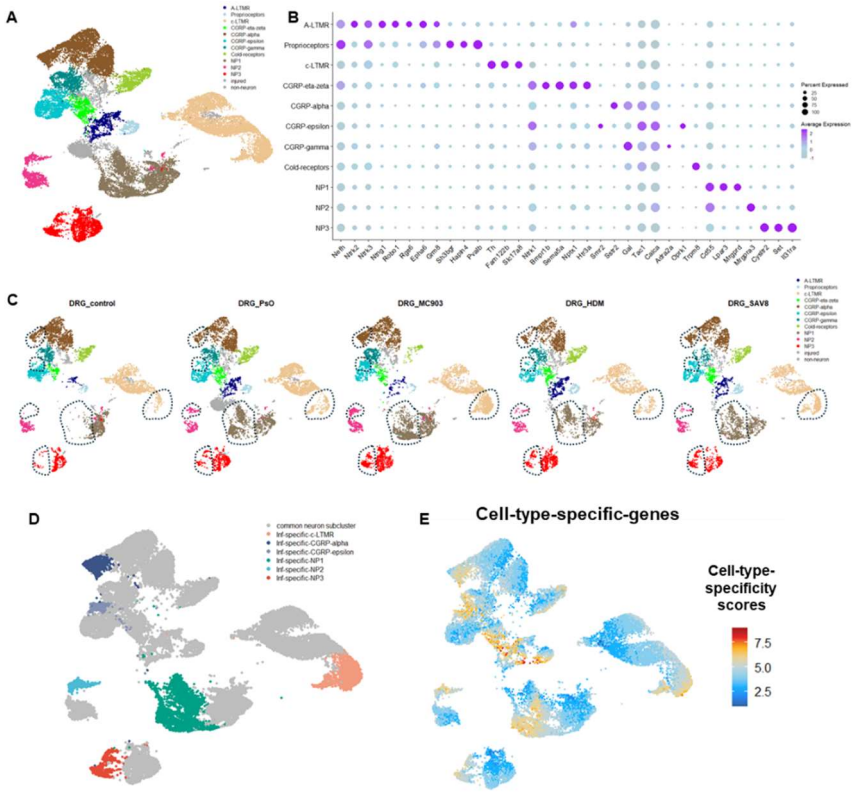

Figure 2. Characterization of DRG sensory neuron subtypes across conditions. (A) UMAP visualization of DRG sensory neurons, color-coded by identified neuronal subtypes. Labels denote distinct clusters, including A-LTMR, proprioceptors, C-LTMR, CGRP+ subsets (eta-zeta, alpha, epsilon, gamma), cold receptors, and NP (NP1, NP2, NP3). (B) Dot plot displaying marker gene expression across neuronal subtypes. Dot size represents the percentage of cells expressing the gene, while color intensity indicates the average expression level. (C) UMAP projections of DRG neurons from different conditions: control, PSO, MC903, HDM, and SAV8. Newly emerging neuronal subclusters are highlighted with

dashed outlines. (D) UMAP projections of DRG neurons with annotation of newly emerging neuronal subclusters (C) Cell-type specificity scores overlaid on the UMAP, indicating the degree of specificity for each neuronal cluster. Higher scores (warmer colors) reflect stronger specificity for subtypes.

The emergence of Inf-specific clusters were accompanied by the higher expression levels of cell type specific marker genes which was calculated with only origin of new clusters (Figure 2E). This upregulation suggests a functional specialization rather than a complete identity shift, reinforcing the subset's role in sensory processing while enabling adaptation to inflammatory cues that amplify pain- or itch-related gene expression, ultimately driving heightened sensory sensitivity or pathological hypersensitivity.

To check whether the Inf-specific clusters are derived from the specific inflammatory stimulation, the relative proportions of neuron clusters were analyzed across inflammatory conditions (Figure 3). When clustering without distinguishing Inf-specific subsets, there was little difference among neuronal subclusters across different inflammatory stimulations (Figure 3A). However, when accounting for Inf-specific clusters, these populations were nearly absent in the control group but were clearly observed across all inflammatory conditions (PSO, MC903, HDM, SAV8) (Figure 3B). Notably, the presence of Inf-specific clusters was most pronounced in MC903, followed by SAV8, with PSO and HDM exhibiting comparatively lower levels.

Additionally, the proportion of clusters observed in the control group closely matched the combined proportion of Inf-specific clusters and their corresponding origin clusters in chronic inflammatory skin diseases conditions. These findings suggest that inflammation-associated neuronal states arise not from *de novo* neurogenesis but through transcriptional reprogramming of pre-existing neurons. The conserved distribution of neuronal subtypes across conditions indicates that sensory neurons undergo phenotypic identity shifts in response to inflammation, adopting distinct transcriptional signatures while maintaining a stable population size.

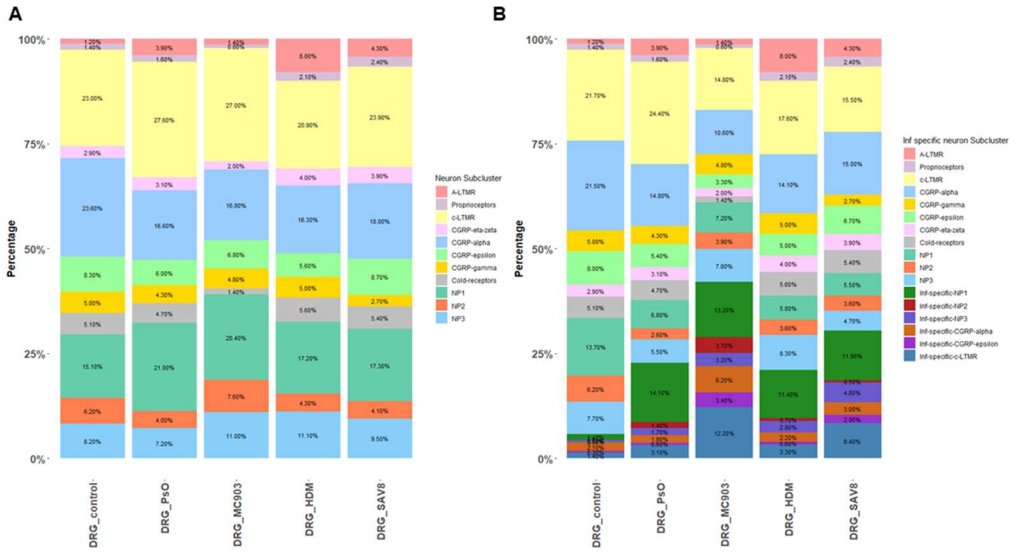

Figure 3. Proportional distribution of DRG sensory neuron subtypes across conditions. (A) Stacked bar plot depicting the percentage composition of neuronal subtypes across different experimental conditions: Control, PSO, MC903, HDM, and SAV8. Each color represents a distinct neuron subcluster. (B) Stacked bar plot illustrating the proportion of inflammation-specific (Inf-specific) neuronal subclusters across conditions. Inf-specific subclusters exhibit condition-dependent enrichment and are identified based on differential gene expression profiles.

Next, to validate the robustness of our pre-processing and clustering pipeline and to rule out methodological artifacts in the identification of Inf-specific clusters, we performed identity mapping using publicly available mouse DRG neuron single-cell and single-nucleus RNA-seq datasets (GSE154659, GSE139088, GSE254789)(Qi et al., 2024; Renthal et al., 2020; Sharma et al., 2020). By applying an anchor-based integration approach with MapQuery, we mapped our neuronal subclusters onto reference DRG neuron clusters reported in these datasets (Figure 4). Notably, Inf-specific clusters were not only retained but also mapped to existing clusters within the public data, reinforcing their

biological relevance. This finding is consistent with the increased cell-type marker signature observed in Inf-specific clusters (Figure 1E), further supporting the notion that these clusters represent inflammation-induced transcriptional states rather than technical artifacts.

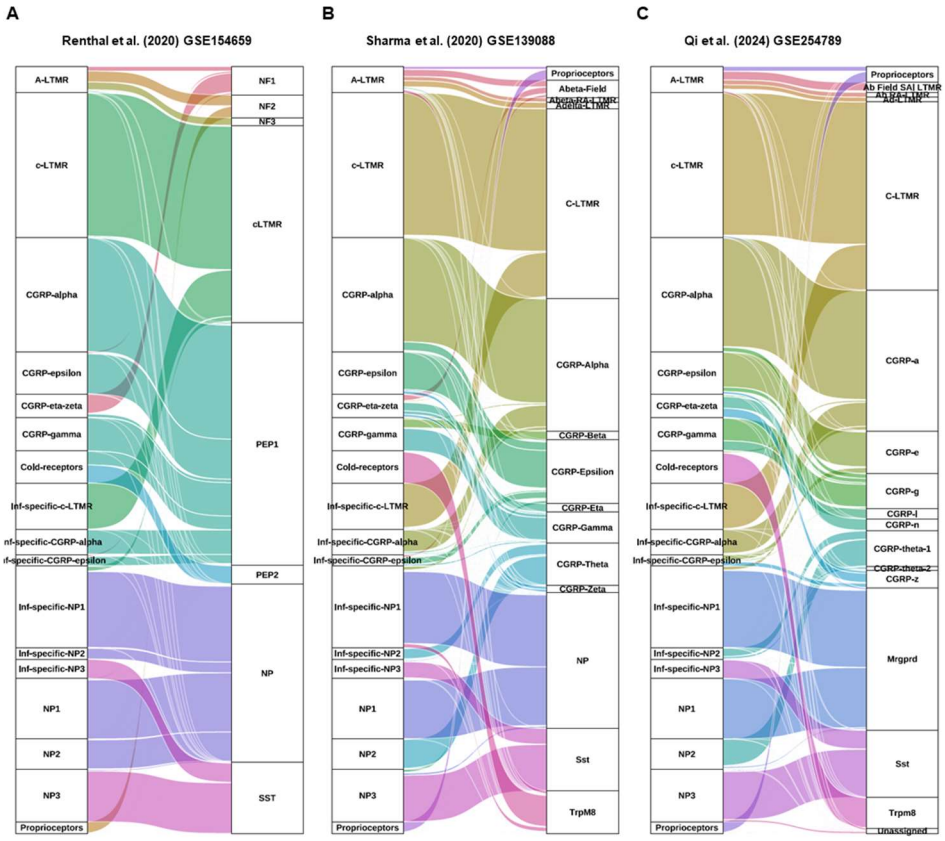

Figure 4. Mapping of annotated DRG sensory neuron subtypes to reference classifications from public datasets. Each panel presents the correspondence between our DRG neuron subtypes and established taxonomies derived from publicly available single-cell transcriptomic datasets. (A) Renthal et al. (GSE154659), (B) Sharma et al. (GSE139088), and (C) Qi et al. (GSE254789). The leftmost column represents our annotation, while right columns display the corresponding classifications from each reference dataset. The width of each flow denotes the relative proportion of mapped cells.

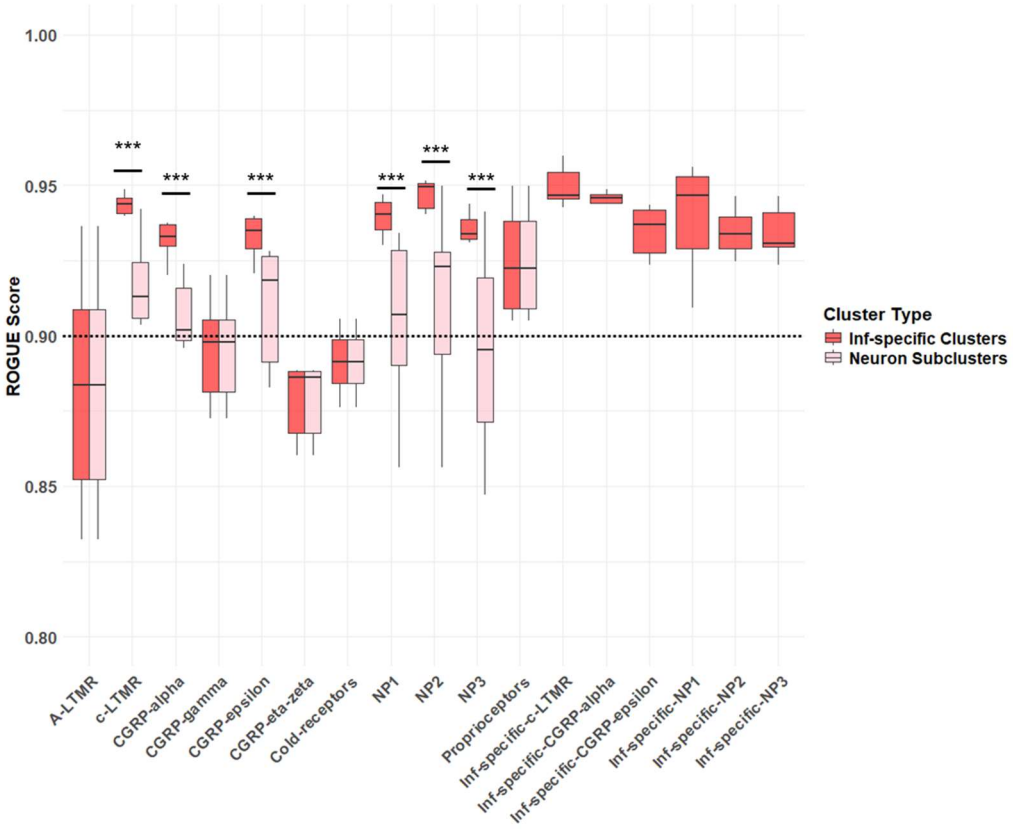

Figure 5. ROGUE Score Comparison Before and After Inclusion of Inflammation-Specific Clusters as Separate Entities. Boxplots depict ROGUE scores for DRG neuron subclusters before and after considering Inf-specific clusters as distinct entities. The y-axis represents the ROGUE score. "Neuron Subclusters" (light pink) represent clustering without separately considering Inf-specific clusters, whereas "Inf-specific Clusters" (dark red) were analyzed as distinct clusters. Wilcoxon rank sum test with Bonferroni post hoc test was used. *$P < 0.05$, **$P < 0.01$, or ***$P < 0.001$, ****$P < 0.0001$.

To confirm the presence of Inf-specific clusters, we used ROGUE, an entropy-based metric of cluster purity (0 = heterogeneous, 1 = homogeneous), to assess cluster integrity (Figure 5)(Liu et al., 2020). Notably, defining Inf-specific clusters as separate clusters significantly increased ROGUE scores in c-LTMR, CGRP-alpha, CGRP-epsilon, NP1, NP2, and NP3—the parent clusters of Inf-specific clusters. After this refinement, ROGUE values exceeded 0.9, the threshold for high cluster purity with statistical significance, indicating a more robust clustering outcome. These findings indicate that isolating Inf-specific clusters into distinct entities prevented them from diluting broader populations, thereby sharpening cluster boundaries and yielding more homogeneous groups. These findings support that DRG sensory neurons undergo transcriptional reprogramming in chronic inflammatory skin disease models.

Having established the robustness of Inf-specific clusters through ROGUE analysis, we next assessed their disease specificity using *MiloR* differential abundance analysis (Figure 6). The AD category included samples from the MC903, SAV8, and HDM models, each inducing chronic pruritus through distinct inflammatory pathways, while the PSO category consisted of the IMQ model, which mimics psoriatic inflammation. Although each model exhibits unique inflammatory signatures, we categorized them into AD and PSO groups to enable a direct comparison between atopic dermatitis and psoriasis.

Neighborhood abundance comparisons revealed substantial alterations in neuronal subpopulations under inflammatory conditions. In AD versus control, Inf-specific clusters were significantly enriched in AD while being depleted in control samples, reflecting the emergence of novel neuronal subtypes under AD-like inflammation (Figure 6B, 6C – left panels). Similarly, in PSO versus control, Inf-specific clusters were also enriched in PSO, though to a lesser extent than in AD, indicating a moderate expansion of these clusters in psoriasis (Figure 6B, 6C – middle panels). Direct comparison between AD and PSO further revealed a striking pattern: nearly all Inf-specific neighborhoods, except for the Inf-specific NP1 cluster, were significantly more abundant in AD than in PSO(Figure 6B, 6C – right

panels). This suggests a stronger inflammatory effect in AD models, leading to greater neuronal plasticity and recruitment of inflammation-associated neuron subpopulations.

To further characterize the specificity of Inf-specific clsuters under inflammatory conditions, we performed unsupervised clustering of MiloR neighborhoods based solely on transcriptomic similarity, without manual annotations (Figure 6D, 6E). This unbiased approach independently identified distinct neuronal groups, many of which corresponded to Inf-specific clusters. Notably, these unsupervised clusters recapitulated the manually annotated Inf-specific subclusters, confirming their inflammation-driven emergence. The numbered neighborhood clusters represent newly formed neuronal subtypes that arise specifically under inflammatory conditions.

Collectively, these findings provide strong evidence that inflammatory skin conditions induce the emergence of distinct DRG neuron clusters. These Inf-specific clusters, absent in healthy controls, become increasingly enriched under inflammation, with a more pronounced effect in AD models.

In summary, scRNA-seq analysis of DRG neurons from various chronic cutaneous inflammation conditions revealed significant transcriptional reprogramming in DRG neurons, leading to the emergence of inflammation-specific (Inf-specific) clusters derived from NP1, NP2, NP3, CGRP-alpha, CGRP-epsilon, and C-LTMR neurons. These clusters were absent in controls but enriched under inflammatory conditions, particularly in AD models. ROGUE analysis validated their robustness, and MiloR differential abundance analysis demonstrated a stronger inflammatory effect in AD than in PSO. Unsupervised clustering further confirmed their distinct transcriptional identity, highlighting inflammation-driven neuronal plasticity. These findings suggest that sensory neurons undergo adaptive changes in response to chronic inflammation, possibly contributing to persistent pruritus and altered sensory processing.

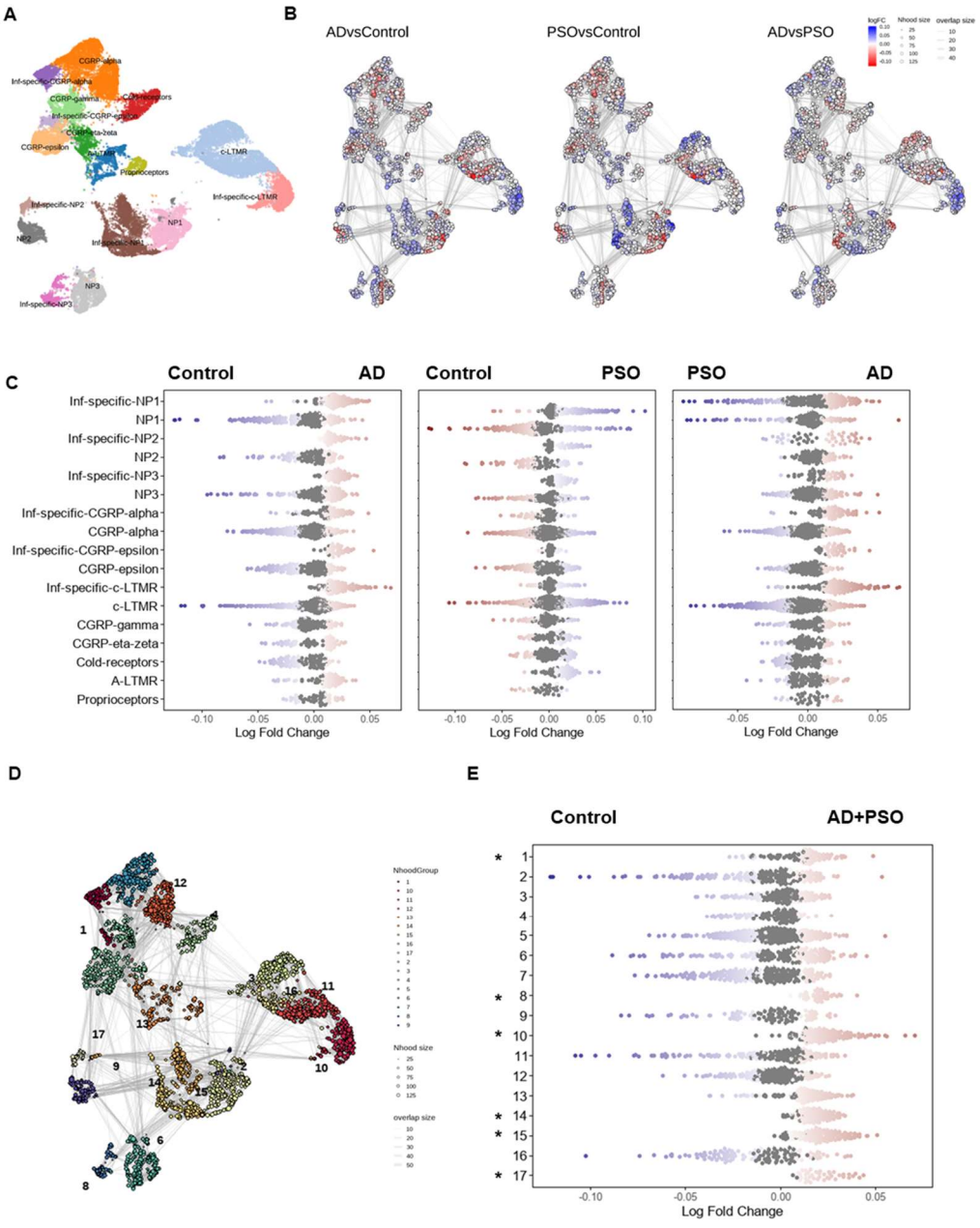

Figure 6. Neighborhood-based differential abundance analysis reveals Inf-specific clusters are specific to chronic inflammatory skin diseases mouse models. (A) UMAP representation of sensory neuron subtypes from dorsal root ganglia (DRG), colored by

cluster annotation. (B) Milo-based differential abundance analysis across conditions. Each node represents a local neighborhood of cells, with edges depicting similarity relationships. Nodes are colored based on log fold change (LFC) in abundance between conditions: AD (MC903, SAV8, and HDM models) vs. Control, PSO (IMQ models) vs. Control, and AD vs. PSO. Blue indicates a decrease, while red represents an increase in abundance. (C) Beeswarm plot of the distribution of LFC across conditions in neighborhoods containing cells from different cell type clusters. Differential abundance neighborhoods at FDR 10% are colored. (D) UMAP representation of neuronal neighborhoods identified via Milo analysis, with neighborhoods grouped and numbered based on similarity. (E) Beeswarm plot of the distribution of LFC across conditions (AD, PSO vs. Control) in neighborhoods identified via Milo analysis. Differential abundance neighborhoods at FDR 10% are colored. Asterisks (*) indicate that the corresponding Inf-specific clsuters (1 : Inf-specific CGRP-alpha & epsilon, 8 : Inf-specific NP3, 10 : Inf-specific c-LTMR, 14&15 : Inf-specific NP1, 17 : Inf-specific NP2)

3.2. The transcriptomics characteristics of inflammation-specific neuron subsets

To investigate the molecular characteristics of Inf-specific cluster neurons, we analyzed key quality control metrics across neuronal subtypes (Figure 7A, 7B, 7C). Inf-specific neurons were characterized by significantly lower number of genes detected (Figure 7A) and total UMI counts (Figure 7B) compared to other neuronal populations. Despite the reduced RNA contents, these neurons showed a markedly higher fraction of mitochondrial reads relative to other clusters (Figure 7C). An elevated mitochondrial reads contents often indicates altered metabolic state or cellular stress.

To validate this possibility, we examined whether Inf-specific neurons display hallmarks of neuronal injury by analyzing the expression of regeneration-associated genes (RAGs), which have been linked to axonal injury responses in bulk DRG transcriptomic studies(Chandran et al., 2016; Costigan et al., 2002; LaCroix-Fralish et al., 2011; Perkins et al., 2014; Xiao et al., 2002). Surprisingly, Inf-specific neurons did not upregulate canonical injury-response genes (Figure 7D). The absence of RAG induction indicates that these neurons are not mounting an injury-associated transcriptional program, consistent with them not experiencing active axonal damage(Seijffers et al., 2007). Likewise, pro-apoptotics (*Bax, Bak1, Casp3, Casp8, Casp9, Fas, Tnf, Bcl2, Bcl2l1, Tradd, Bid*) and stress-response genes (*Ddit3, Atf4, Atf6, Xbp1, Hspa5, Nfe2l2, Sod1, Sod2, Gpx1, Hmox1*) remain low in Inf-specific neurons (Figure 7E). Specifically, there were no upregulation of key cell stress markers such as Ddit3/CHOP, a transcription factor that mediates ER stress-induced neuronal apoptosis(Ajoolabady et al., 2022). Markers of ongoing apoptosis or oxidative stress were also not increased in this clusters. This lack of stress gene induction suggests that Inf-specific neurons are not undergoing cell death or severe stress, despite their high mitochondrial RNA content.

Instead of injury markers, Inf-specific neurons exhibited increased expression of genes related to neuronal plasticity (*Fos , Jun, Egr1, Arc, Nr4a1, Dusp1, Npas4, Bdnf, Camk2a,*

Grin1, Gria1, Syn1) and inflammatory signaling (*Il1b, Il6, Ifng, Ccl2, Ccl5, Cxcl10, Rela, Nfkb1, Nfkb2, Jak1, Stat3*). Many of these cells highly expressed immediate-early genes and other activity-dependent transcription factors associated with synaptic plasticity. This suggests that these neurons may be in an active or recently stimulated state, potentially undergoing synaptic remodeling. In parallel, these neurons upregulated genes involved in cytokine and chemokine signaling, implicating neuroimmune interactions. The co-expression of plasticity regulators and inflammatory mediators indicates that Inf-specific neurons are actively adapting their synapses and interacting with an inflammatory environment, rather than being quiescent.

Alongside these transcriptional changes, Inf-specific neurons exhibited broad downregulation of oxidative phosphorylation (OXPHOS) and mitochondrial metabolic genes (Figure 7E). These findings suggest a metabolic shift away from mitochondrial respiration, likely to accommodate the increased energetic and biosynthetic demands associated with neuronal remodeling and inflammatory activation(Willemen et al., 2023). Rather than reflecting mitochondrial dysfunction, this pattern aligns with metabolic adaptation(Cheng et al., 2022), potentially analogous to the Warburg-like effect observed in immune cells under inflammatory conditions(Vander Heiden et al., 2009). Such reprogramming may support the energetic demands of synaptic remodeling while mitigating oxidative stress.

To exclude the possibility that the Inf-specific transcriptomic signature results from technical artifacts, we applied ambient RNA correction using SoupX (Figure 7F). After correction, the Inf-specific cluster remained distinctly identifiable (Figure 7F). The persistence of this cluster after stringent quality control confirms its biological relevance, establishing Inf-specific neurons as a bona fide subset with a distinct molecular state characterized by enhanced plasticity, inflammatory activation, and metabolic reprogramming.

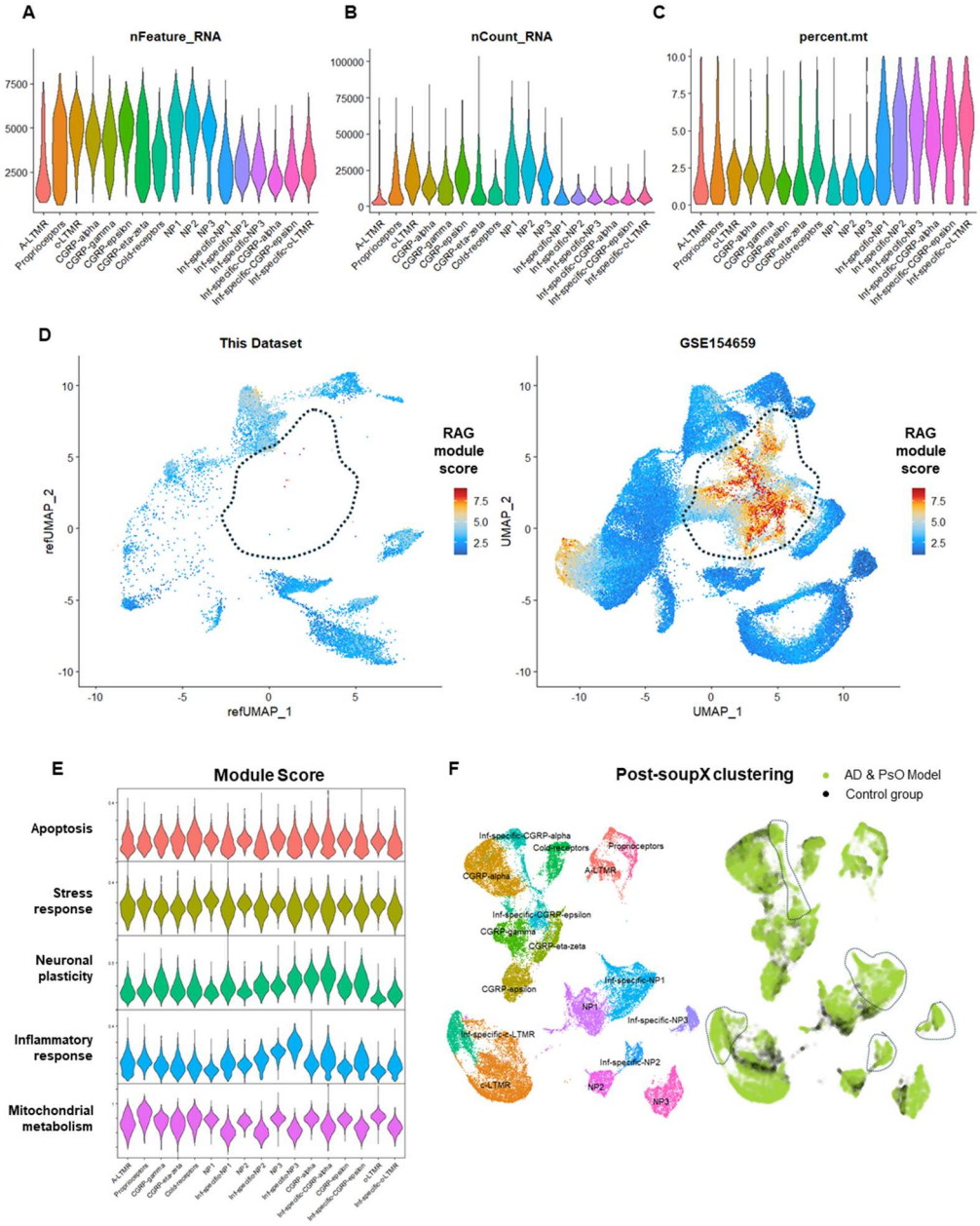

Figure 7. Inf-specific neurons represent a distinct neuronal state with low

transcriptional complexity, high mitochondrial content, and inflammation-associated plasticity. (A) Violin plots illustrating key quality control metrics across neuronal subtypes, including the number of detected genes (nFeature_RNA), total transcript counts (nCount_RNA), and mitochondrial gene fraction (percent.mt). Certain neuronal subsets exhibit lower transcript detection and total RNA counts with a relatively higher mitochondrial fraction, suggesting metabolic or stress-related differences.

(B) UMAP visualization of RAG (regeneration-associated gene) module scores in this dataset (left) and the GSE154659 dataset (right). Cells are colored based on RAG module activity, with higher scores in red and lower scores in blue. The dotted lines highlight regions with notable RAG module enrichment.

(C) Violin plots showing expression distributions of selected genes across neuronal subtypes, indicating differential expression patterns among distinct neuronal clusters.

(D) UMAP representation of neuronal subclusters with annotated labels (left) and an alternative visualization highlighting inferred trajectories (right), providing insights into potential neuronal lineage relationships and functional transitions.

Next, to define the transcriptional identity of Inf-specific neuron clusters, we examined the expression of genes regulating neuronal excitability (ion channels and peripheral sensitization), synaptic function (plasticity-related molecules and neuropeptides), neuroimmune interactions (cytokines, chemokines, and their receptors), and transcriptional control (sensory identity factors, injury response programs, and epigenetic modulators) across neuronal subtypes (Figure 8).

Inf-specific neurons showed substantial upregulation of voltage-gated ion channels, particularly sodium (*Scn9a, Scn10a, Scn11a*) and calcium channels (*Cacna1c, Cacna1h, Cacna1b, Cacna2d1*), indicating an increased capacity for neuronal firing. In parallel, key potassium channels (*Kcnq2, Kcnq3, Kcna1, Kcna2*) were downregulated, a shift known to lower the threshold for action potential generation (Tsantoulas & McMahon, 2014). Moreover, TRP channels (*Trpv1*, *Trpa1*, *Trpv3*) was significantly upregulated across multiple Inf-specific clusters, which parallels known inflammation-induced increases in TRP channels that heighten neuronal responsiveness and promote neuropeptide release(Misery et al., 2023). This pattern was most pronounced in Inf-specific-NP1 and Inf-specific-NP3, which displayed the strongest induction of sodium and calcium channels. Inf-specific neurons also upregulated *P2rx3*, an ATP-gated ion channel implicated in sensory hypersensitivity(Shiratori-Hayashi et al., 2019), particularly in Inf-specific-NP3 and Inf-specific-CGRP-epsilon, suggesting increased sensitivity to ATP-mediated signaling.

Beyond excitability and plasticity, Inf-specific neurons displayed broad neuroimmune activation. Compared to their original neuronal counterparts, Inf-specific neurons showed increased expression of pro-inflammatory cytokines (*Il1b, Il6, Tnf*), chemokines (*Ccl2, Ccl5, Ccl8, Ccl11, Ccl24, Ccl26, Ccl20, Tslp*), and cytokine receptors (*Il1r1, Il4ra, Il6st, Il17ra*). Among the neuropeptidergic subclusters, Inf-specific-CGRP-alpha neurons exhibited a transcriptional profile that diverged significantly from their original counterparts, with changes that suggested a dual role in neurogenic inflammation and immune modulation. Compared to CGRP-alpha neurons, Inf-specific-CGRP-alpha

neurons displayed marked upregulation of *Vgf*, a neuropeptide implicated in pain modulation and neurotrophic signaling(Soliman et al., 2019), while *Cartpt* were downregulated, suggesting functional shifts in peptide-mediated signaling. Concurrently, these neurons exhibited a strong decrease in *Ccr8* expression but a substantial increase in *Ccl5*, *Ptger4*, and *Il6*, highlighting their increased participation in inflammatory cascades. The upregulation of *Il4ra* and *Il13ra1*, further supports a functional shift toward an immune-interactive state, especially Th2 immune response which is crucial in chronic pruritus(Oetjen et al., 2017). Notably, *Il17ra* expression was highly specific to Inf-specific-CGRP-alpha, distinguishing these neurons from all other Inf-specific populations. The specificity of *Il17ra* induction suggests a potential role in IL-17-mediated neuroimmune interactions.

Despite shared neuroimmune adaptations, individual Inf-specific subclusters exhibited distinct functional specializations. Inf-specific-NP3 neurons displayed a dominant pruritus-related gene signature, with upregulation of *Mrgpra3*, *Mrgprx1*, *Hrh1*, *Ptger4*, *Il31ra*, *Osmr*, and *Cysltr2*, suggesting an enhanced response to both histaminergic and non-histaminergic itch stimuli. Also, Inf-specific-NP3 neurons specifically up-regulated the expression of *Ccl24*, a chemokine linked to eosinophil recruitment, suggesting a neuron-mediated mechanism of Th2-driven inflammation.

In parallel with these neuroimmune adaptations, Inf-specific neurons displayed transcriptional changes indicative of sustained neuronal plasticity and epigenetic reprogramming. Inf-specific clusters showed increased expression of key epigenetic modulators (*Ebf1*, *Brd4*, *Kdm6b*, *Hdac3*, *Dnmt3a*, *Ezh2*), suggesting inflammation-induced chromatin remodeling that may drive long-term alterations in neuronal function. Ebf1, a transcription factor critical for sensory neuron identity, was notably enriched across Inf-specific populations, particularly in Inf-specific-NP3, suggesting its role in subtype-specific regulatory programs. The histone acetylation reader *Brd4* and H3K27 demethylase *Kdm6b* were upregulated, consistent with an epigenetic shift that facilitates pro-nociceptive and pro-inflammatory gene expression.

Consistent with these regulatory changes, Inf-specific neurons also exhibited broad upregulation of plasticity-associated transcription factors (TFs), including *Creb1*, *Egr1*, *Egr2*, *Gata3*, and immediate early genes (*Fos*, *Jun*, *Arc*). These factors are known to enhance activity-dependent neuronal remodeling and synaptic strengthening, a hallmark of sensory sensitization(Kim et al., 2018). The increase in *Creb1*, a master regulator of synaptic plasticity(Yee et al., 2024), suggests enhanced transcriptional activity supporting hyperexcitability and persistent signaling. Similarly, *Egr1* and *Egr2*, which are rapidly induced by neuronal activation, were significantly upregulated, pointing to sustained transcriptional adaptation under inflammatory conditions.

At the functional level, Inf-specific neurons exhibited reinforced synaptic plasticity and excitatory signaling, as indicated by increased expression of synaptic regulators (*Grin2b*, *Dlg4*, *Camk2a*). The upregulation of *Grin2b* (encoding the NR2B subunit of NMDA receptors) suggests enhanced glutamatergic transmission, contributing to heightened excitability and central sensitization. Additionally, *Dlg4* (PSD-95) and *Camk2a* point to structural and functional reinforcement of excitatory synapses. This transcriptional profile suggests that Inf-specific neurons not only become more excitable but also undergo long-term synaptic reorganization, providing a molecular basis for chronic inflammatory pain and pruritus.

Together, these findings indicate that Inf-specific neurons undergo a coordinated transcriptional and epigenetic shift, reinforcing neuronal hyperexcitability, synaptic remodeling, and neuroimmune interactions. The convergence of epigenetic modulation, activity-dependent TF induction, and enhanced synaptic function suggests that these neurons acquire a persistent, inflammation-adapted phenotype, potentially sustaining sensory hypersensitivity even after the resolution of acute inflammation.

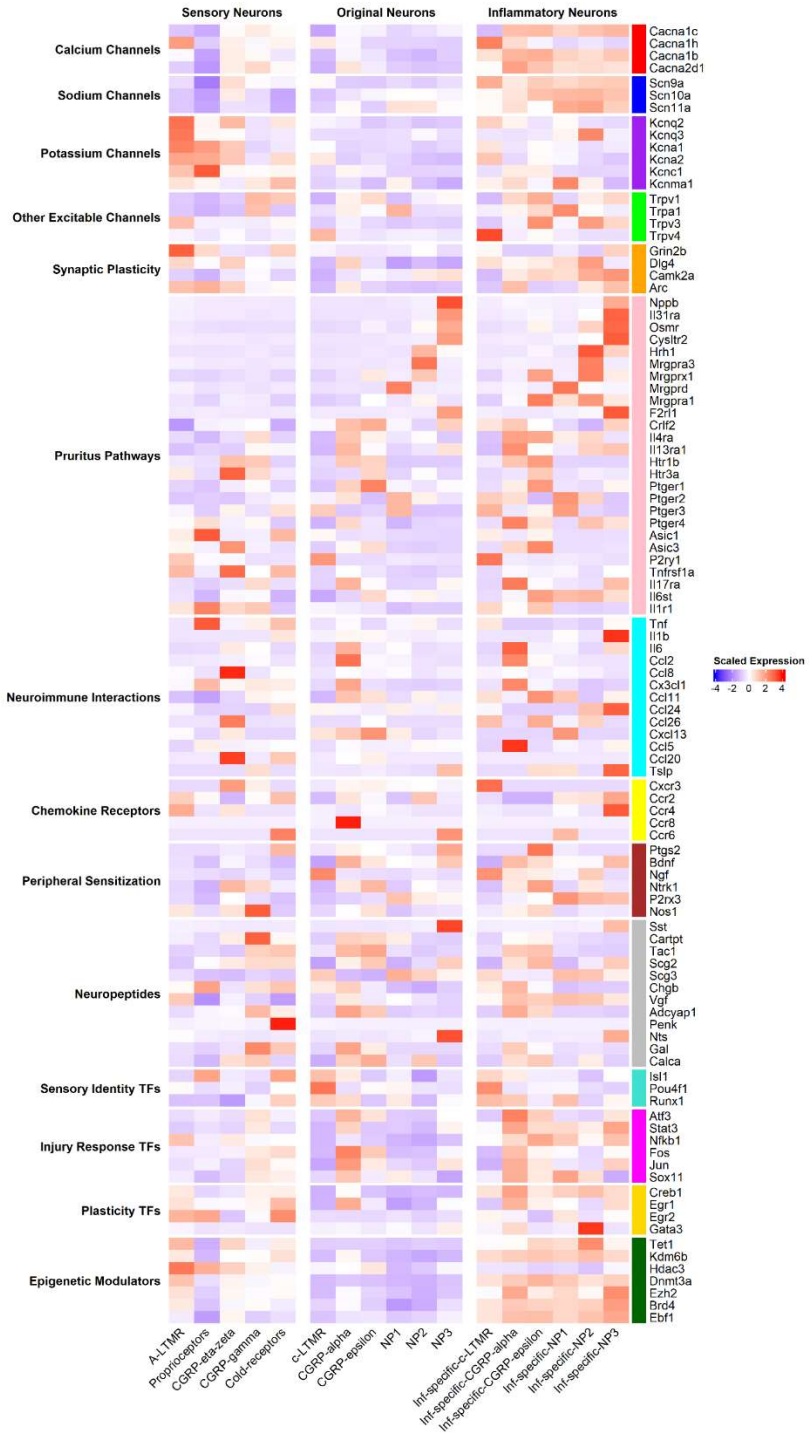

Figure 8. Transcriptional changes in Inf-specific neurons reveal alterations in excitability, synaptic plasticity, and neuroimmune interactions. Heatmap depicting scaled expression of representative genes across sensory neuron subtypes, including Inf-specific neurons. Gene categories include ion channels (calcium, sodium, potassium, and TRP channels), synaptic plasticity factors, pruritus-related pathways, neuroimmune mediators (cytokines, chemokines, and their receptors), peripheral sensitization factors, neuropeptides, sensory identity TFs, injury response TFs, plasticity TFs, and epigenetic modulators.

Next, to capture the shared transcriptomic characteristics of Inf-specific clusters beyond individual gene-level changes, we conducted gene set enrichment analysis (GSEA) and pathway-level differential analysis to identify the broader molecular programs distinguishing Inf-specific neurons from their original counterparts (Figure 9). This analysis revealed widespread upregulation of pathways associated with neuronal excitability, synaptic plasticity, and neuroimmune interactions, highlighting key transcriptional signatures underlying sensory adaptation under inflammatory conditions.

Inf-specific neurons exhibited significant enrichment of ion transport and excitability pathways, including voltage-gated ion channel activity, potassium and sodium ion transport, and glutamatergic synaptic transmission. These findings suggest a molecular basis for heightened sensory responsiveness, likely contributing to neuronal hyperexcitability and sensitization. Concurrently, pathways involved in cell adhesion and synaptic organization were upregulated, indicating structural remodeling of sensory neurons in response to inflammation.

Beyond excitability and plasticity, neuroimmune interactions emerged as a dominant transcriptional feature of Inf-specific neurons. The enrichment of neuroactive ligand-receptor interactions suggests that these neurons actively engage in immune modulation, reinforcing their role in the inflammatory microenvironment.

To further dissect the contributions of individual gene sets, we employed decoupleR to calculate AUC scores for each pathway and then treated these terms as features for differential analysis using MAST (Figure 10). Inf-specific neurons exhibited a relative downregulation of mitochondrial metabolism and oxidative phosphorylation pathways, which were instead enriched in common clusters. The suppression of ATP synthesis and mitochondrial electron transport suggests a shift away from oxidative phosphorylation (OXPHOS) toward alternative energy metabolism. Such metabolic reprogramming may serve to limit excessive ROS production, which is known to exacerbate oxidative stress and neuronal dysfunction in inflammatory conditions. The observed pattern is reminiscent of metabolic shifts in immune and glial cells during inflammation, where glycolysis is favored over mitochondrial respiration to support biosynthetic demands rather than ATP production. This reduction in mitochondrial output in Inf-specific neurons may contribute to a state of energy conservation and stress adaptation, potentially sustaining a prolonged sensitized state.

Despite the suppression of mitochondrial metabolism, Inf-specific neurons displayed enrichment of pathways linked to neuronal excitability and synaptic plasticity. Increased expression of genes involved in calcium ion transport, voltage-gated channel activity, and spontaneous neurotransmitter release suggests an intrinsic shift toward a hyperexcitable state. Enrichment of synaptic remodeling and cell adhesion pathways further indicates that structural and functional synaptic changes contribute to the sustained sensitization of these neurons. The combination of metabolic suppression and heightened neuronal activity suggests that Inf-specific neurons undergo a shift in resource allocation, prioritizing prolonged synaptic responsiveness over mitochondrial efficiency.

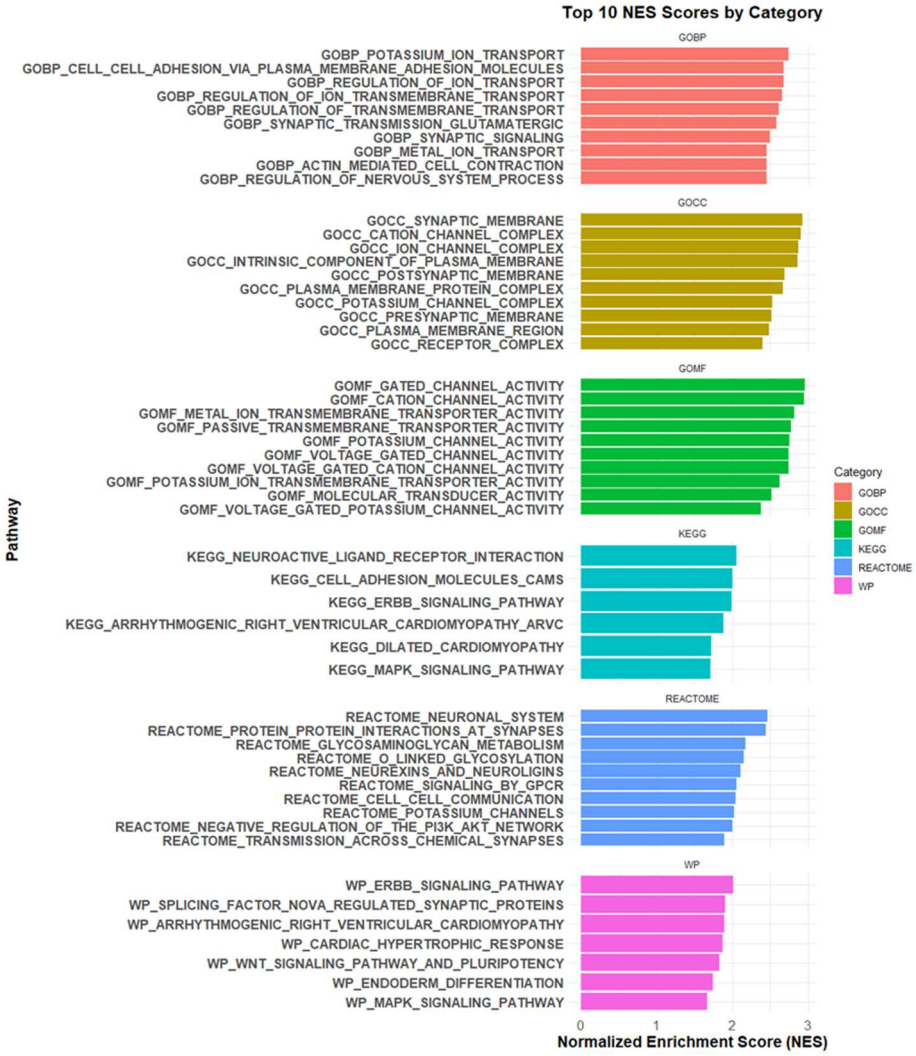

Figure 9. Enrichment of Ion Transport, Synaptic Plasticity, and Neuroimmune Pathways in Inf-Specific Neurons. Bar plots represent the top 10 pathways ranked by normalized enrichment score (NES) across five major pathway databases: Gene Ontology Biological Process (GOBP, pink), Gene Ontology Cellular Component (GOCC, yellow-green), Gene Ontology Molecular Function (GOMF, green), KEGG (cyan), Reactome (blue), and WikiPathways (WP, purple). Each bar corresponds to a pathway, with NES values displayed on the x-axis, indicating the strength and direction of enrichment.

Figure 10. DecoupleR with differential enrichment analysis reveals Synaptic Plasticity, and Ion Transport Pathways Are Enriched in Inf-Specific Clusters. Dot plot showing the top enriched GOBP terms identified using decoupleR for differential gene expression analysis with MAST methods. The x-axis represents the Inf-specific-cluster and common (origin) clsuter. The dot size corresponds to the average log2 fold change (avg_log2FC), representing the magnitude of gene expression changes within each pathway.

A detailed examination of decoupleR-derived pathway scores highlighted key biological processes contributing to the functional reprogramming of Inf-specific neurons (Figure 11). Despite significant downregulation of oxidative phosphorylation (OXPHOS)-related genes, the hypoxia-inducible factor 1-alpha (HIF1A) pathway remained largely inactive, suggesting mitochondrial suppression independent of classical hypoxic adaptation. Instead, these neurons displayed robust upregulation of inflammatory pathways, including NF-κB, JAK-STAT, and TNFα signaling, implicating immune-driven neuronal response.

Notably, JAK-STAT signaling is a well-established driver of neuronal sensitization in chronic itch, and its activation in DRG neurons has been linked to key cytokine-mediated pathways. IL-31 signaling via JAK1/STAT3 and JAK2/STAT5A/5B, as well as IL-4 and IL-13 signaling through JAK1/JAK3/STAT3/STAT6, have been implicated in promoting neuronal hyperexcitability. The observed enrichment of JAK-STAT components in Inf-specific neurons suggests an inflammation-induced sensitization mechanism, potentially driving persistent itch-related hypersensitivity(Fang et al., 2015; Oetjen et al., 2017).

Concurrently, pathways linked to neurodevelopmental and regenerative processes—including WNT, TGF-β, VEGF, and EGFR—were enriched, suggesting inflammation-induced remodeling of neuronal structure and function. While p53 and TRAIL signaling were also upregulated, apoptotic and stress-response module scores (Figure 7) remained low, indicating that these neurons are not in a dying state but may instead engage these pathways for stress adaptation or synaptic plasticity.

Pathway-level analyses further revealed that Inf-specific neurons exhibited significant upregulation of long-term potentiation (LTP) pathways (Figure 12), including KEGG and Reactome-defined LTP as well as memory-associated gene sets. Enrichment of calcium-dependent signaling cascades, including calcium ion import, neurotransmitter exocytosis, calcineurin-mediated signaling, and voltage-gated calcium channel activity (Figure 13), suggests that chronic inflammation promotes sustained neuronal hyperexcitability. Additionally, positive regulation of CREB transcription factor activity, a key mediator of synaptic plasticity and memory formation, was significantly enriched, reinforcing the role of inflammatory signaling in persistent sensory adaptation.

Together, these findings indicate that inflammation reshapes sensory neurons through a complex interplay of metabolic suppression, immune signaling, and structural remodeling, reinforcing the role of neuroimmune interactions—particularly JAK-STAT-mediated sensitization and calcium-dependent synaptic potentiation—in chronic itch.

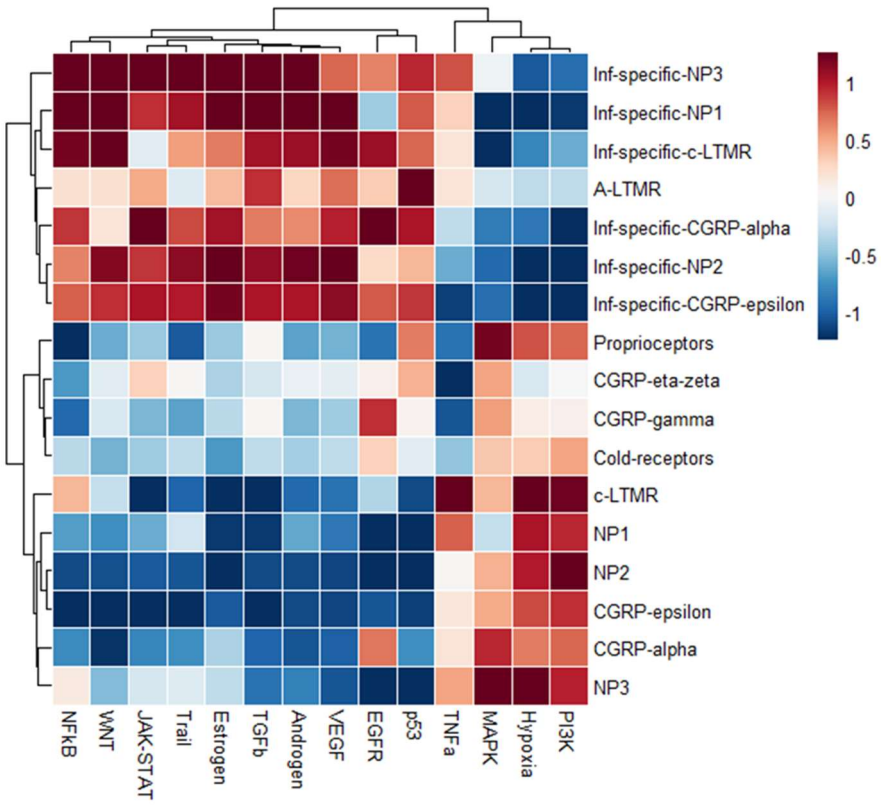

Figure 11. Inf-Specific Neurons Exhibit Distinct Activation of Inflammatory, Apoptotic, and Growth Factor Signaling Pathways. heatmap displays the scaled activity scores of PROGENy signaling pathways across neuronal subtypes, with a focus on Inf-specific clusters. Columns represent pathways, including inflammatory (TNF-α, NF-κB, JAK-STAT, MAPK), apoptotic (p53, TRAIL), growth factor-related (VEGF, EGFR, TGF-β, PI3K), metabolic stress (Hypoxia), and neurodevelopmental (WNT, Androgen, Estrogen) signaling. Rows represent neuronal clusters, and columns represent individual pathways.

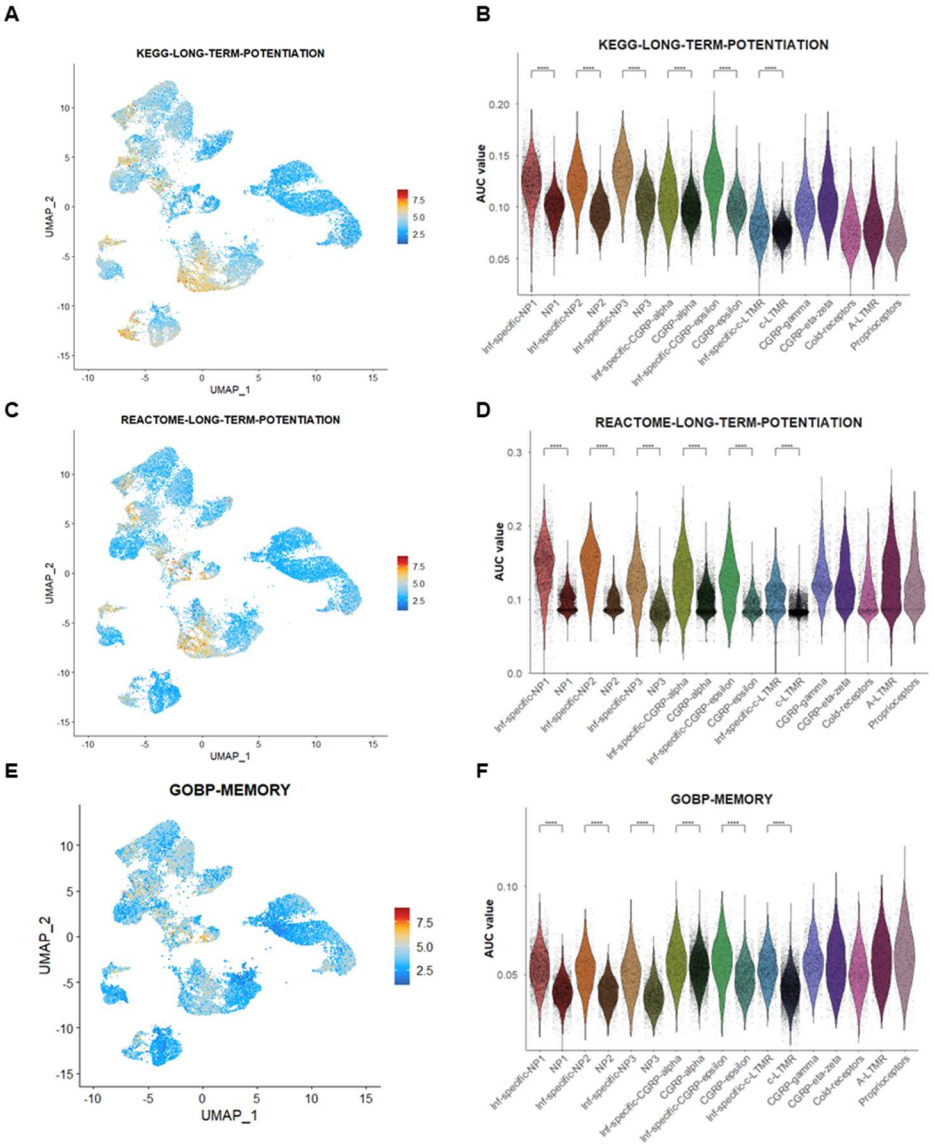

Figure 12. Inf-specific neuron clusters show enriched long-term potentiation and memory gene sets suggesting enhanced plasticity. Inf-specific neuron clusters show enrichment of long-term potentiation and memory-related gene sets from various gene set database. UMAP projections displaying the enrichment scores of (A) KEGG long-term potentiation, (C) Reactome long-term potentiation, and (E) Gene Ontology biological

process (GOBP) memory gene sets, respectively. (B, D, F) Violin plots showing the distribution of enrichment scores across neuronal subsets. Wilcoxon rank sum test with Bonferroni post hoc test was used. *$P < 0.05$, **$P < 0.01$, or ***$P < 0.001$, ****$P < 0.0001$.

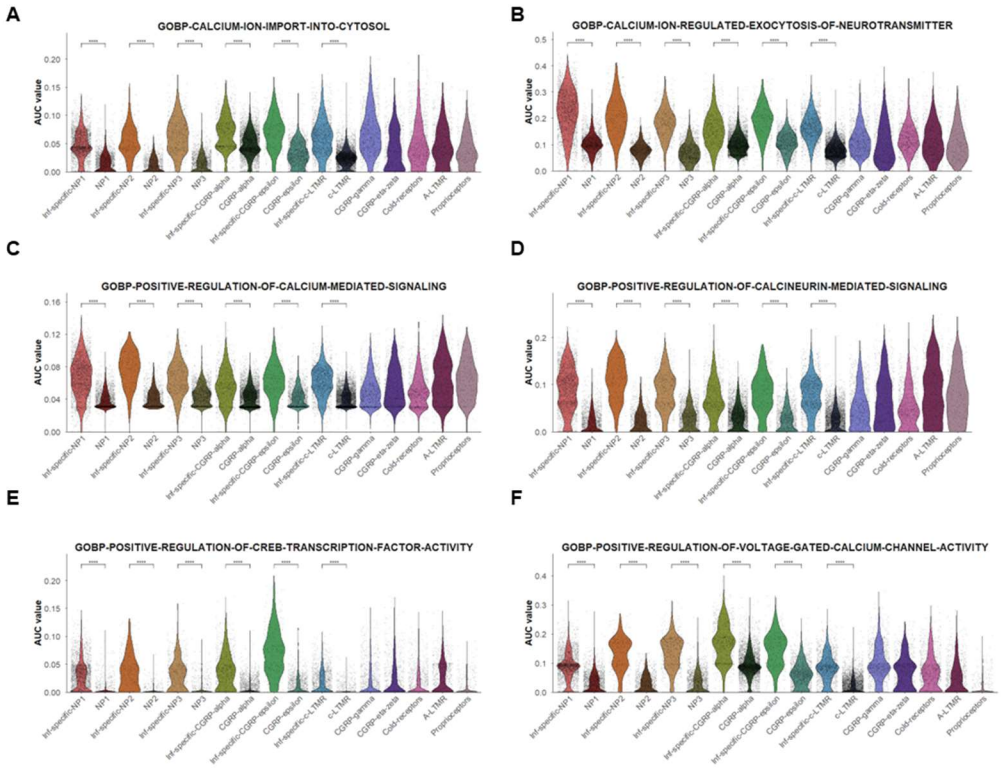

Figure 13. Inf-specific neuron clusters show enrichment of intracellular calcium signaling and their downstream pathways. Violin plots showing enrichment scores for gene ontology biological process (GOBP) terms related to calcium signaling across neuronal subsets. (A) Calcium ion import into the cytosol. (B) Calcium ion-regulated exocytosis of neurotransmitters. (C) Positive regulation of calcium-mediated signaling. (D) Positive regulation of calcineurin-mediated signaling. (E) Positive regulation of CREB transcription factor activity. (F) Positive regulation of voltage-gated calcium channel activity. Wilcoxon rank sum test with Bonferroni post hoc test was used. *$P < 0.05$, **$P < 0.01$, or ***$P < 0.001$, ****$P < 0.0001$.

3.3. Regulon Analysis Identifies Transcriptional Drivers of Inf-Specific Neurons

To elucidate the transcriptional regulatory mechanisms underlying the transition from the origin cluster to the Inf-specific cluster, we performed SCENIC-based regulon activity analysis and identified TFs with significantly increased regulon activity in the Inf-specific cluster. Notably, several of these TFs were closely linked to neuronal plasticity, chronic itch, and sustained neuronal sensitization. While the overall regulon activity patterns in Inf-specific neurons were largely comparable between the AD and PSO conditions, a striking divergence was observed between the original neuron cluster and the Inf-specific cluster, suggesting substantial transcriptional reprogramming during this transition (Figure 14, Figure 15).

Notably, Ebf1, Stat3, Nfat5, and Klf4 exhibited a marked increase in regulon activity within the Inf-specific cluster. Ebf1 is a well-established regulator of sensory neuron identity and has been implicated in peripheral neuron excitability(Liang et al., 2024). Consistent with its role in chronic pruritus, Ebf1 activity was significantly upregulated, supporting its involvement in sustained neuronal sensitization. Stat3 and Stat5b, a key mediator of neuroinflammatory responses(Flayer et al., 2024; Li et al., 2017; Takahashi et al., 2023), displayed elevated activity, suggesting its role in the transcriptional remodeling of pruriceptive neurons.

Additionally, Nfat5, a regulator of osmotic stress response(Chen et al., 2024), has been linked to sensory neuron adaptation and persistent excitability, further reinforcing its role in chronic pruritus pathophysiology. Moreover, Nfatc1 and Nfatc3, components of Calcineurin/NFAT signaling, exhibited increased activity. Nfatc1 and Nfatc3 have been implicated in nociceptor hyperexcitability, pro-inflammatory gene expression, and upregulation of ion channels, which contribute to long-term neuronal sensitization(Huang et al., 2022). Klf4, known for its role in neuronal reprogramming and axonal regeneration(Qin et al., 2013), exhibited increased activity, suggesting its involvement in

injury-induced neuronal plasticity. Also, Nr3c1 (glucocorticoid receptor), Fosb, and Esrra displayed robust regulon activity enhancement. Nr3c1, a key mediator of stress responses(Hong et al., 2015), has been implicated in neuropathic pain and pruritus, indicating its potential role in chronic itch mechanisms. Fosb, a well-known immediate early gene, is a critical regulator of activity-dependent neuronal plasticity, and its increased activity suggests persistent neuronal activation in the Inf-specific cluster. Esrra, an orphan nuclear receptor, has been associated with metabolic adaptation in neurons(Xie et al., 2022) and is linked to chronic pain and itch pathways. In addition to these factors, Runx1, Runx3, and Tead1 were identified as key regulators with increased activity. Runx1 is essential for the differentiation of nociceptive neurons, and its upregulation in the Inf-specific cluster suggests a potential role in chronic itch transmission. Similarly, Runx3, a critical determinant of sensory neuron subtype identity, exhibited increased activity, highlighting its potential contribution to neuron subtype-specific plasticity. Tead1, a downstream effector of the Hippo signaling pathway, has been implicated in neuronal survival and regeneration(Sahu & Mondal, 2021), indicating a potential role in the adaptive response of pruriceptive neurons.

Cluster-specific regulon analysis provided additional insights. Sox11 was particularly elevated in Inf-specific-NP1 and Inf-specific-NP2, suggesting its involvement in neuronal differentiation and plasticity, given its role for neuropathic pain (Ma et al., 2011; K. Wang et al., 2021; Xiao et al., 2002). Irf2 exhibited heightened activity specifically in Inf-specific-NP1, suggesting its involvement in neuroimmune interaction in chronic inflammatory skin dieases(Barragán-Iglesias et al., 2020; Gao et al., 2012; Ray et al., 2023). Meanwhile, Irf6 was prominently enriched in Inf-specific-CGRP-alpha, which suggests its role in chronic pruritus(Donnelly et al., 2020). Hmga2, chromatin-associated proteins that play a pivotal role in activating the transcription of several key inflammatory and immune-related genes(Barrette et al., 2010), displayed pronounced activity in Inf-specific-NP3, supporting its role in transcriptional reprogramming and chronic sensitization.

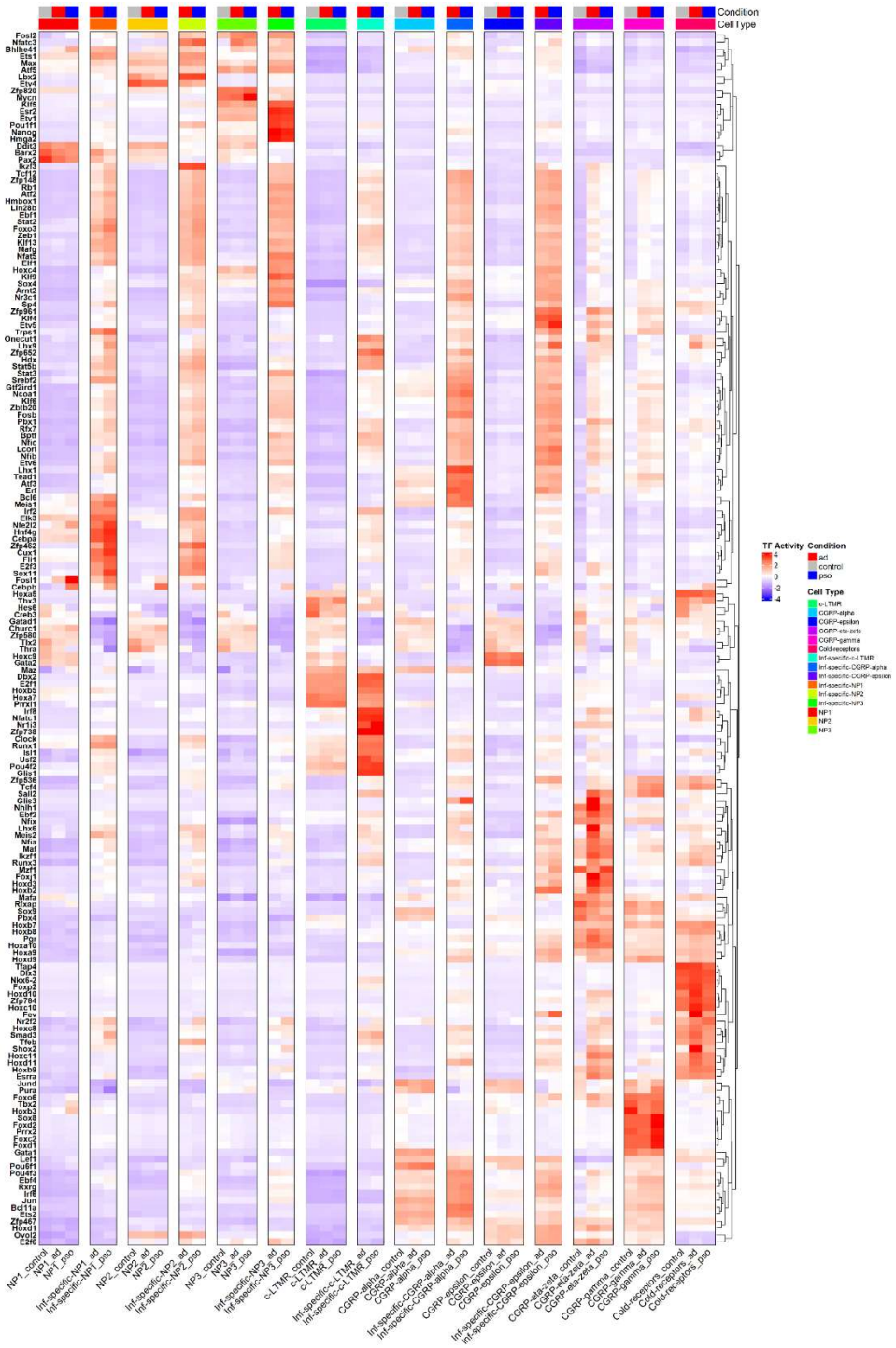

Figure 14. Transcription Factor Activity in Sensory Neurons Across Conditions. Heatmap depicting regulon activity across sensory neuron subclusters under control, AD, PSO conditions. Columns represent individual neuron subclusters, with Inf-specific neurons analyzed separately. Rows represent the union of transcription factors from the top 20 differentially active regulons per cluster, identified using FindMarkers on regulon activity scores. The color scale indicates Z-scored regulon activity. Top annotations indicate condition categories (*control* = gray, *AD* = red, *PSO* = blue) and neuron subtypes.

Building upon the overall transcriptional landscape, we specifically examined TFs implicated in chronic neuronal sensitization and found a consistent pattern reinforcing our previous findings (Figure 15). Regulons associated with neuroinflammation and sensitization, including those containing *Nfkb*, *Rel*, *Jun*, and *Fos*, exhibited increased activity in Inf-specific clusters, irrespective of AD or PSO conditions. Among them, *Rela* and *Relb* displayed differential activity between AD and PSO, with higher activation in Inf-specific NP1, NP2, and NP3 subsets of PSO compared to AD. Additionally, Inf-specific NP1 in PSO exhibited a general trend toward higher regulon activity relative to AD.

TFs associated with neuronal activity and plasticity also showed increased activity within Inf-specific clusters in both AD and PSO conditions. Notably, *Creb1*, a key regulator of neuronal plasticity, was particularly prominent. In contrast, *Egr4*, a transcription factor involved in activity-dependent neuronal gene expression, exhibited a condition-specific pattern: in AD, its activity did not increase in Inf-specific clusters, whereas in PSO, it was strongly upregulated in Inf-specific NP2.

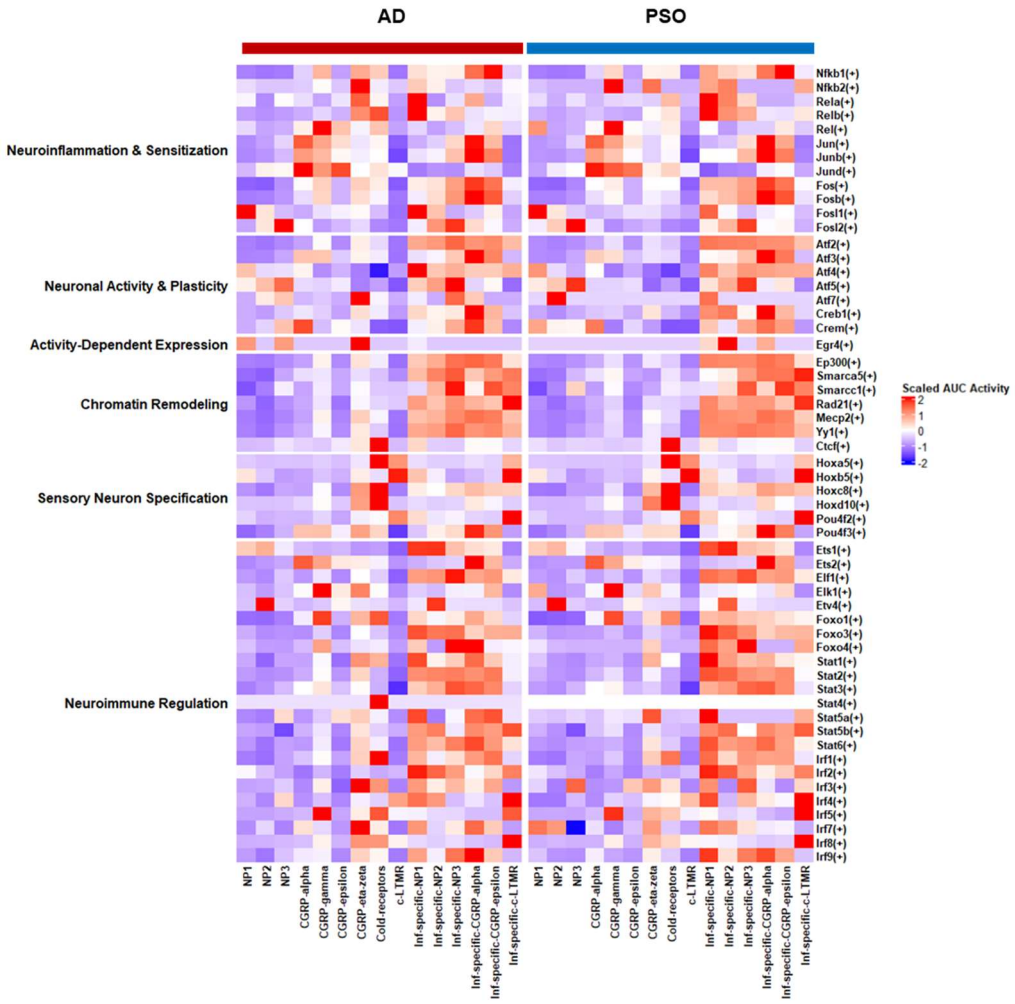

Figure 15. Transcription Factor Activity in Sensory Neurons Across Conditions for selected Transcription factors. Heatmap depicting regulon activity of key regulons categorized into functional groups, including Neuroinflammation & Sensitization, Neuronal Activity & Plasticity, Activity-Dependent Expression, Chromatin Remodeling, Sensory Neuron Specification, and Neuroimmune Regulation. Columns represent neuronal clusters, Inf-specific clusters. The color scale indicates relative regulon activity (red: high, blue: low).

For neuroimmune regulation, *Irf1* and *Irf2* showed higher regulon activity in Inf-specific clusters of PSO compared to AD, suggesting a potential role in PSO-specific sensory neuron adaptation. Further analysis of STAT family transcription factors revealed a significant increase in the regulon activity of *Stat3*, *Stat6*, and *Stat5b*, all of which are key mediators of Th2 inflammation and chronic pruritus, particularly through *Il4*, *Il13*, and *Il31* signaling. Notably, *Stat3* exhibited the highest activity in Inf-specific NP3, aligning with its established role as a downstream effector of Il31 signaling (Figure 16). In parallel, we identified selective upregulation of *Rfx1*, *Rfx3*, and *Rfx7* regulon activity in inflammation-enriched neuronal clusters, with corresponding increases in transcript expression (Figure 17). Functional enrichment of RFX target genes highlighted a prominent association with chromatin remodeling pathways, including histone modification and chromatin assembly, as well as neuron projection development, and glutaminergic synaptic transmission. These findings suggest that, in addition to canonical immune mediators such as IRFs and STATs, RFX family transcription factors may contribute to inflammation-induced transcriptional reprogramming in peripheral sensory neurons via epigenetic regulation.

Furthermore, regulons associated with chromatin remodeling displayed a uniform increase in activity within Inf-specific clusters, particularly for *Ep300*, *Smarca5*, *Smarcc1*, *Mecp2*, and *Yy1*. Given these findings, we further examined chromatin remodeling-associated regulons (Figure 17), revealing key factors linked to histone modifications, nucleosome remodeling, and higher-order chromatin architecture.

Among these, histone acetylation regulators exhibited heightened activity, with *Ep300*, a histone acetyltransferase (HAT) essential for enhancer activation and transcriptional plasticity(Yang & Hansen, 2024), showing significant upregulation. This suggests that Ep300-mediated histone acetylation may facilitate sensory neuron-specific transcriptional programs, contributing to the transition toward a pruriceptive state.

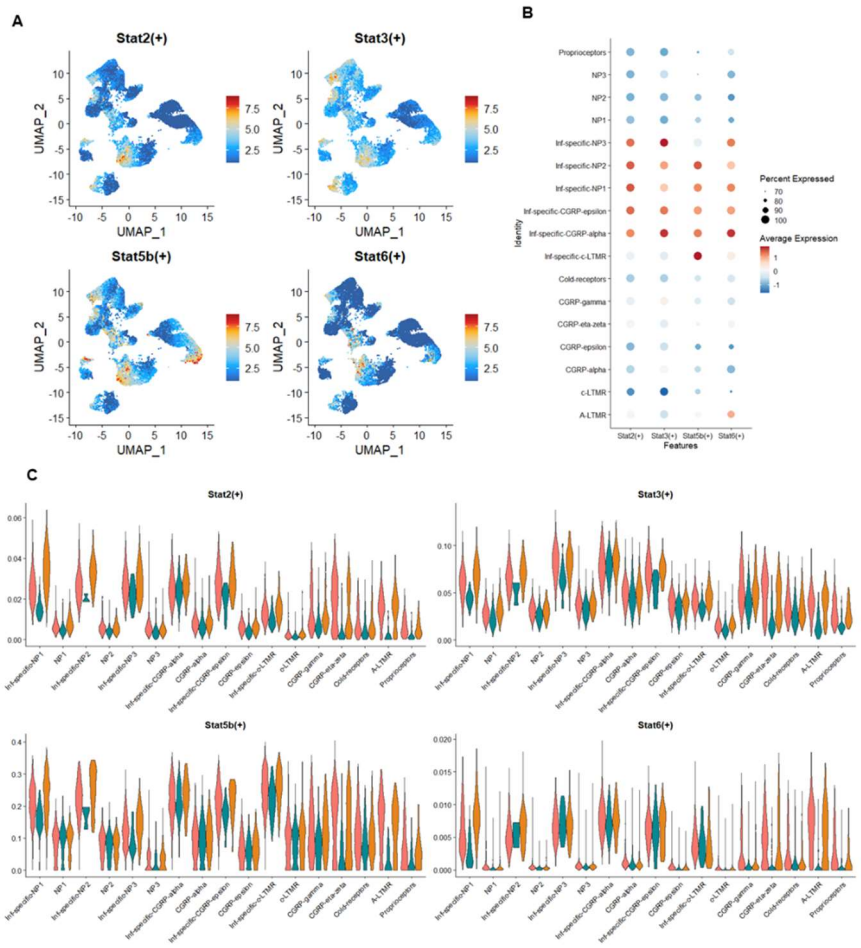

Figure 16. STAT family transcription factors exhibit distinct activity patterns in DRG sensory neuron clusters. (A) UMAP feature plots showing the regulon activity (AUC scores) of Stat2, Stat3, Stat5b, and Stat6 across DRG sensory neuron populations. Warmer colors (red) indicate higher regulon activity, while cooler colors (blue) represent lower activity. (B) Dot plot displaying the percentage of cells expressing Stat2, Stat3, Stat5b, and Stat6 across neuronal clusters, including Inf-specific subsets. The dot size represents the proportion of cells expressing each transcription factor, while the color scale indicates average expression levels. (C) Violin plots illustrating the distribution of Stat2, Stat3, Stat5b, and Stat6 regulon activity across neuronal clusters separating conditions.

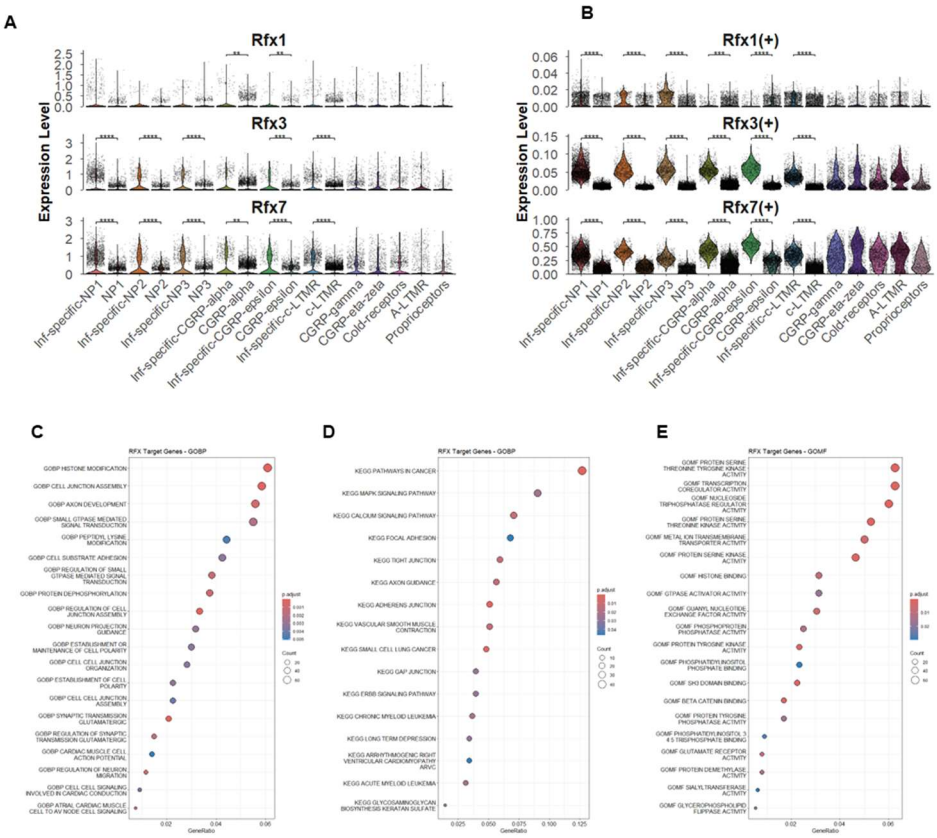

Figure 17. Inflammation-specific upregulation of RFX transcription factor activity in sensory neurons and its association with chromatin remodeling. (A) Expression levels of Rfx1, Rfx3, and Rfx7 across DRG sensory neuron subtypes. (B) Regulon activity scores of RFX1(+), RFX3(+), and RFX7(+) regulons demonstrate increased transcriptional activity specifically in inf-specific neuron clusters. (C–E) Functional enrichment analysis of RFX target genes. (C) GO:BP terms highlight significant enrichment in chromatin remodeling–associated pathways, including histone modification and chromatin assembly. (D) KEGG pathway analysis reveals association with cytokine signaling, cell adhesion, and inflammatory cascades. (E) GO:MF terms indicate regulatory roles of RFX targets in transcription factor binding, DNA interaction, and chromatin regulatory complexes.

Key chromatin remodelers also demonstrated increased regulon activity. *Smarca5*, a member of the ISWI chromatin remodeling complex, and *Smarcc1*, a core component of the SWI/SNF (BAF) complex, were both upregulated, suggesting a shift in nucleosome positioning and enhancer accessibility, potentially priming sensory neurons for persistent transcriptional changes associated with chronic itch. Additionally, *Rad21*, a cohesin complex component responsible for chromatin looping and three-dimensional genome organization, exhibited increased activity, indicating that epigenetic reprogramming extends beyond local histone modifications to higher-order chromatin architecture, possibly reinforcing enhancer-promoter interactions sustaining chronic neuronal sensitization.

DNA methylation-associated factors also demonstrated increased activity. *Mecp2*, a well-established reader of DNA methylation and a regulator of neuronal gene repression and activation, exhibited enhanced regulon activity within pruriceptive subsets. Given its dual role, *Mecp2* may contribute to transcriptional reprogramming by selectively repressing pain-inhibitory genes while promoting pro-pruritic gene expression.

Among zinc finger transcription factors, *Zbtb7a* and *Yy1* were significantly upregulated. *Zbtb7a* functions as a chromatin repressor by recruiting histone deacetylases (HDACs), potentially restricting alternative sensory neuron fates while reinforcing pruriceptive transcriptional states. Meanwhile, *Yy1*, known for its interaction with Polycomb group proteins, exhibited strong activity, suggesting a role for Polycomb-mediated transcriptional repression in stabilizing chronic pruritus-associated neuronal states.

Finally, *Ebf1*, a pioneer transcription factor capable of binding closed chromatin and facilitating enhancer activation, exhibited one of the most pronounced increases in regulon activity. Given its role in neuronal identity specification, the heightened activity of Ebf1 strongly suggests its involvement in sensory neuron lineage plasticity and pruriceptive state maintenance. Notably, *Ebf1* collaborates with chromatin remodelers such as *Smarca5* and *Smarcc1(Zolotarev et al., 2022)*, further supporting the hypothesis that pruriceptive DRG

neurons undergo a coordinated epigenetic reprogramming process to sustain their hyperexcitable state.

Together, these findings highlight an intricate regulatory network driving transcriptional and epigenetic reprogramming in chronic pruritus, reinforcing the role of neuronal plasticity, immune signaling, and chromatin remodeling in maintaining sensory neuron sensitization.

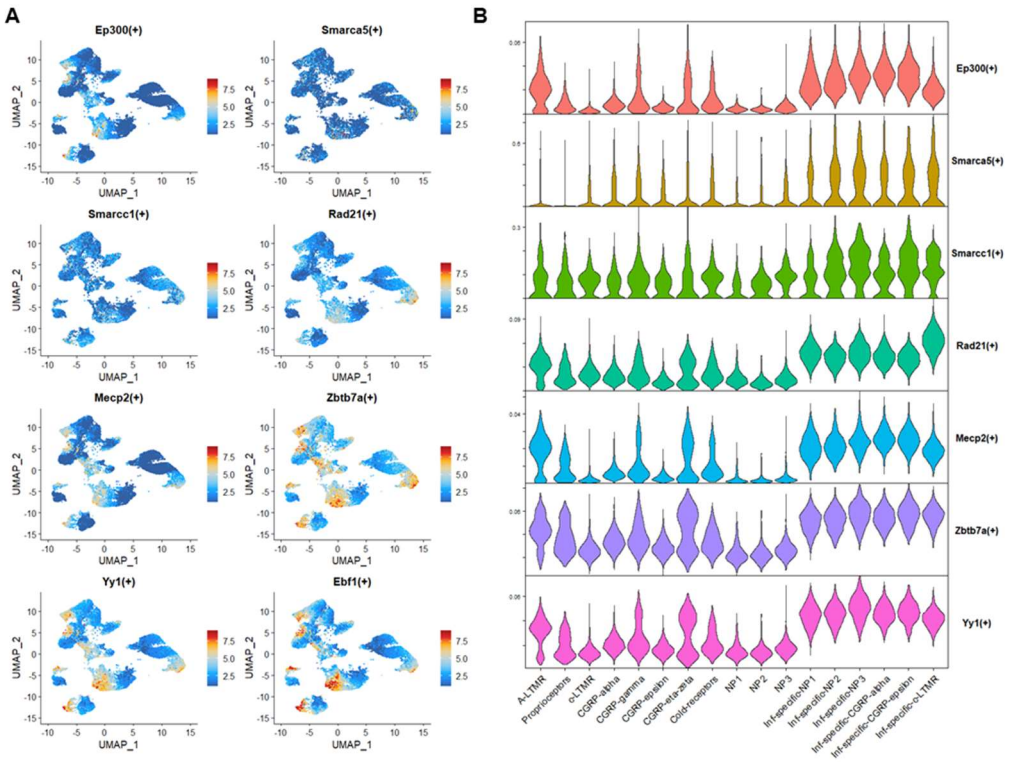

Figure 178. Chromatin remodeling-associated regulons exhibit distinct activity patterns in DRG sensory neuron subsets. (A) UMAP feature plots depicting the regulon activity (AUC scores) of chromatin remodeling-associated transcription factors, including Ep300, Smarca5, Smarcc1, Rad21, Mecp2, Zbtb7a, Yy1, and Ebf1, across DRG sensory neuron populations. Warmer colors (red) indicate higher regulon activity, while cooler colors (blue) represent lower activity. (B) Violin plots illustrating the distribution of regulon activity across neuronal subtypes, including A-LTMR, proprioceptors, cNILs, CGRP-expressing neurons, NP1, NP2, NP3, and Inf-specific subsets. Notably, certain regulons, such as Ep300 and Smarca5, exhibit broad activation, while others, like Yy1 and Ebf1, show distinct enrichment patterns in specific neuronal populations. These results suggest a transcriptional reprogramming of chromatin regulators in Inf-specific neurons.

3.4. Trajectory Inference Suggests Inf-Specific Clusters originate from original neuron clusters

To investigate whether Inf-specific neuron clusters undergo transcriptional conversion from their original neuronal counterparts, we performed pseudotime trajectory analysis using Monocle3 (Figure 18). Clustering results from Monocle3 were consistent with those from Seurat, confirming that Inf-specific clusters and original clusters were assigned to distinct transcriptional states (Figure 18A, 18B, 18C). Furthermore, unsupervised partitioning revealed five major neuronal groups: PEP and large-diameter mechanosensors (A-LTMR, Proprioceptors), NP1, NP2, NP3, and C-LTMR (Figure 18D). Notably, within each of these partitions, Inf-specific and original clusters were co-localized, suggesting that despite transcriptional reprogramming, the fundamental neuronal identity of these subclusters remains largely preserved.

Trajectory inference analysis demonstrated transcriptional state transitions within each partition, with Inf-specific clusters generally connected to their original neuronal counterparts via a single trajectory (Figure 18E). Pseudotime analysis of NP1, NP2, NP3, and C-LTMR partitions revealed transcriptional state conversion from original clusters toward Inf-specific clusters (Figure 19A, 19B, 19C, 19D). Furthermore, expression analysis of key regulatory genes previously identified as upregulated in Inf-specific clusters (*Ebf1*, *Ep300*, *Stat3*, and *Stat6*) showed a significant increase along the inferred trajectory, further supporting the transcriptional reprogramming hypothesis.

In contrast, PEP and large-diameter mechanosensory neurons exhibited more heterogeneous subcluster compositions, suggesting that transcriptional state transitions within these populations are more variable and less constrained to a single trajectory.

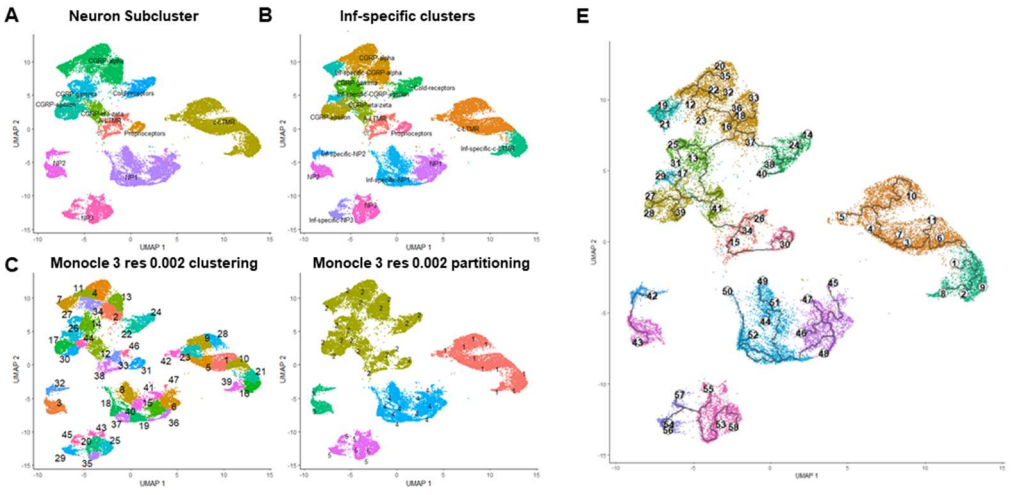

Figure 189. Clustering and partitioning of DRG sensory neurons in chronic itch conditions using Seurat and Monocle 3. (A) UMAP visualization of neuron subclusters identified using Seurat in the DRG sensory neuron dataset. Major neuronal subtypes are labeled. (B) UMAP representation highlighting Inf-specific clusters identified using Seurat. (C) Clustering of DRG sensory neurons using Monocle 3 at a resolution of 0.002, showing finer subcluster differentiation. (D) Monocle 3 partitions at resolution 0.002, demonstrating global organization of neuronal subsets. (1 : c-LTMR, 2 : CGRP (Peptidergic), 3 : NP2, 4 : NP1, 5 : NP3) (E) Trajectory graph of DRG neurons, with nodes and edges overlaid to indicate potential trajectory relationships between subpopulations.

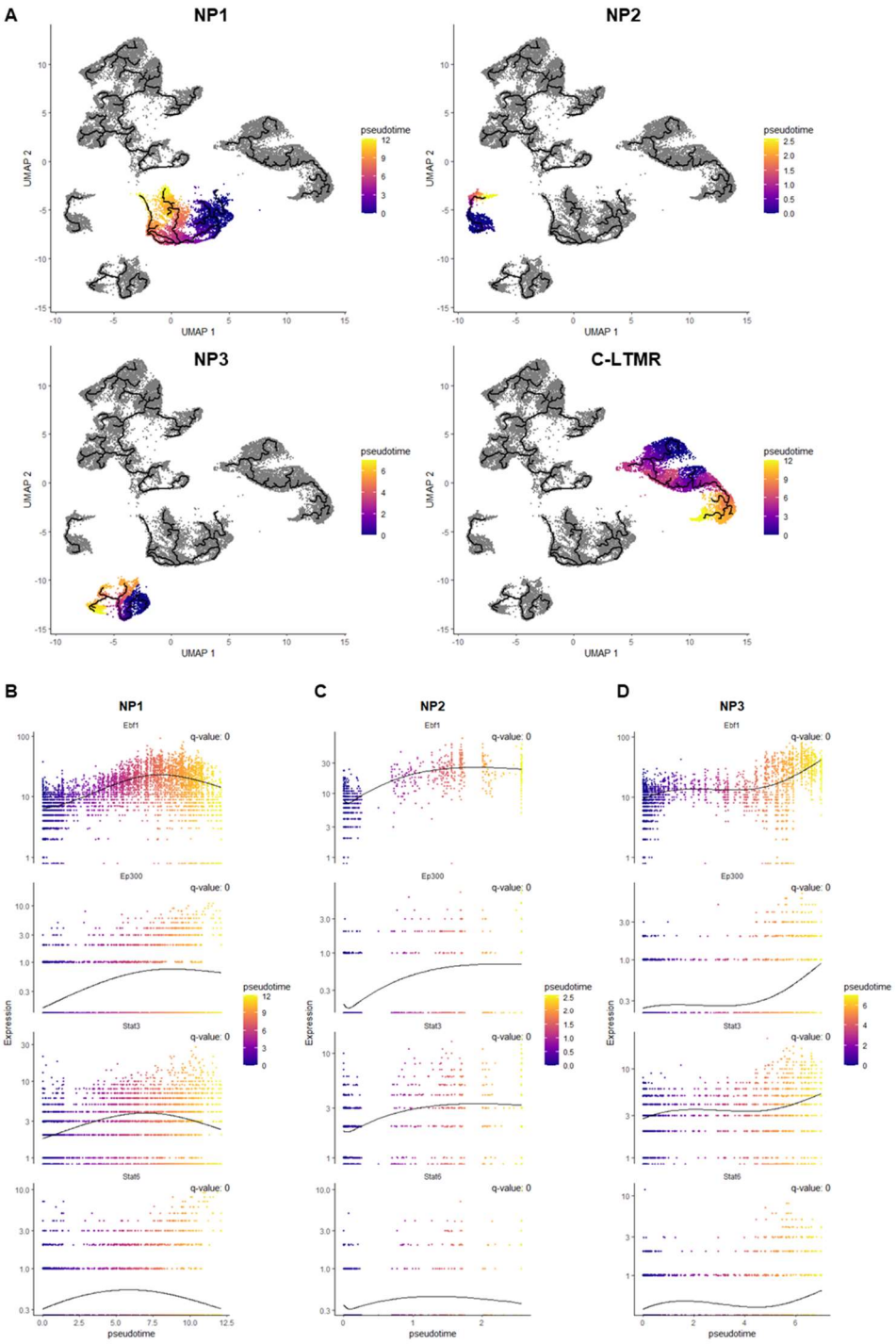

Figure 20. Pseudotime trajectory and gene expression dynamics in Inf-specific NP1, NP2, NP3, and C-LTMR sensory neuron subsets. (A) UMAP projection of single-cell transcriptomes showing pseudotime trajectory inference for NP1, NP2, NP3, and C-LTMR neuronal subsets. Cells are color-coded based on their pseudotime progression, ranging from early (dark blue) to late (yellow), indicating a potential transition from the original neuronal state to Inf-specific clusters. (B-D) Pseudotime-dependent expression dynamics of Ebf1, Ep300, Stat3, and Stat5 in NP1 (B), NP2 (C), and NP3 (D). Each dot represents a single cell, with expression levels plotted along the pseudotime axis. Color gradient corresponds to pseudotime progression. The black curve represents a smoothed trend line. Q-values indicate statistical significance for gene expression changes along pseudotime.

To validate the pseudotime trajectory analysis, we employed scVelo to assess RNA velocity, which estimates differentiation trajectories based on the ratio of spliced to unspliced transcripts (Figure 20). Inf-specific clusters exhibited a higher proportion of spliced transcripts compared to original clusters (Figure 20A), suggesting a transition in transcriptional state toward a more stabilized gene expression program. This shift suggests a transition from dynamic transcriptional bursts to a more persistent state(La Manno et al., 2018), a phenomenon often observed in neurons undergoing long-term transcriptional reprogramming. Epigenetically, a higher spliced/unspliced ratio may reflect chromatin stabilization, where transcriptionally active loci remain accessible but are no longer undergoing de novo activation. Chromatin remodelers such as *Smarca5* and *Smarcc1*, along with the pioneer transcription factor *Ebf1*, likely contribute to this stabilization. Furthermore, Ep300-mediated histone acetylation may reinforce transcriptional stabilization, ensuring sustained expression of key regulatory genes critical for pruritic and inflammatory responses.

Consistently, RNA velocity analysis revealed a markedly higher velocity length in Inf-specific clusters compared to original clusters (Figure 20B). UMAP projection of the

computed RNA velocity demonstrated a transcriptional state transition aligning with the pseudotime trajectory inferred from Monocle 3, with transcriptional shifts directed toward the Inf-specific cluster (Figure 20C). The elevated RNA velocity in these clusters suggests a robust transcriptional state transition, reinforcing the notion that these neurons are undergoing active reprogramming rather than maintaining a static identity.

Unlike proliferating or differentiating cells, DRG neurons retain their lineage identity but can transition between distinct functional states in response to external stimuli, such as inflammation, chronic injury, or pruritic conditions. The increased velocity length observed in Inf-specific clusters suggests that these neurons are undergoing a pronounced shift in transcriptional programs, transitioning from a baseline state to a maladaptive, hyperexcitable phenotype characteristic of chronic pruritus. This transition likely involves extensive remodeling of gene regulatory networks governing neuronal excitability, synaptic plasticity, and neuroimmune interactions.

Taken together, the concurrent increase in the spliced/unspliced transcript ratio and RNA velocity suggests that DRG neurons in Inf-specific clusters are actively remodeling their transcriptional landscape in response to persistent inflammatory stimuli.

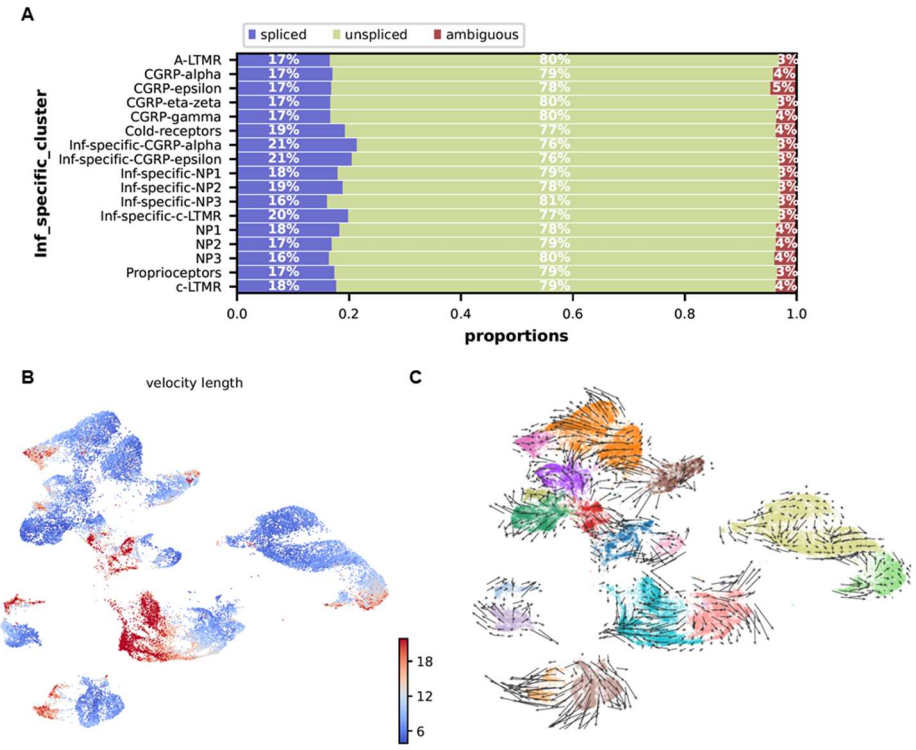

Figure 191. RNA velocity analysis reveals transcriptional state transitions from original clusters to Inf-specific neuron clusters. (A) Proportions of spliced, unspliced, and ambiguous mRNA fractions across different neuronal subsets, including Inf-specific clusters and original clusters. The majority of transcripts are classified as unspliced (green), indicating active transcription, with varying proportions of spliced (blue) and ambiguous (red) reads. (B) RNA velocity length projected onto the UMAP embedding of DRG neurons. Cells with higher velocity magnitudes (red) indicate stronger transcriptional activity and potential transcriptional conversion, while lower velocity magnitudes (blue) suggest a more stable transcriptional state. (C) RNA velocity streamlines overlaid onto the UMAP of DRG neurons. Arrows represent the predicted transcriptional trajectories, showing directional flows between neuronal clusters. Inf-specific clusters exhibit clear directional transitions from their original neuronal states, supporting a transcriptional conversion process.

3.5. Epigenome data inferred transcription factor activity reveals differential regulatory dynamics across stimulations, with enrichment of Ebf1 in AD conditions

To investigate the epigenomic regulatory landscape underlying the transcriptional state conversion of Inf-specific neurons observed in scRNA-seq of DRG neurons, we performed ATAC-seq on DRG neurons from the same groups as the scRNA-seq dataset, including MC903, SAV8, and HDM (AD mouse models) as well as PSO (psoriasis mouse model).

ATAC-seq libraries were assessed for quality and complexity using PEPATAC, confirming high data quality across all samples. Sequencing yielded ~87-89 million raw paired-end reads per sample, with high retention post-trimming (~99%). Library complexity was well maintained, as indicated by NRF (~0.8), PBC1 (~0.89), and PBC2 (~9.2-9.4), ensuring minimal duplication and optimal nucleosome-free fragment recovery. TSS enrichment scores (~9.6-9.7) confirmed strong transcriptional accessibility, while FRiP values (~0.52-0.54) indicated a high proportion of reads mapping to regulatory elements. These results confirm the successful generation of high-quality ATAC-seq data, enabling robust downstream analysis of chromatin accessibility and transcription factor activity across conditions.

To investigate the epigenomic changes underlying transcriptional state conversion in DRG neurons following MC903 stimulation, ATAC-seq was first analyzed in the MC903 group. A consensus peak set was generated using an iterative peak merging approach(Corces et al., 2018), ensuring robust identification of accessible chromatin regions. To assess differential chromatin accessibility, DiffBind was performed using the EdgeR method, optimizing sensitivity for detecting differentially accessible regions (DARs). This analysis identified 14,995 peaks with increased accessibility and 10,832 peaks with decreased accessibility in MC903 compared to control (Figure 21).

To further delineate the regulatory landscape, distal intergenic (DI) and promoter-associated peaks (TSS ±3 kb) were separately analyzed. In the DI regions, 4,085 peaks exhibited increased accessibility, whereas 2,140 peaks showed decreased accessibility. In contrast, promoter regions demonstrated an opposite trend, with 4,728 peaks exhibiting decreased accessibility and only 1,502 peaks showing increased accessibility. Log2-normalized read counts confirmed these patterns, showing global accessibility increases in DI regions upon MC903 stimulation, while promoter regions exhibited no significant differences between MC903 and control (Figure 21A, 21B).

To determine the genomic distribution of significantly altered peaks, annotation of differentially accessible peaks was performed (Figure 21C, 21D). Among increased peaks, distal intergenic regions (26.77%) and intronic regions (47.4%, including 1st intron: 17.87% and other introns: 29.53%) accounted for the majority, indicating that putative enhancer elements represented over 50% of the upregulated regions(Carullo et al., 2020). In contrast, promoters dominated among the decreased peaks (59.7%), suggesting that enhancer accessibility is predominantly increased, whereas promoter accessibility is reduced upon MC903 stimulation. These findings suggest that enhancer-driven regulatory changes play a key role in DRG neuronal transcriptional reprogramming in response to pruritic stimulation.

To identify transcription factors potentially governing these accessibility changes, Homer *de novo* motif enrichment analysis was conducted on increased DI and promoter peaks (Figure 21E). Notably, Ebf-related motifs were the second most enriched in DI peaks with increased accessibility, suggesting a role for Ebf1 in enhancer-mediated transcriptional regulation following MC903 stimulation. Intriguingly, Ebf1 motifs were the top enriched motifs in promoter peaks with increased accessibility, whereas no Ebf1 motif enrichment was detected in DI or promoter peaks with decreased accessibility. These results indicate that Ebf1 may act as a key transcription factor driving enhancer activation in DRG neurons in response to chronic itch stimulation.

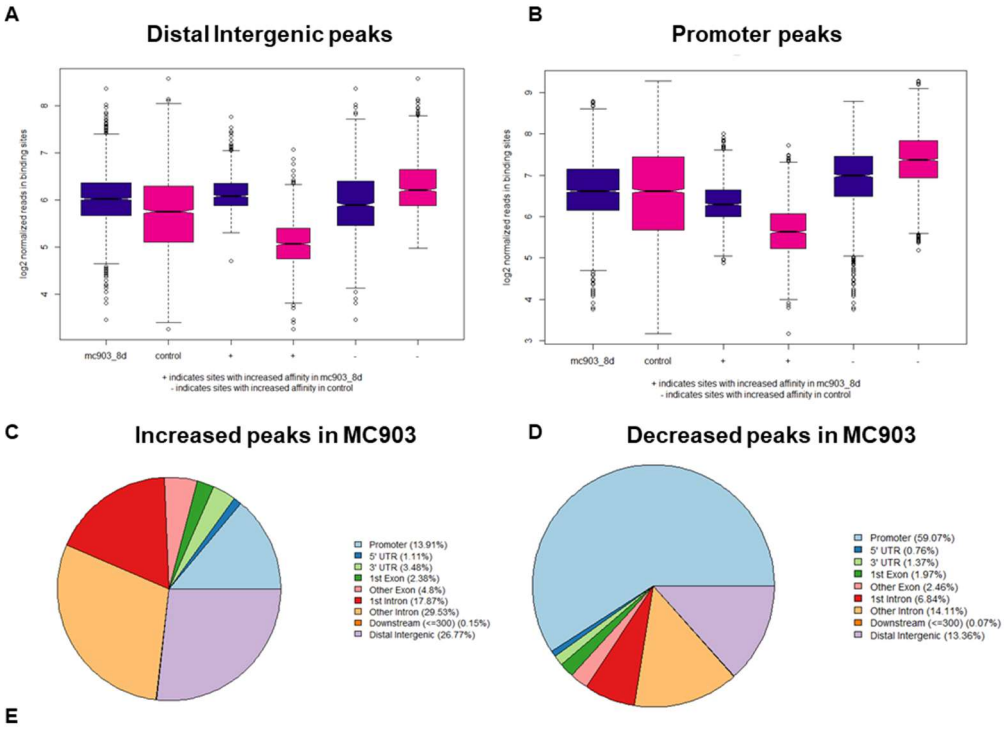

E

Rank	Motif	P-value	log P-pvalue	% of Targets	% of Background	STD(Bg STD)	Best Match/Details
1		1e-290	-6.689e+02	29.62%	9.38%	54.2bp (69.4bp)	Isl1/MA1608.1/Jaspar(0.965) More Information | Similar Motifs Found
2		1e-226	-5.226e+02	26.41%	9.05%	55.8bp (61.2bp)	EBF2(EBF)/BrownAdipose-EBF2-ChIP-Seq(GSE97114)/Homer(0.950) More Information | Similar Motifs Found
3		1e-139	-3.216e+02	21.37%	8.50%	52.3bp (68.5bp)	ISL2/MA0914.1/Jaspar(0.930) More Information | Similar Motifs Found
4		1e-76	-1.750e+02	5.61%	1.24%	52.1bp (65.1bp)	Six1(Homeobox)/Myoblast-Six1-ChIP-Chip(GSE20150)/Homer(0.976) More Information | Similar Motifs Found
5		1e-67	-1.552e+02	69.08%	55.77%	52.7bp (69.6bp)	PB0099.1_Zfp691_1/Jaspar(0.768) More Information | Similar Motifs Found
6		1e-61	-1.418e+02	12.71%	5.75%	51.0bp (66.6bp)	Fra1(bZIP)/BT549-Fra1-ChIP-Seq(GSE46166)/Homer(0.971) More Information | Similar Motifs Found
7		1e-52	-1.200e+02	58.36%	46.43%	53.8bp (68.5bp)	POL010.1_DCE_S_III/Jaspar(0.696) More Information | Similar Motifs Found
8		1e-47	-1.092e+02	2.20%	0.29%	47.1bp (64.5bp)	CTCF/MA0139.1/Jaspar(0.856) More Information | Similar Motifs Found
9		1e-45	-1.050e+02	20.24%	12.34%	52.9bp (69.2bp)	Tlx?(NR)/NPC-H3K4me1-ChIP-Seq(GSE16256)/Homer(0.845) More Information | Similar Motifs Found
10		1e-43	-1.003e+02	8.59%	3.77%	55.0bp (68.8bp)	Atf2(bZIP)/3T3L1-Atf2-ChIP-Seq(GSE56872)/Homer(0.961) More Information | Similar Motifs Found

Figure 202. Epigenomic profiling of distal intergenic and promoter peaks in MC903-treated DRG neurons. (A-B) Boxplots showing log2-normalized read counts for distal intergenic peaks (A) and promoter peaks (B) in MC903-treated (mc903_8d) and control DRG neurons. Sites with increased chromatin accessibility in MC903_8d are indicated in pink, while sites with increased affinity in control are shown in blue. (C-D) Genomic

distribution of distal intergenic (C) and promoter peaks (D). The percentage of peaks overlapping with different genomic features (e.g., promoter, UTRs, exons, introns, and distal intergenic regions) is shown in the pie charts. (E) Homer *de novo* motif enrichment analysis of significanly increased distal intergenic peaks in MC903 condition. The table displays the top-ranked motifs enriched in distal intergenic peaks, along with associated transcription factors, p-values, percentage of target sites, and best match details.

To examine the TF accessibility landscape in MC903-stimulated DRG neurons, diffTF analysis was performed to identify TFs that exhibit condition-specific activation or repression (Figure 22). This analysis revealed that COE1 (Ebf1) displayed the most statistically significant activation in MC903 compared to all other TFs (Figure 22A).

Integrative analysis incorporating bulk RNA-seq of MC903-treated DRG neurons further demonstrated that Ebf1 expression was positively correlated with chromatin accessibility (Figure 22B). Among all TFs, Ebf1 exhibited the second strongest correlation between RNA expression and chromatin accessibility, supporting its role as a transcriptional activator in MC903-stimulated neurons.

To determine whether Ebf1 activation was specific to MC903 or extended to other inflammatory conditions, diffTF analysis was conducted across additional ATAC-seq datasets from PSO, SAV8, and HDM mouse models (Figure 22C). Interestingly, while Ebf1 activation in PSO reached statistical significance (adjusted p-value < 0.0001), its log2FC was notably lower compared to AD models (log2FC: MC903 = 0.188, SAV8 = 0.18, HDM = 0.125, PSO = 0.088; adjusted p-value < 0.001 for all conditions). These findings align with previous DRG neuron scRNA-seq results, where Inf-specific neuron clusters were predominantly enriched in AD models (MC903, SAV8, HDM) compared to PSO, except for Inf-specific NP1 (Figure 6). This suggests that Ebf1-driven transcriptional reprogramming is more pronounced in AD-like chronic cutaneous inflammatory stimulation.

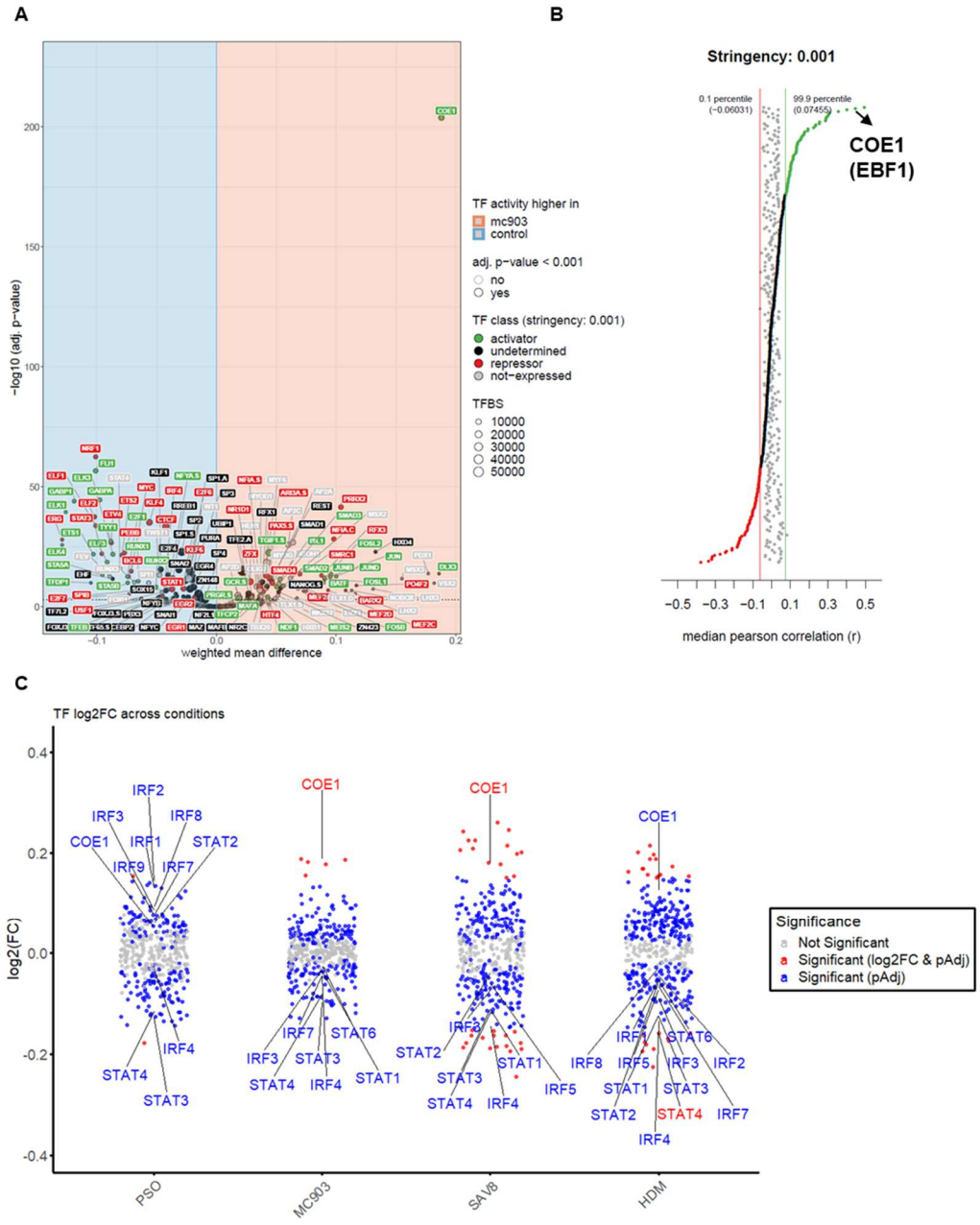

Figure 213. diffTF analysis of transcription factor activity identifies COE1 (Ebf1) as a significantly activated regulator in AD mouse models. (A) Volcano plot showing

differentially active TFs between MC903-treated and control conditions. The x-axis represents the weighted mean difference in TF activity, while the y-axis shows statistical significance. TFs with significantly increased activity in MC903-treated samples are highlighted in red, while those enriched in controls are in blue. The size of the dots represents the number of transcription factor binding sites (TFBS). (B) Diagnostic plots displaying the distribution of median Pearson correlations for TF activity across samples, ordered from bottom (lowest) to top (highest). The transcription factor *COE1 (EBF1)* is highlighted as a significantly enriched activator in MC903-treated conditions. (C) Strip plots describing distribution of Log2 fold-change (log2FC) of TF activity across different conditions (Psoriasis (PSO), MC903, SAV8, HDM). Transcription factors that are significantly upregulated (red) or significantly different based on adjusted p-values (blue) are labeled.

Additionally, PSO exhibited increased activation of the IRF transcription factor family compared to AD models, suggesting distinct regulatory mechanisms of DRG neurons underlying imiquimod induced psoriasis-like cutaneous inflammation. Notably, STAT3 and STAT6 showed reduced activation in AD models, which contrasts with previous DRG scRNA-seq findings, where STAT factors exhibited increased activity. This discrepancy is likely attributable to the inherent limitations of bulk ATAC-seq, as neuronal cluster composition varies across libraries, potentially diluting cell-type-specific regulatory signals. Despite these limitations, the data robustly demonstrate that Ebf1 is a top-ranking, significantly activated transcription factor in AD models, reinforcing its potential role in driving chronic pruritus-associated transcriptional reprogramming in DRG neurons.

To further validate the TF activation patterns identified via diffTF analysis, chromVAR analysis was independently conducted to assess TF activity dynamics across conditions (Figure 23). To ensure robustness, TF motif enrichment was analyzed using three distinct

motif databases—JASPAR 2022, HOCOMOCO v12, and HOMER—providing a comprehensive assessment of TF accessibility changes.

Principal component analysis (PCA) based on chromVAR-calculated deviation scores demonstrated clear separation among control, AD, and PSO groups (Figure 23A, 23B, 23C), reinforcing the distinct transcriptional regulatory landscapes associated with these conditions. Additionally, hierarchical clustering of the top 50 most variable TFs across conditions, identified through chromVAR, provided a global overview of TF activation patterns. Strikingly, across all three motif databases, Ebf1 exhibited the highest activity in MC903, followed by SAV8 and HDM, confirming its prominent activation in AD models.

Consistent with DRG neuron scRNA-seq findings, immediate early gene (IEG)-associated TFs, including FOS, JUN, and ATF3, displayed increased activity in MC903, suggesting rapid transcriptional responses to inflammatory stimuli. Moreover, TFs linked to neuronal plasticity, such as CREB, also showed elevated activation in MC903, indicating potential transcriptional remodeling of DRG neurons in response to chronic pruritic stimulation.

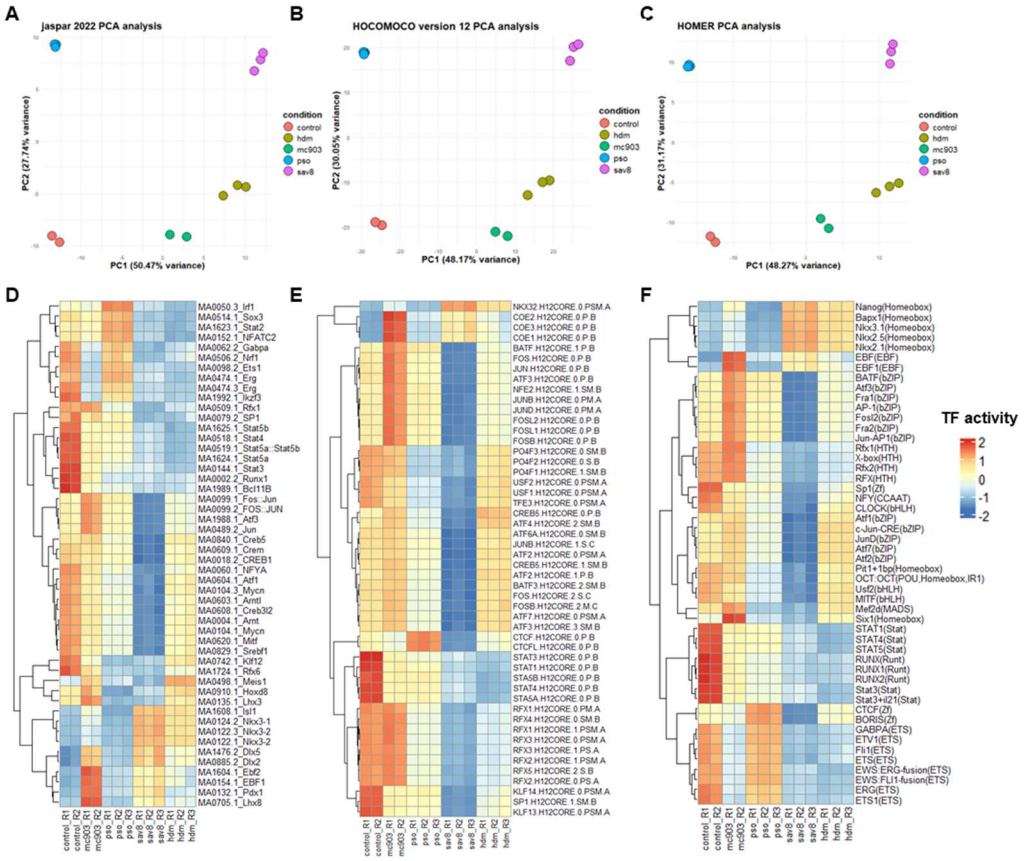

Figure 224. ChromVAR analysis identifies Ebf1 as a significantly activated transcription factor in AD mouse models. (A–C) Principal Component Analysis (PCA) plots of TF deviation scores computed using chromVAR with different motif databases: (A) JASPAR 2022, (B) HOCOMOCO version 12, and (C) HOMER. Each point represents a sample, and colors indicate different conditions (control, MC903, PSO, SAV8, HDM). The first two principal components (PC1 and PC2) are plotted, showing the variance explained by each axis. (D–F) Heatmaps displaying the top 50 most variable TFs based on chromatin accessibility variability scores for the same motif databases: (D) JASPAR 2022, (E) HOCOMOCO version 12, and (F) HOMER. TF accessibility scores are row-scaled (Z-score normalization). Samples are hierarchically clustered based on chromVAR deviation scores.

Expanding the analysis to TF binding events in bulk ATAC-seq data, TOBIAS footprinting analysis was applied using broad peak calling instead of motif-matched peak quantification (Figure 24). Unlike standard ATAC-seq peak calling, which predominantly captures narrow peaks, promoter regions often span broader regions and may be missed or fragmented. TOBIAS addresses this limitation by applying broad peak calling, enabling a more comprehensive assessment of TF occupancy, particularly in promoter regions.

In MC903, the representative chronic pruritus model, EBF1 exhibited statistically significant activation and ranked within the top 10 most activated TFs (Figure 24A). Examining broad peaks predicted to be bound by EBF1 revealed 998 peaks uniquely enriched in control conditions and 1,891 peaks uniquely bound in AD conditions (MC903, SAV8, and HDM) (Figure 24B). This substantial increase in EBF1 binding under AD conditions suggests its involvement in chromatin remodeling linked to chronic pruritic inflammation.

Functional annotation of the EBF1-bound peaks through GOBP enrichment analysis revealed an association with learning, regulation of synapse assembly, and neuron action potential in AD conditions (Figure 24C). These terms highlight long-term neuronal adaptations, synaptic remodeling, and excitability modulation, processes linked to DRG neuron sensitization in chronic itch.

These findings suggest that Ebf1 plays a central role in transcriptional reprogramming of DRG neurons in chronic pruritic conditions by driving enhancer-mediated regulatory changes. The increased chromatin accessibility at distal intergenic regions, coupled with enhanced Ebf1 binding and activation in AD models, points to a putative epigenetic mechanism underlying neuronal sensitization. This highlights enhancer-driven transcriptional regulation as a key process in chronic itch-associated neuroplasticity.

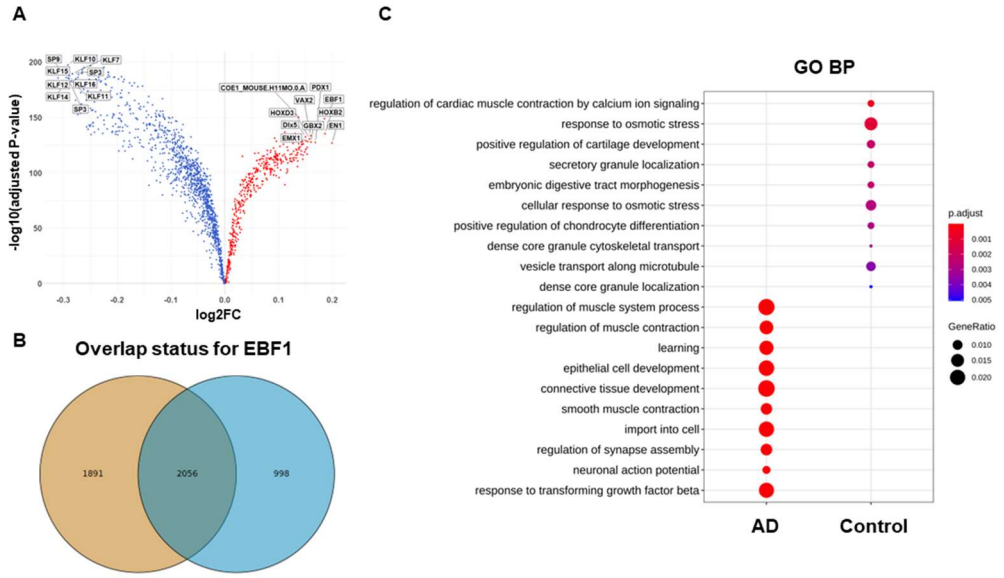

Figure 235. TOBIAS ATAC footprinting analysis identifies Ebf1 activation in AD mouse models. (A) Volcano plot displaying differentially bound transcription factors (TFs) identified through TOBIAS footprinting analysis in MC903 mouse models. The x-axis represents the log2 fold-change (log2FC) of TF binding activity, while the y-axis shows the statistical significance. Red dots indicate significantly upregulated TFs, and blue dots represent downregulated TFs (adjusted $P < 0.05$). (B) Venn diagram illustrating the overlap of differentially bound TF target genes between AD conditions (MC903, SAV8, and HDM) and controls. The overlapping region represents shared TF target genes, brown for unique binding genes for AD condition, and blue for control. (C) GO enrichment analysis of differentially bound TF target genes. The dot plot highlights significantly enriched biological processes (BP), with the size of dots representing the gene ratio (proportion of genes associated with each GO term) and the color scale indicating adjusted P-values. Larger dots indicate a higher number of associated genes.

3.6. Enhancers activated in MC903 show Ebf1 motif enrichment and regulate chronic pruritus-related genes

Bulk ATAC-seq analysis not only confirmed the increased transcription factor activity of EBF1 observed in scRNA-seq of DRG neurons but also revealed that MC903 stimulation preferentially enhanced accessibility at distal intergenic peaks over promoter regions. Notably, EBF1 motifs were among the most significantly enriched within these distal elements, suggesting a potential role in enhancer regulation. In epigenomic analyses, distal intergenic peaks are often considered putative enhancers, particularly when they exhibit hallmark chromatin features associated with enhancer activity, such as H3K4me1 and H3K27ac enrichment(Andersson & Sandelin, 2020).

To further investigate whether EBF1 contributes to enhancer remodeling under MC903 stimulation, we performed Cleavage Under Targets and Release Using Nuclease sequencing (CUT&RUN-seq) targeting H3K4me1 and H3K27ac in DRG neuron nuclei from the MC903 mouse model. This analysis allowed us to define active and primed enhancers, thereby providing deeper insights into how EBF1 influences the enhancer landscape in the context of chronic pruritus. Active and primed enhancers were systematically identified using H3K27ac and H3K4me1 CUT&RUN-seq in conjunction with ATAC-seq profiling.

Active enhancers were defined as genomic regions where H3K27ac CUT&RUN broad peaks overlapped with ATAC-seq narrow peaks within each condition. In contrast, primed enhancers were identified as H3K4me1-enriched regions that exhibited ATAC-seq accessibility but lacked H3K27ac, ensuring the exclusion of fully activated enhancers. To avoid promoter-associated elements, we removed peaks overlapping ±5 kb from the transcription start site (TSS). Finally, condition-specific and shared enhancers were merged to generate a consensus enhancer set (Figure 25A, 25B).

This analysis identified 38,337 active enhancers, including 9,207 Control-specific, 9,085 MC903-specific, and 20,045 shared enhancers. Similarly, we identified 48,181 primed enhancers, of which 14,202 were control-specific, 25,359 were MC903-specific, and 8,620 were shared between conditions. These numbers align with previous estimates of enhancer landscapes in sensory neurons, where 50,000–200,000 enhancers are predicted per neuronal subtype, the majority being intergenic or intronic regulatory elements (Gray et al., 2017; Kundaje et al., 2015; Malik et al., 2014; Moore et al., 2020; Palmisano et al., 2019).

The emergence of condition-specific enhancers in both control and MC903-treated DRG neurons suggests that chronic inflammatory stimulation in the skin can transmit signals to distant DRG neurons, leading to profound remodeling of the epigenomic enhancer landscape. Notably, while the number of condition-specific active enhancers was comparable between groups, MC903-specific primed enhancers were markedly more abundant. This imbalance suggests that MC903 stimulation not only induces enhancer activation but also establishes a broader priming effect, potentially preparing a subset of enhancers for future activation in response to sustained or additional stimuli(Malik et al., 2014; Marco et al., 2020) (Figure 25A, 25B).

Next, we applied chromVAR to the defined consensus active and primed enhancers (Figure 25C, 25D). Among all transcription factors, EBF1 exhibited one of the highest variability scores, suggesting a dominant role in shaping the enhancer landscape under chronic inflammatory conditions. Subsequently, we ranked the top 50 transcription factors by variability score and examined their deviation scores across active and primed enhancers (Figure 26A, 26B). Hierarchical ordering of these factors enabled a direct comparison of their activity between conditions. EBF1 displayed a striking increase in deviation scores in the MC903 condition, not only at active enhancers (Figure 26A) but also at primed enhancers (Figure 26B), suggesting that its regulatory influence extends beyond enhancer activation to the priming of regulatory elements. These findings position EBF1 as a central driver of enhancer-mediated transcriptional reprogramming in DRG neurons, potentially

linking inflammatory signaling in the skin to widespread epigenomic modifications in sensory circuits.

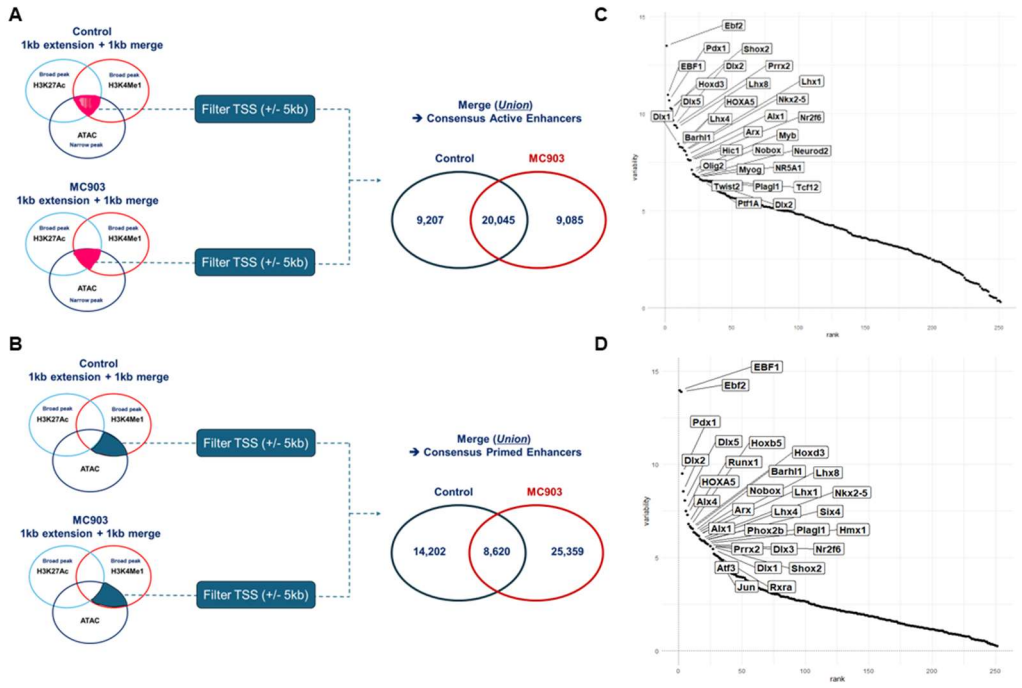

Figure 26. EBF1 is preferentially activated in active and primed enhancers of DRG neurons in the MC903 mouse model. Identification of consensus (A) active and (B) primed enhancers. Active enhancers were identified as regions exhibiting both ATAC-seq peaks and active enhancer-associated histone modifications (H3K27ac & H3K4me1 CUT&RUN peaks), while primed enhancers were defined by the overlap of ATAC-seq peaks with H3K4me1 CUT&RUN peaks only. Peaks were merged within each condition using a 1 kb extension and 1 kb merging window, followed by filtering to exclude transcription start site (TSS)-proximal regions (±5 kb). The Venn diagrams show the distribution of consensus active and primed enhancers. Transcription factor variability analysis with chromVAR in (C) active and (D) primed enhancers. Motif accessibility variability scores for TFs associated with active and primed enhancers. The rank plots display TFs with the highest variability scores.

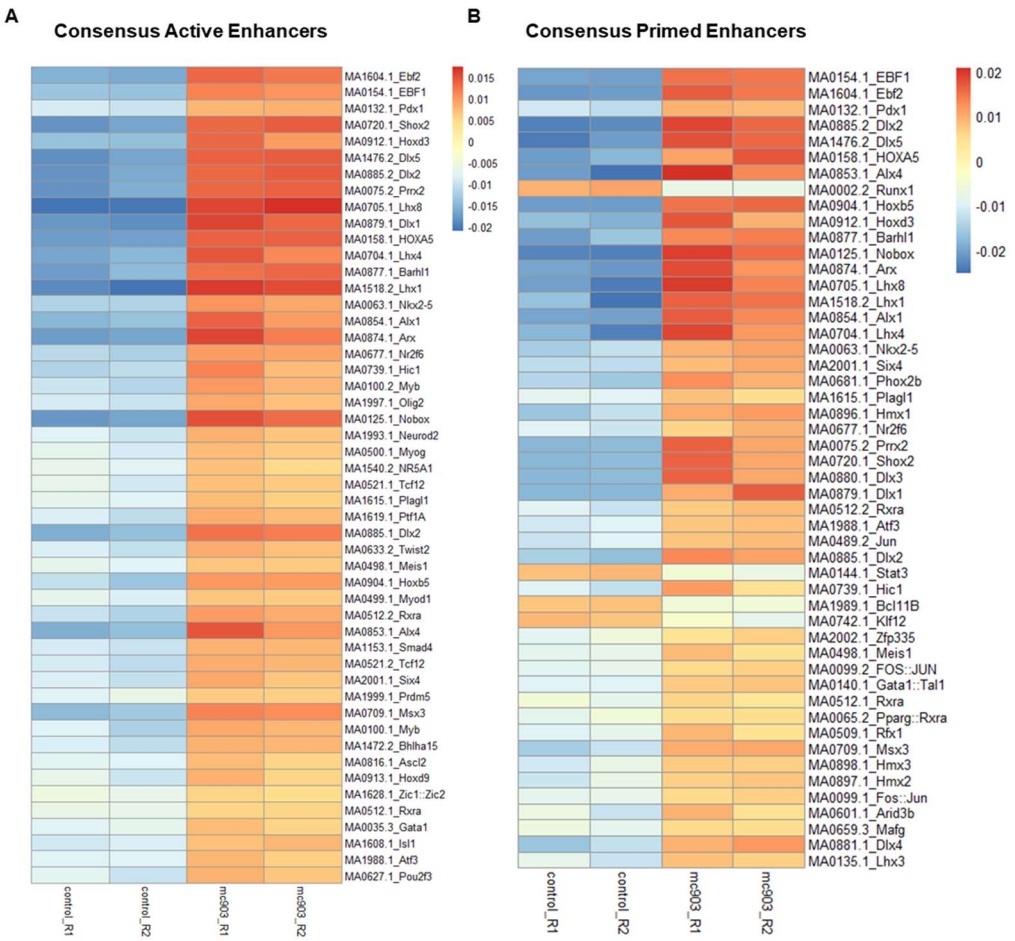

Figure 7. Transcription factor motif accessibility changes in active and primed enhancers of DRG neurons in the MC903 mouse model. Heatmaps showing chromVAR-derived deviation scores across control and MC903-stimulated DRG neurons for TFs associated with (A) active enhancers and (B) primed enhancers. Rows represent TF motifs ranked by chromVAR-calculated variability, while columns correspond to individual replicates from control and MC903 conditions. warmer colors indicate increased motif accessibility, while cooler colors represent decreased accessibility upon MC903 application.

To assess whether Ebf1-binding enhancers and promoters are associated with genes implicated in itch sensation, we employed the Activity-by-Contact (ABC) model(Fulco et al., 2019) to predict enhancer–promoter interactions. This analysis identified Ebf1 motif-containing regulatory elements linked to key genes involved in neuronal sensitization and chronic itch, including Trpv1 and Trpa1, as well as Il13ra1 and Il4ra (Figure 27), both of which play central roles in Type 2 immune-driven pruritus and sensory neuron hypersensitivity.

While some enhancer–promoter pairs were shared between control and MC903 conditions, global analysis revealed a marked increase in H3K4me1 and H3K27ac signal intensity in MC903-treated neurons, consistent with enhancer activation under chronic itch conditions. These findings suggest that Ebf1 orchestrates chromatin remodeling at itch-associated regulatory elements, facilitating the transcriptional reprogramming of sensory neurons in response to chronic inflammation.

These findings suggest that EBF1 plays a central role in enhancer dynamics in sensory neurons, linking chronic inflammation to widespread epigenomic remodeling. The preferential activation of distal enhancers over promoters suggests that transcriptional changes in chronic pruritus are primarily governed by enhancer-mediated gene regulation. Moreover, the expansion of MC903-specific primed enhancers implies that inflammatory stimuli not only activate immediate transcriptional responses but also precondition the enhancer landscape, potentially sensitizing sensory neurons for heightened reactivity to future inflammatory cues. This enhancer priming may provide a mechanistic basis for the persistent neuronal hypersensitivity observed in chronic itch, wherein pre-established regulatory elements facilitate rapid transcriptional responses upon subsequent immune stimulation. Together, these results suggest that chronic pruritus is epigenetically encoded through enhancer remodeling, offering a potential framework for therapeutic intervention targeting EBF1-driven regulatory networks in chronic pruritus.

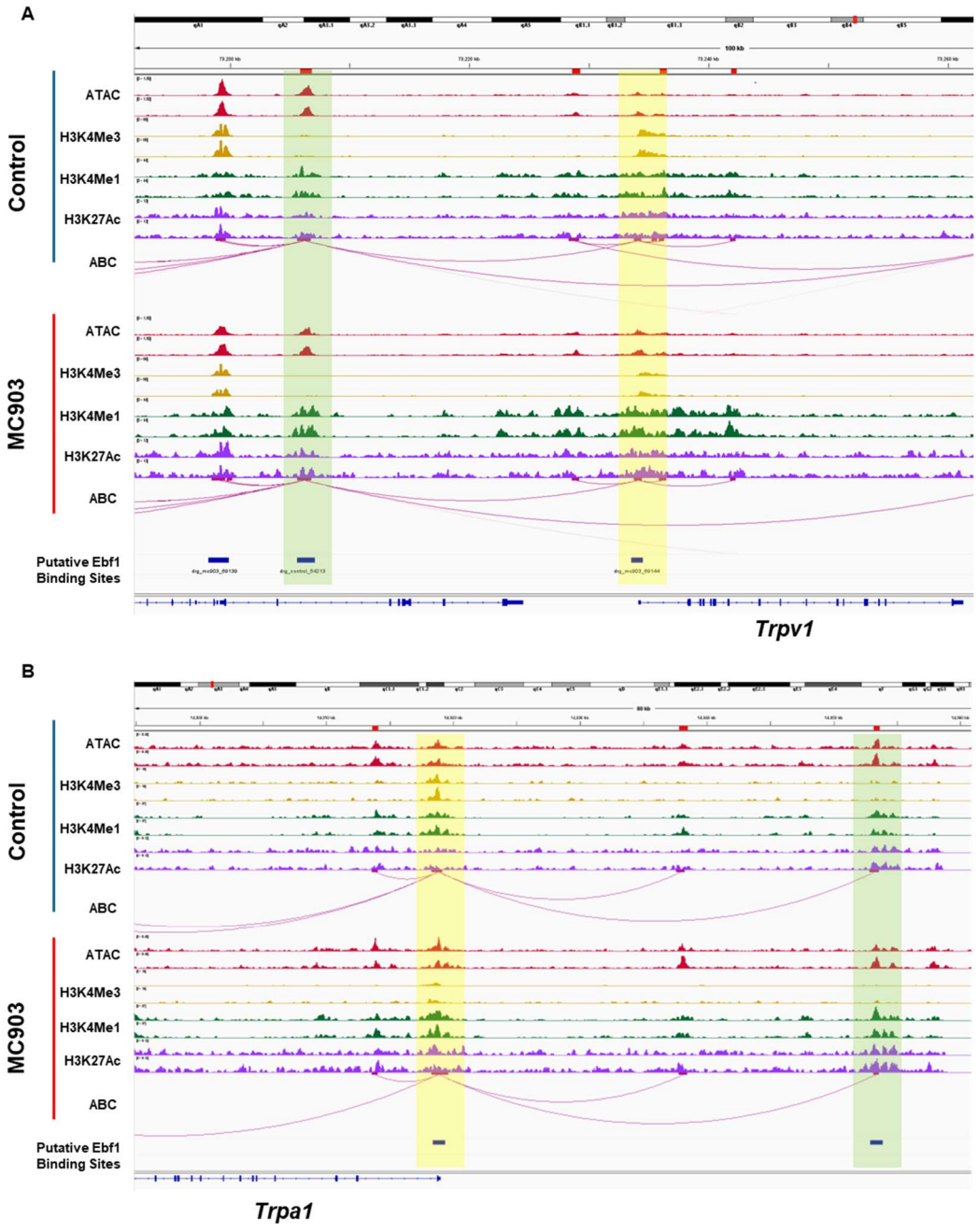

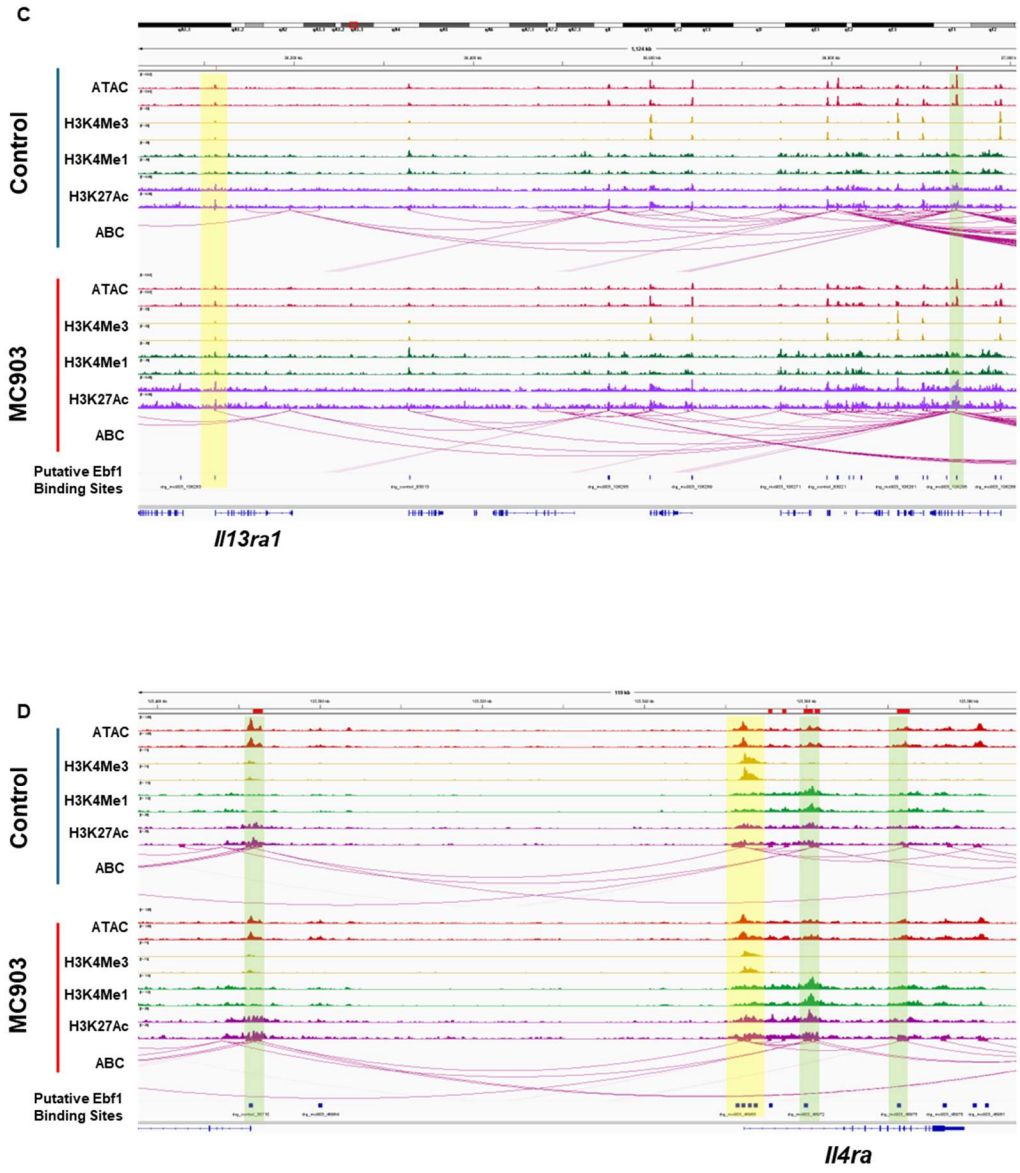

Figure 28. Genome browser tracks highlighting the activation of Ebf1 motif-containing enhancers in the MC903 condition and their potential regulation of itch-related genes. IGV genome browser snapshots showing chromatin accessibility and histone modifications at putative regulatory elements near key itch-related genes, including

(A) Trpv1, (B) Trpa1, (C) Il13ra1, and (D) Il4ra. Tracks represent chromatin accessibility (ATAC-seq, red), active promoter (H3K4me3, yellow), general enhancer marks (H3K4me1, green), and active enhancer marks (H3K27Ac, purple). Highlighted regions indicate Ebf1 motif-containing enhancers (green fluorescence) and promoters (yellow fluorescence) that exhibit differential activation in the MC903 condition. Purple arcs denote chromatin interactions which was predicted by Activity-by-Contact (ABC) model.

3.7. Integrated epigenome and scRNA-seq analysis uncovers Ebf1-driven enhancer activation in MC903, linking JAK-STAT signaling to inflammation-specific sensory neuron reprogramming

Through scRNA-seq of DRG neurons, we identified an EBF1-activated, Inf-specific neuronal cluster that emerges exclusively in inflammatory skin disease mouse models, with the MC903 model displaying the most prominent induction of this cluster. Independently, bulk epigenomic profiling of purified DRG neurons—which lacks cell type resolution—revealed a significant increase in distal intergenic accessibility under MC903 conditions, with these accessible peaks enriched for EBF1 binding sites. DiffTF, chromVAR, and TOBIAS footprinting analyses further confirmed elevated EBF1 activity under MC903 stimulation, particularly at active and primed enhancers, suggesting a role in enhancer-mediated transcriptional regulation. Notably, these enhancers were strongly linked to chronic itching sensation-associated genes, implicating EBF1 as a key regulator of sensory neuron transcriptional plasticity.

To assess whether findings from these two datasets align, we examined the expression of ABC-identified target genes associated with EBF1 motif-containing active enhancers of MC903 condition in DRG neuron scRNA-seq data. After consolidating duplicate target genes, we quantified their expression in individual cells using AddModuleScore (Figure 28A). Remarkably, despite utilizing epigenomic datasets derived from bulk-level analyses, target gene expression was selectively enriched in Inf-specific clusters, aligning with the predicted enhancer activity. Further validation via violin plot (Figure 28B) confirmed a statistically significant increase in target gene expression scores across all Inf-specific clusters compared to their original counterparts. These findings demonstrate a strong concordance between single-cell omics and bulk epigenome analysis, supporting the notion that EBF1 plays a pivotal role in transcriptional regulation within inflammation-responsive sensory neurons.

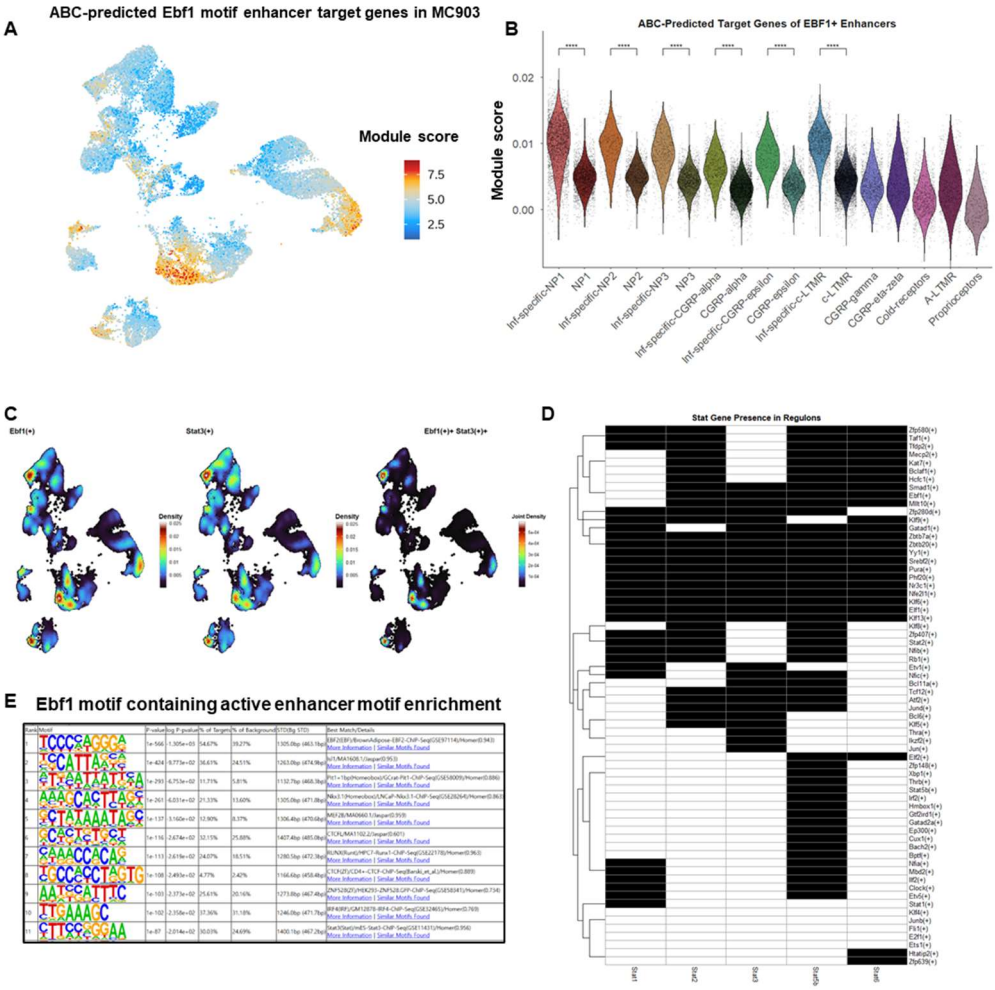

Figure 249. Ebf1-STAT3 Co-regulated Enhancer Landscape in Sensory Neurons Under Chronic Itch Conditions. (A) UMAP projection of single-cell RNA-seq data displaying the module score for ABC-predicted Ebf1 motif-containing enhancer target genes in MC903-treated DRG neurons. Warmer colors indicate higher module scores, highlighting enrichment in specific neuronal subpopulations. (B) Violin plot showing the distribution of module scores across different neuronal subtypes, revealing distinct enrichment patterns in Inf-specific neuron clusters (C) Nebulosa density plots depicting the

regulon activity landscape of Ebf1, Stat3, and their co-activation (Ebf1+Stat3+) in UMAP space. High-density regions indicate neuronal clusters where Ebf1 and Stat3 are likely to co-regulate enhancer activity, suggesting functional cooperation in transcriptional control. (D) Heatmap of STAT gene presence in regulon target genes, illustrating the distribution of STAT family genes across predicted regulatory elements. Black regions indicate the presence of STAT motifs within regulon target genes, revealing differential transcription factor occupancy. (E) Sequence motifs and predicted binding sites for Ebf1 motif containing active enhancer in MC903 mouse model. Wilcoxon rank sum test with Bonferroni post hoc test was used. *$P < 0.05$, **$P < 0.01$, or ***$P < 0.001$, ****$P < 0.0001$.

Given that Ebf1 functions as a pioneer factor and a key regulator of enhancer remodeling(Boller et al., 2016; Lenaerts et al., 2022; Zolotarev et al., 2022), we hypothesized that it may cooperate with other transcription factors to modulate the enhancer landscape in inflammation-responsive sensory neurons. scRNA-seq analysis of DRG neurons previously revealed that STAT transcription factor activity is significantly elevated in Inf-specific clusters, suggesting a potential interaction between Ebf1 and STAT signaling. Consistent with this, the JAK-STAT pathway is a well-established regulator of DRG neuron sensitization in chronic pruritus(Nicolas et al., 2012; Oetjen et al., 2017). Among its components, JAK1 and STAT3 are central mediators of IL-31 receptor signaling, a key driver of chronic itch(Takahashi et al., 2023).

To explore the relationship between Ebf1 and Stat3, we first assessed their transcriptional activity using Nebulosa plots, which visualize co-activation density at the single-cell level (Figure 28C). This analysis revealed a notable increase in Ebf1 and Stat3 co-activation within Inf-specific clusters, with the highest density observed in Inf-specific NP3 neurons, suggesting potential transcriptional cooperation. Further investigation of regulon target genes confirmed that Stat3, along with Stat2, Stat5b, and Stat6, are direct

targets of the Ebf1 regulon (Figure 28D), supporting a hierarchical regulatory relationship between Ebf1 and STAT factors in inflammation-responsive neurons.

At the chromatin level, HOMER de novo motif enrichment analysis of MC903-induced active enhancers containing EBF1 motifs revealed a significant co-enrichment of STAT3 motifs, ranking 11th in statistical significance (Figure 28E). This suggests that Ebf1 and Stat3 may function cooperatively at enhancer elements, particularly within NP3 pruriceptors, which are critical for inflammatory itch sensation(Wang & Kim, 2020). Collectively, these findings propose that Ebf1 and Stat3 coordinate enhancer-driven transcriptional regulation in chronic pruritus, further linking epigenomic remodeling in sensory neurons to persistent inflammatory signaling.

3.8. Skin-neuron crosstalk predicts OSM-LIF/LIFR as an upstream trigger of Ebf1 activation, converging with STAT3 in inflammation-specific neurons

Despite the topical application of MC903 to the skin, *Ebf1* activation was observed in DRG sensory neurons, which are anatomically distant from the site of treatment. This suggests that cutaneous immune activation triggered by MC903 generates signals that are transmitted to sensory neurons via receptors expressed on peripheral nerve terminals. Notably, DRG sensory neurons are known to express receptors for key cytokines, including *Il4r*, *Il31ra*, and *Il13ra1*, enabling them to respond to immune-derived signals(Akinyemi et al., 2024). To elucidate the neuroimmune interactions that drive *Ebf1* activation within DRG sensory neurons, we performed single-cell RNA sequencing (scRNA-seq) of skin from MC903-treated and control mice.

Following 8 days of MC903 application, we generated scRNA-seq libraries from dorsal skin samples of MC903-treated and control mice. After standard quality control and doublet removal, we obtained 26,381 single cells from MC903-treated mice and 9,722 single cells from controls. Cell type annotation was performed based on established marker genes, identifying six major cellular populations: keratinocytes, fibroblasts, endothelial cells, smooth muscle cells, Schwann cells, and immune cells (Figure 29A-B). Quantification of cell population shifts revealed significant changes in fibroblast and immune cell abundance following MC903 treatment (Figure 29C). In MC903-treated skin, the number of immune cells increased more than 2.7-fold (1,516 in controls vs. 4,161 in MC903-treated skin), while fibroblasts exhibited a dramatic 7.3-fold expansion (2,104 in controls vs. 15,296 in MC903-treated skin) (Figure 29D). Proportional analysis of cell composition within the total skin cell population further demonstrated that the expansion of fibroblasts and immune cells reduced the relative abundance of keratinocytes (Figure 29E). This finding indicates that MC903 application induces a profound reorganization of the cutaneous tissue microenvironment, characterized by fibroblast proliferation and immune cell infiltration. Notably, cell-type-specific comparisons revealed that while keratinocyte numbers

remained relatively stable, both immune cell and fibroblast populations expanded significantly in the MC903-treated group (Figure 29F). These results are consistent with previous findings from human AD skin scRNA-seq studies, which similarly reported fibroblast expansion as a hallmark of AD-associated tissue remodeling(He et al., 2020; Mitamura et al., 2023).

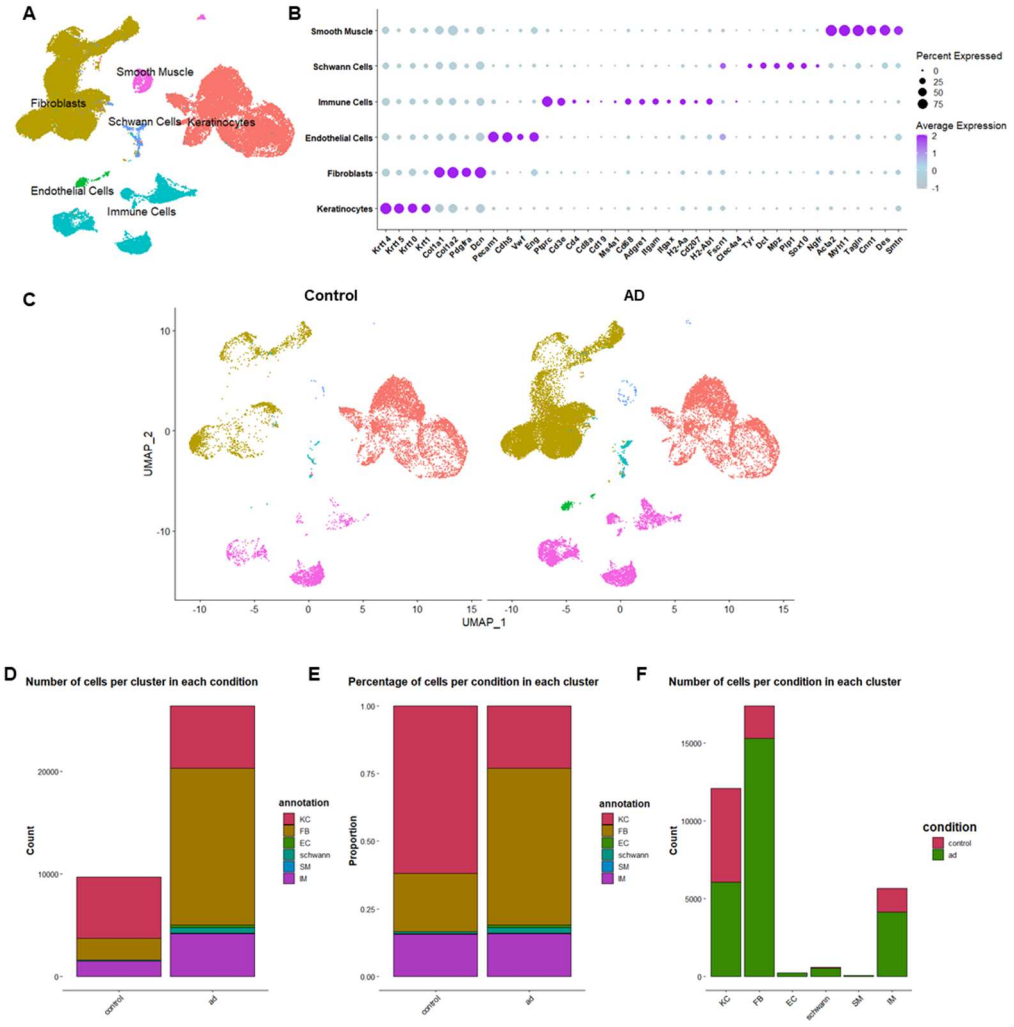

Figure 30. Skin scRNA-seq dataset preparation for cell-to-cell interaction with DRG

neuron scRNA-seq dataset. (A) UMAP visualization of annotated cell types, including fibroblasts (FB), keratinocytes (KC), endothelial cells (EC), immune cells (IM), Schwann cells (Schwann), and smooth muscle cells (SM). (B) Dot plot illustrating the expression of key genes across different cell types. The dot size represents the percentage of cells expressing each gene, while the color intensity indicates average expression levels (C) UMAP projections of cells from control, atopic dermatitis (AD) conditions. (D-F) Quantification of cell type distributions across conditions. (D) Bar plot showing the total number of cells per cluster in each condition. (E) Stacked bar plot depicting the relative proportion of each cell type within control, AD, and PSO conditions. (F) Bar plot displaying the number of cells per cluster in each condition.

To investigate the overall landscape of neuroimmune interactions, including those involving the Inf-specific neuron cluster, we integrated the skin scRNA-seq dataset with our previously analyzed DRG neuron scRNA-seq data. Using CellComm, we systematically mapped ligand-receptor interactions between skin cells and sensory neurons based on the recently constructed neuroimmune interactome database(Jain et al., 2024) (Figure 30). This analysis revealed that NP1, NP2, and CGRP-epsilon neurons exhibited the strongest interactions with fibroblasts and keratinocytes, suggesting a preferential neuroimmune communication axis between these neuronal subtypes and structural skin cells. Notably, this trend was observed in both skin-to-neuron and neuron-to-skin signaling directions, indicating bidirectional crosstalk between these cell types (Figure 30A-B).

The dominance of fibroblast- and keratinocyte-mediated interactions over immune cell-derived signaling can be attributed to their stable anatomical and functional relationships with sensory neurons. Unlike immune cells, which engage with neurons in a transient, context-dependent manner during inflammation, fibroblasts and keratinocytes form continuous paracrine and juxtacrine interactions with DRG terminals in the skin(Cai et al., 2023; Chen et al., 2021). Fibroblasts serve as key regulators of neuronal function by

secreting neuroactive factors, such as NGF, LIF, and IL-6, while also providing an extracellular matrix scaffold that facilitates integrin-mediated adhesion between neurons and their surrounding tissue(Shin et al., 2021). Similarly, keratinocytes modulate neuronal excitability through ATP, prostaglandins, and cytokines (including alarmin), reinforcing their role in sensory signaling(Liu et al., 2016; Pang et al., 2015; Takahashi et al., 2019; Talagas et al., 2020; Wilson et al., 2013). This persistent neuroepithelial crosstalk is essential for sensory neuron development, axonal patterning, and homeostatic maintenance(Simmons & Gallo, 2024), whereas immune-neuron interactions, though functionally significant, are more dynamic and primarily activated under pathological conditions.

Interestingly, Inf-specific neurons, which were the primary focus of our transcriptomic analysis, exhibited a marked reduction in interaction strength with keratinocytes, fibroblasts, and immune cells compared to their original cluster counterparts (Figure 30A-B). This finding suggests that Inf-specific neurons might transform toward a semi-autonomous mode of operation, potentially reducing interactions observed in their original cluster to prioritize those specifically involved in itch sensitization and transmission. Insights from recent itch and pain studies support this model, revealing that what may seem paradoxical at the surface—high activity but low external interaction—is, in fact, a hallmark of neurons that have been persistently stimulated and have reached a new homeostasis. These findings indicate the need to consider temporal and adaptive neuroimmune changes: while cytokine blockade may halt itch initiation, disrupting the itch cycle may require targeting intrinsic neuronal changes like Ebf1 activation.

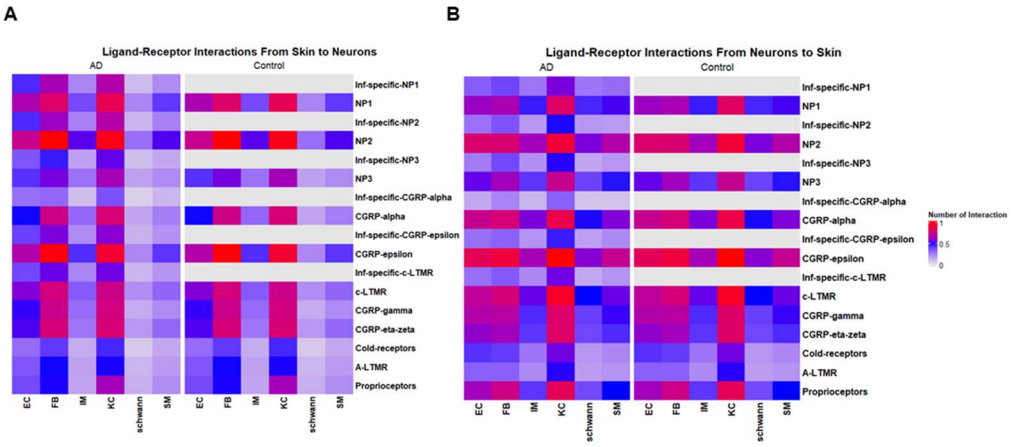

Figure 251. CellComm analysis shows reduced cell-to-cell interactions in Inf-specific clusters of AD compared to control and original AD neuronal clusters. Heatmaps display cell-to-cell interaction strength derived from CellComm analysis, showing ligand-receptor communication between skin and neurons in AD and control conditions. (A) Ligand-receptor interactions from skin to neurons. (B) Ligand-receptor interactions from neurons to skin. (FB; fibroblasts, KC; keratinocytes, EC; endothelial cells, IM; immune cells, Schwann; Schwann cells, SM; smooth muscle cells)

Next, to examine immune-to-neuron interactions that may contribute to the transcriptional reprogramming of Inf-specific clusters, we focused on small-fiber nociceptors, including CGRP-alpha, CGRP-epsilon, NP1, NP2, and NP3 (Figure 31). Comparative analysis revealed that Inf-specific clusters exhibited distinct interaction patterns compared to their original clusters (Figure 31A).

Pathway analysis of interactions unique to Inf-specific clusters identified several intracellular regulatory pathways. Specifically, Inf-specific CGRP-alpha neurons exhibited a *Nrxn1* → *Stat3* interaction, while Inf-specific CGRP-epsilon neurons displayed *Nrxn* → *Ncoa2* and *Cadm1* → *Crebbp* interactions. Similarly, Inf-specific NP1 neurons were enriched for the *Itgb1* → *Hnrnpk* pathway, whereas Inf-specific NP2 neurons exhibited a

Nrxn1 → *Ago1* interaction. Notably, Inf-specific NP3 neurons showed a strong *Lifr* → *Stat3* and *Lifr* → *Stat2* regulatory pathway. Since *Lifr* is a receptor for *Osm* and *Lif*, and *Osm* has been specifically implicated in chronic itch (Tseng & Hoon, 2021), we sought to identify the cellular sources of *Osm* and *Lif* in the skin scRNA-seq dataset (Figure 31B). As a result, *Osm* expression was highest in the *Cd68*+, *Lyz2(LyzM)*+, and *Itgam(Cd11b)*+ macrophage cluster. Further re-clustering of immune cells followed by *Osm* and *Lif* expression analysis (Figure 31C) confirmed a significant upregulation of *Osm* in the macrophage, neutrophil, and T/NK clusters under MC903 condition compared to control. Similarly, *Lif* expression was significantly elevated in macrophage and T/NK clusters in MC903 condition.

Interestingly, basophils were absent in the control group but emerged exclusively in the MC903 condition, where they exhibited the highest expression of both *Lif* and *Osm* among all immune cell clusters. This finding aligns with previous studies demonstrating that basophils play a crucial role in allergic itch by interacting with sensory neurons(F. Wang et al., 2021), further supporting the hypothesis that basophil-derived *Osm* and *Lif* contribute to Inf-specific NP3 activation in the chronic itch setting.

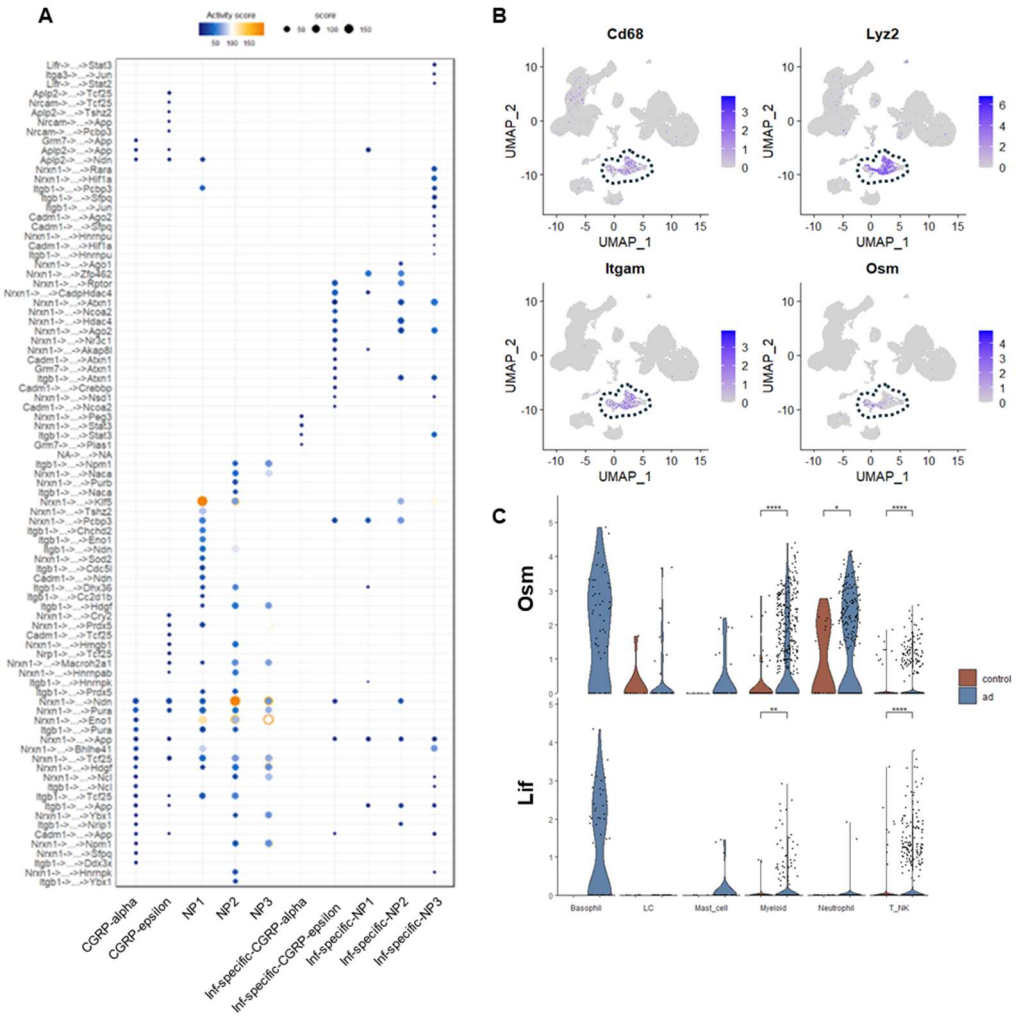

Figure 262. Inf-specific-NP3 shows potential interaction with cutaneous immune cells via Lifr-Stat3 pathways. (A) Predicted DRG neuron signaling pathways from skin immune cells in the MC903 group to transcriptional regulators. (B) Feature plot displaying the expression of Cd68, Lyz2 (LyzM), Itgam (Cd11b), and Osm (Oncostatin M) in skin scRNA-seq data. The dotted region marks the macrophage/monocyte cluster. (C) Violin plot showing the expression of Lif and Osm across immune subclusters. Wilcoxon rank sum test with Bonferroni post hoc test was used. *$P < 0.05$, **$P < 0.01$, or ***$P < 0.001$, ****$P < 0.0001$.

CellComm infers receptor-to-TF pathways by integrating ligand-receptor interactions with PPI networks. However, its accuracy is constrained by database completeness. In our dataset, Ebf1 was not linked to any receptor pathway, likely due to limited upstream interactions in iRefIndex(Razick et al., 2008). To address this, we used DominoSignal, which infers regulatory pathways based on expression patterns rather than predefined PPIs .

DominoSignal utilizes regulon scores calculated by SCENIC to define downstream target transcription factors associated with ligand-receptor pairs. Using this approach, we identified DRG neuron-expressed receptors most strongly correlated with Ebf1 regulon activity, revealing *Scn10a* (Nav1.8), *Lifr*, *Robo2*, and *Ret* as the top four correlated receptors (Figure 32A). To validate these findings, we examined the expression of these four receptors in the DRG neuron scRNA-seq dataset (Figure 32B-E) and found that they were particularly enriched in Inf-specific clusters. This enrichment suggests that these receptors may play a crucial role in mediating the upstream signals that regulate *Ebf1* activity in these neuronal subsets.

Furthermore, network analysis of immune-to-neuron interactions in Inf-specific NP1, NP2, and NP3 clusters revealed that *Osm* or *Lif*, secreted by immune cells, interacts with *Lifr*, leading to the downstream activation of *Ebf1* (Figure 32F-H). These findings provide mechanistic insight into how immune-derived signals mediate Ebf1 activation in specific neuronal subsets under chronic itch conditions.

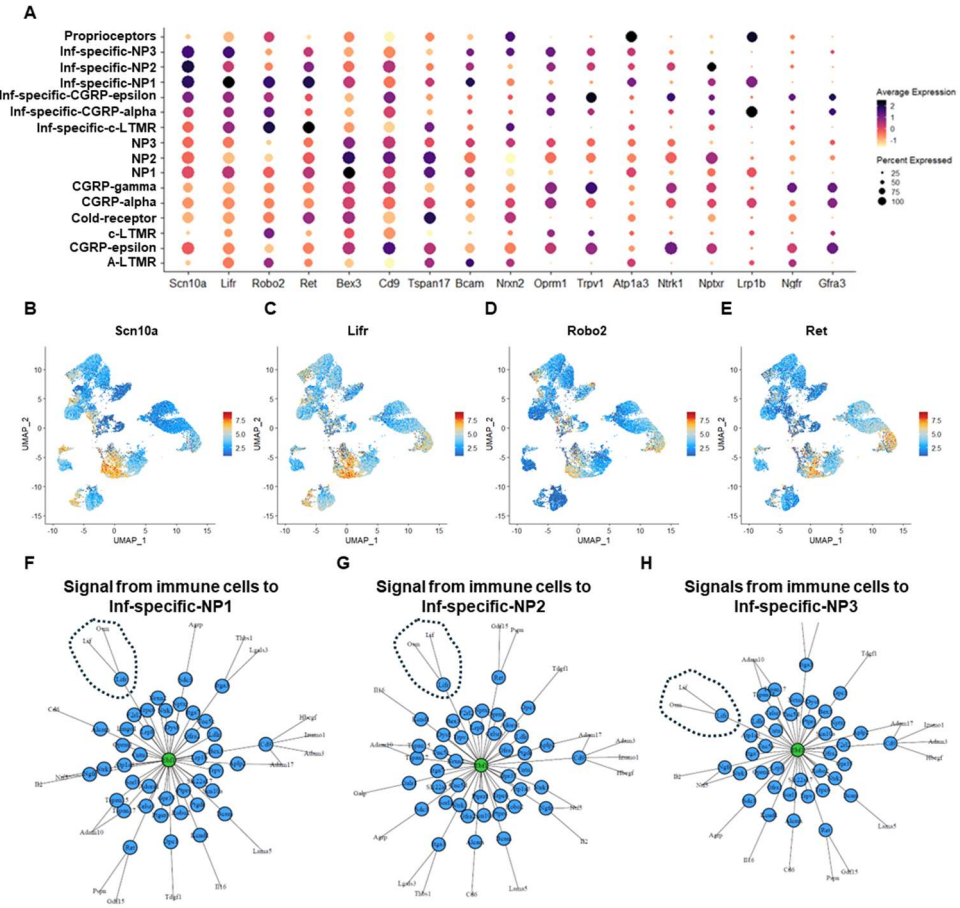

Figure 273. DominoSignal analysis reveal the interaction between Inf-specific-NP subclusters with skin immune cells via Lif/Osm-Lifr-Ebf1 pathway. (A) A dot plot displays the top receptors correlated with Ebf1 regulon score, where dot size represents the percentage of expressing cells, and color intensity indicates average expression levels. (B-E) Feature plots show the spatial distribution of the top four correlated receptors in UMAP space, highlighting their expression is specific to Inf-specific neurons : (B) Scn10a (Nav1.8), (C) Lifr, (D) Robo2, and (E) Ret. (F-H) Network diagrams depict neuroimmune interactions from immune cells to inflammation-specific neuronal clusters, demonstrating potential ligand-receptor signaling pathways targeting (F) Inf-specific-NP1, (G) Inf-specific-NP2, and (H) Inf-specific-NP3.

3.9. Scn10a-specific Ebf1 deletion mitigates skin inflammation and pruritus, rewiring NP3 sensory neurons and suppressing chronic itch-associated transcriptional programs

Ebf1 was thought to be a possible key regulator of chronic itch based on scRNA-seq analysis of DRG neurons and bulk epigenome profiling in the MC903 chronic pruritus model. To explore its functional significance *in vivo*, Scn10a-Cre;Ebf1$^{fl/fl}$ conditional knockout (cKO) mice were generated, allowing selective deletion of Ebf1 in small-fiber nociceptors. Both cKO and littermate wild-type (WT, Ebf1$^{fl/fl}$) controls were treated with MC903 for 8 days, followed by an assessment of scratching behavior and skin inflammation (Figure 33).

At the macroscopic level, cKO mice displayed markedly reduced erythema, scaling, edema, and lichenification compared to WT controls, suggesting an attenuation of MC903-induced skin inflammation (Figure 33A). This observation was further supported by SCORAD-based dermatitis scoring, which revealed a statistically significant reduction in skin inflammation in cKO mice (Figure 33B). To quantify scratching behavior, spontaneous scratching was monitored using an infrared behavioral observation box (iBOB) on day 9 following MC903 application. Compared to WT controls, cKO mice exhibited a significant reduction in spontaneous scratching, indicating a diminished pruritic response (Figure 33C).

Histological examination of H&E-stained back and ear skin sections provided additional evidence of reduced inflammation (Figure 33D–F). In back skin, cKO mice exhibited notably less epidermal acanthosis, with a significant reduction in epidermal thickness, though total skin thickness remained unchanged (Figure 33D, E). In ear skin, both epidermal acanthosis and dermal thickening were significantly diminished in cKO mice compared to WT controls (Figure 33F). This regional difference likely reflects intrinsic anatomical properties, as back skin is structurally thicker, mechanically stable, and less prone to inflammatory remodeling, whereas ear skin, being thinner and more vascularized, exhibits greater sensitivity to inflammatory resolution and extracellular matrix remodeling.

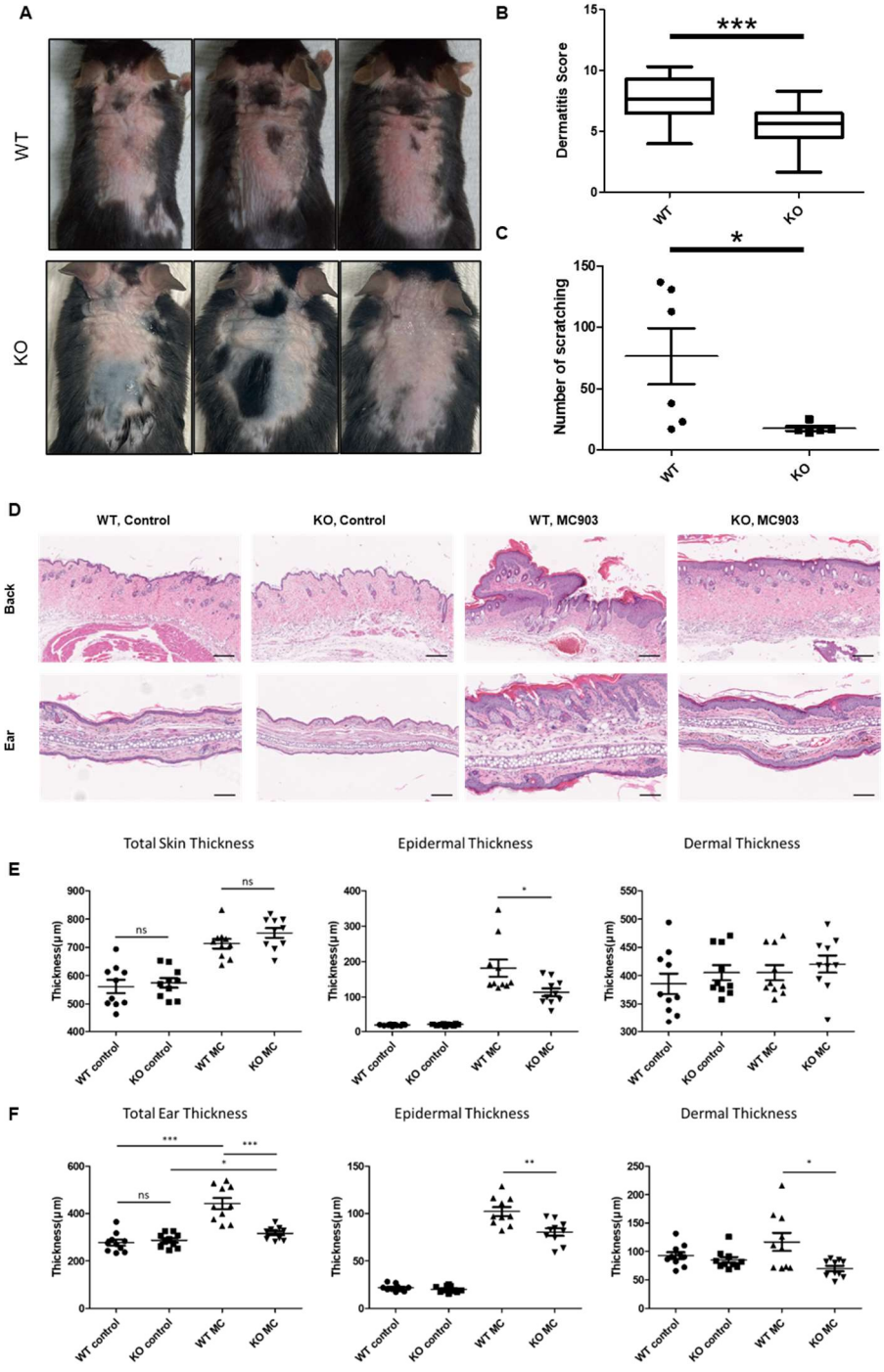

Figure 284. Ebf1 deletion in scn10a expressing sensory neurons attenuates MC903-induced chronic itch and epidermal pathology. (A) Representative images of dorsal skin lesions in WT ($Ebf^{fl/fl}$) and Nav1.8-Cre;$Ebf^{fl/fl}$ (Ebf1 cKO) mice following MC903 treatment. Erythema, scaling, edema was reduced in Ebf1 cKO mouse. (B) Quantification of dermatitis severity using a SCORAD-based scoring system adapted for mice. (WT mouse, n=21; KO mouse, n=21) (C) Spontaneous scratching behavior, measured as the number of scratching bouts per 30 min. (WT mouse, n=21; KO mouse, n=21) (D) H&E-stained sections of dorsal and ear skin from control and Ebf1 cKO mice following MC903 application. Control mice develop epidermal hyperplasia, hyperkeratosis, and dermal inflammation, whereas Ebf1 cKO mice exhibit markedly reduced pathological changes. Scale bars: (back) 200 μm, (ear) 100 μm. (E, F) Quantification of skin thickness in dorsal (E) and ear (F) skin sections. Epidermal thickening is significantly attenuated in Ebf1 cKO mice, consistent with reduced inflammation-induced hyperplasia. two-tailed Student's t-test was used. *$P < 0.05$, **$P < 0.01$, or ***$P < 0.001$, ****$P < 0.0001$, ns, not significant.

To better understand the molecular basis of the observed reduction in inflammation and scratching behavior above, we performed scRNA-seq analysis on DRG tissues isolated from cKO and littermate control mice following 8-day MC903 treatment. Consistent with the developmental role of Ebf1 in neurons(Garel et al., 1999; Wang et al., 1997), the number of neurons detected in cKO mice (11,997 neurons) was markedly lower compared to littermate controls (25,813 neurons), whereas non-neuronal cell counts remained comparable (cKO: 37,924, control: 39,947). Despite the reduced neuronal population in cKO mice, Louvain clustering followed by UMAP visualization confirmed that all known sensory neuron subclusters reported in B6 and public datasets were well-defined (Figure 34A-B).

We next identified genes significantly up- or downregulated (adjusted $p < 0.05$) by MC903 treatment in the B6 dataset and examined those that were inversely regulated in cKO mice, thereby assessing the extent to which Ebf1 modulates the MC903-driven transcriptional response (Figure 34C-D). To enhance the reliability of our data analysis, we first performed harmonization-based batch correction between the B6 and cKO datasets and subsequently re-clustered the data to redefine neuronal subpopulations. Following this correction, we re-identified differentially expressed genes (DEGs) in each cluster and reassessed the transcriptional changes associated with MC903 treatment and Ebf1 cKO. This analysis revealed that MC903-upregulated genes that were downregulated in cKO were highly enriched in NP2, NP3, and CGRP-epsilon clusters, while MC903-downregulated genes that were upregulated in cKO were enriched in NP2, NP3, CGRP-epsilon, and CGRP-alpha (Figure 34C-D). Notably, the proportion of MC903-up genes downregulated by Ebf1 loss (maximal value ~5%) was higher across all clusters compared to the opposite case (maximal value ~2%), indicating that Ebf1 primarily functions to sustain MC903-induced transcriptional activation of chronic itch-related genes.

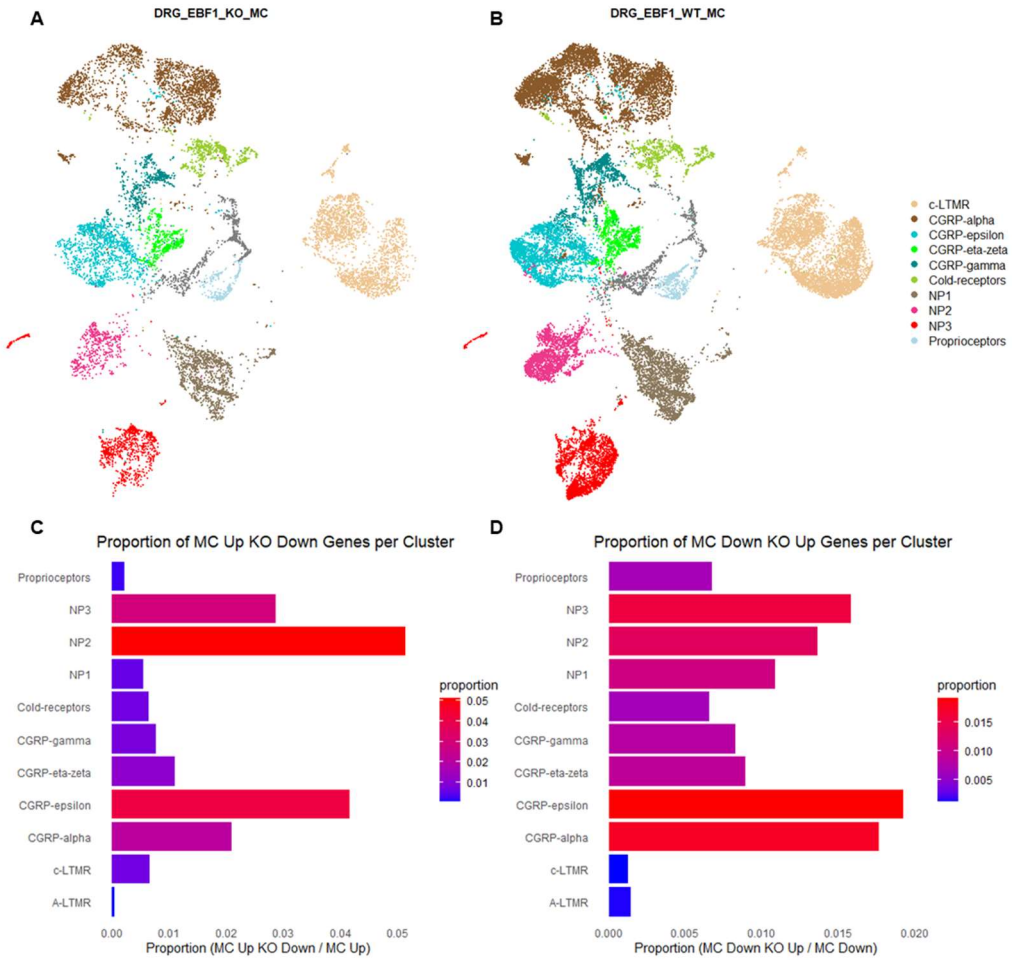

Figure 295. Preferential impact of Ebf1 deletion on specific DRG neuronal clusters in MC903-induced chronic itch. (A, B) UMAP projections of DRG sensory neurons from (A) Ebf1 cKO and (B) control mice, both treated with MC903 for 8 days. (C) Proportion of MC903-upregulated genes that are downregulated in Ebf1 cKO neurons across neuronal clusters (both adjusted p-value < 0.05). The proportion was determined relative to the total number of MC903-upregulated genes per cluster. (D) Proportion of MC903-downregulated genes that are upregulated in Ebf1 cKO neurons across neuronal clusters (both adjusted p-

value < 0.05). The proportion was determined relative to the total number of MC903-downregulated genes per cluster.

Building on previous reports identifying NP3 neurons as central mediators of inflammatory chronic itch and the result that NP3 exhibited the highest activation levels of Ebf1 and Stat3, we further examined the transcriptomic changes induced by Ebf1 cKO within the NP3 cluster (Figure 35). Volcano plot of genes upregulated by MC903 in B6 datasets but downregulated in cKO datasets (Figure 35A-B) revealed a significant reduction in *Il31ra*, the receptor for IL-31, a key itch-associated cytokine. Additionally, several genes implicated in itch signal transmission were significantly downregulated, including *Nppb*, a neurotransmitter essential for conveying itch signals to spinal interneurons, as well as *Scn7a* and *Scn9a* (sodium channels), *Htr1a*, *Htr1f*, *F2rl1* (PAR2), and *Mrgprx1* (itch receptors), *Smarca5* and *Smarca1* (epigenomic regulators), and *Camk2a*, which mediates intracellular calcium signaling (Figure 35B).

To identify functional transcriptomic changes beyond individual genes, we performed Overrepresentation Analysis (ORA) on NP3-specific genes that were upregulated by MC903 but downregulated in Ebf1 cKO (Figure 35C-E). This analysis revealed significant enrichment for pathways related to neuroplasticity and chronic sensitization, including mitochondrial organization, ATP metabolism, and OXPHOS, as well as neuronal activation-associated terms such as transmission of nerve impulse and neuronal action potential. These findings indicate that, at least in NP3 neurons, Ebf1 not only regulates chronic itch-related gene expression but also modulates mitochondrial function and energy metabolism, highlighting a potential link between Ebf1-driven metabolic regulation and chronic neuronal sensitization, warranting further investigation.

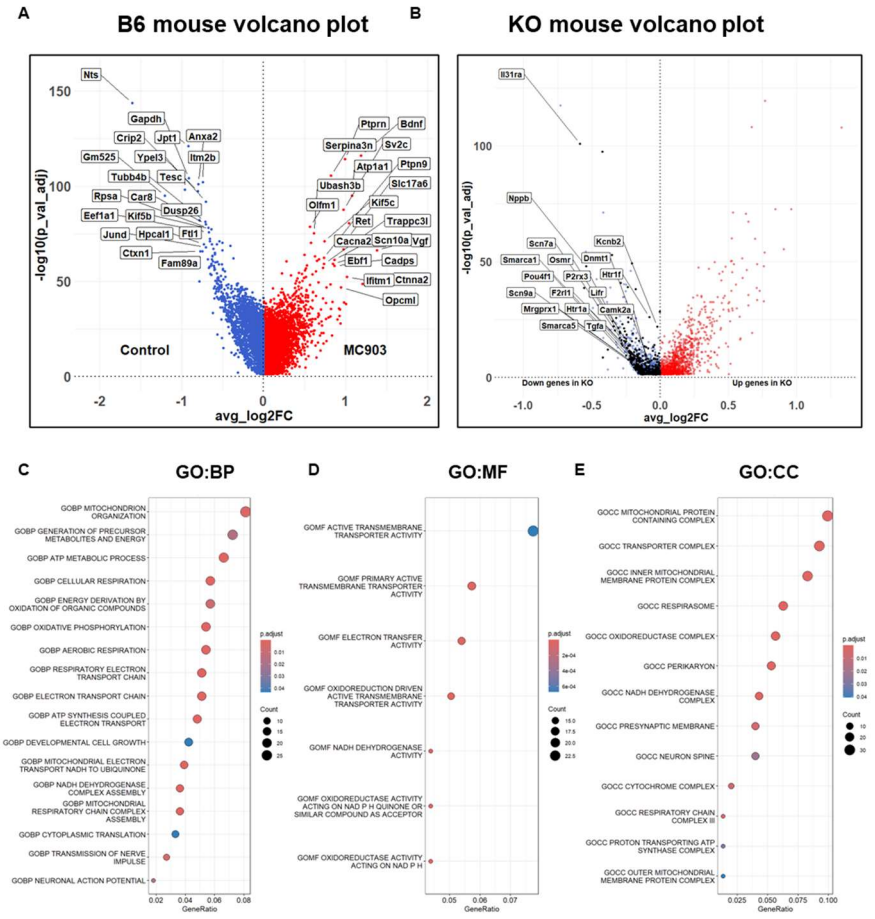

Figure 306. Ebf1 deletion alters the MC903-induced transcriptional program in NP3. (A) Volcano plot of DEGs in NP3 neurons from the B6 mouse dataset. Red indicating significantly upregulated genes and blue representing significantly downregulated genes (both adjusted p-value < 0.05). Labeled top 10 DEGs. (B) Volcano plot of DEGs in NP3 neurons comparing Ebf1 cKO and control mice. Black dots denote genes that are upregulated by MC903 but downregulated in Ebf1 cKO, indicating Ebf1-dependent transcriptional changes. (C–E) Overrepresentation Analysis of MC903-upregulated, Ebf1 KO-downregulated genes in NP3 neurons : (C) GO Biological Process, (D) GO Molecular Function, and (E) GO Cellular Component. Dot size represents gene count. Dot color corresponds to adjusted p-value.

4. DISCUSSION

In this study, we demonstrate that *Ebf1*, a transcription factor with known pioneer activity(Boller et al., 2016; Wang et al., 2020), plays a critical role in sensory neuron reprogramming under chronic itch conditions. Through integrative analyses of scRNA-seq, ATAC-seq, and CUT&RUN-seq, we show that *Ebf1* activity is selectively upregulated in a previously uncharacterized neuronal subset, referred to as Inf-specific neurons, which emerge exclusively in the chronic inflammatory dermatitis mouse models. Our findings further reveal that *Osm* and *Lif*, cytokines upregulated in skin-resident immune cells preferentially in AD condition, act through *Lifr* on DRG sensory neurons to induce *Ebf1* activation, potentially acting in concert with *Stat3*. This study provides mechanistic insight into how cutaneous inflammation triggers transcriptional and epigenetic remodeling in sensory neurons, establishing a molecular framework for the neuronal plasticity associated with chronic pruritus.

Inf-specific sensory neuron exhibit coordinated transcriptional reprogramming involving Ebf1, RFX, STAT, and IRF family factors

Using single-cell transcriptomic analyses, we identified a discrete subset of DRG neurons—termed Inf-specific clusters—that emerge in mouse models of inflammation-associated skin diseases, including AD and psoriasis. These subsets exhibit unique transcriptional signatures that are distinct from canonical nociceptor or pruriceptor classes, suggesting state-specific reprogramming in response to cutaneous inflammation. Our SCENIC-based regulon analysis revealed robust upregulation of transcriptional activity for the RFX family, specifically within Inf-specific subsets. These RFX factors are known for their roles in chromatin accessibility (Zhao et al., 2010), ciliogenesis (Lemeille et al., 2020), and neurodevelopment (Choi et al., 2024). Enrichment analysis of RFX target genes in these neurons revealed strong associations with histone modification, synaptic signaling, and cell–cell junction assembly, suggesting that RFX-driven regulons may coordinate

epigenetic remodeling alongside structural and functional reprogramming of neuronal circuitry in the inflammatory milieu.

Mechanistically, RFX family has been shown to recruit chromatin modifiers such as DNMT1 and HDAC1 in immune cells(Zhao et al., 2010), and its loss results in DNA hypomethylation and histone hyperacetylation at target gene promoters, thereby reinforcing long-lasting changes in gene expression through chromatin-level regulation. By analogy, in sensory neurons, RFX family may induce the expression of histone-modifying enzymes or directly interact with epigenetic remodeling complexes, reshaping the chromatin landscape at inflammation-responsive loci and establishing a “locked-in” pro-inflammatory transcriptional state. Concurrently, the enrichment of genes involved in cell junction organization and glutamate synaptic transmission suggests that RFX factors may also regulate synaptic architecture or neuron–glia interactions, potentially stabilizing maladaptive circuits engaged during chronic inflammation.

Complementing these findings, we also identified selective activation of *Irf1* and *Irf2* regulons within PSO-derived Inf-specific neurons. As canonical transcriptional mediators of type I and II interferon signaling, IRFs (especially *Irf1* and *Irf2*) are closely linked to Th1-polarized inflammatory programs(Wang et al., 2024), in contrast to the Th2-biased responses that characterize AD. Notably, *Irf1* has been shown to antagonize Th2-associated pathways by repressing *Il4* and *Gata3* expression (Elser et al., 2002), suggesting a potential repressive influence on Th2-centered pruritic neuroimmune signaling. This distinction raises the possibility that enhanced IRF activity in PSO neurons may contribute to the relatively lower itch burden observed in psoriasis compared to AD, by dampening Th2 cytokine responsiveness or restricting downstream effectors such as the *Il31–Stat3* axis.

Together, these results suggest that Inf-specific neurons undergo coordinated transcriptional reprogramming involving not only *Ebf1* but also RFX and IRF family transcription factors, leading to both epigenetic remodeling and altered neuroimmune responsiveness. This reprogramming may represent a transitional neuronal state specialized

for inflammatory sensing and may underlie the persistence of chronic itch or heightened sensitivity to cytokines in inflammatory skin disorders.

Ebf1 as a Regulator of Sensory Neuron Plasticity in Chronic Itch

While *Ebf1* is widely recognized for its role in B cell differentiation(Palmisano et al., 2019) and enhancer priming(Lenaerts et al., 2022), its function in sensory neurons has remained poorly defined. Recent studies have suggested a role for Ebf1 in neuropathic pain(Liang et al., 2024), yet its contribution to chronic itch and pruriceptive plasticity has not been previously investigated. Our study provides compelling evidence that *Ebf1* is transcriptionally upregulated and epigenetically activated in DRG sensory neurons under chronic itch conditions.

Epigenomic profiling of DRG neurons revealed that *Ebf1* motif accessibility is significantly increased in MC903-treated mice, particularly in distal intergenic enhancer regions, suggesting that *Ebf1* plays a regulatory role in enhancer activity during sensory neuronal reprogramming. Given that pioneer factors facilitate chromatin accessibility and promote transcriptional rewiring, our findings suggest that Ebf1 may contribute to long-term neuronal sensitization in chronic itch by modulating enhancer landscapes. This aligns with recent work demonstrating that sensory neuron excitability in chronic pain states is driven by persistent transcriptional reprogramming rather than transient gene expression changes(Renthal et al., 2020).

The selective enrichment of *Ebf1* activity in Inf-specific neurons, rather than across all nociceptors, raises important questions regarding the functional divergence of pruriceptive neuronal subtypes. Inf-specific clusters, particularly Inf-specific NP3, exhibit the highest levels of *Ebf1* regulon activity, suggesting that *Ebf1*-dependent transcriptional reprogramming may be a defining feature of this subset. Notably, Inf-specific neurons display reduced neuroimmune interaction strength compared to their original clusters, implying that *Ebf1*-driven reprogramming may alter how these neurons respond to peripheral immune signals. This is particularly intriguing given that neuronal plasticity

often involves a shift from immune cue-dependent activation to heightened intrinsic excitability(Kourrich et al., 2015). Thus, it is possible that *Ebf1*-mediated enhancer remodeling contributes to a sustained hyperexcitable state that persists beyond acute immune activation.

Neuroimmune Interactions in Chronic Itch: The Lif/Osm-Lifr-Ebf1 Axis

A key finding of this study is the identification of a neuroimmune signaling axis linking cutaneous inflammation to sensory neuron epigenetic remodeling. Through CellComm and DominoSignal analyses, we demonstrate that *Osm* and *Lif*, secreted primarily by skin-resident immune cells, signal through *Lifr* on DRG neurons, ultimately leading to *Ebf1* activation. This Lif/Osm-Lifr-Ebf1 axis provides a mechanistic explanation for how cutaneous immune activation translates into sensory neuronal reprogramming in chronic itch.

Our skin scRNA-seq data revealed that *Osm* and *Lif* are significantly upregulated in myeloid and T/NK cell populations under MC903 treatment, with particularly high expression in Cd68+, Lyz2+, and Itgam+ macrophages. Notably, basophils were entirely absent in control skin but emerged exclusively in the MC903 condition, where they exhibited the highest expression levels of *Lif* and *Osm* among all immune cell clusters. This is consistent with prior studies implicating basophils in allergic itch and suggests that basophil-derived cytokines may contribute to sensory neuron plasticity in atopic dermatitis-associated chronic pruritus(F. Wang et al., 2021).

The identification of *Lifr* as one of the top receptors correlated with *Ebf1* regulon activity further supports the functional relevance of this signaling pathway. Our network analysis demonstrated that *Osm* or *Lif* binds to *Lifr* on DRG neurons, leading to downstream activation of *Stat3*, a well-established transcriptional regulator in immune signaling. Given that *Stat3* motifs are highly enriched within *Ebf1*-bound enhancers, our findings suggest that Osm/Lif-Lifr signaling may serve as an upstream trigger for *Ebf1*-dependent chromatin remodeling in sensory neurons.

Transcriptional Reprogramming in Inf-Specific Neurons and Functional Implications

One of the most intriguing aspects of our findings is that Inf-specific neurons, despite displaying high *Ebf1* and *Stat3* activity, exhibit reduced neuroimmune interaction strength compared to their original clusters. This diminished ligand-receptor connectivity raises the possibility that these neurons transition from an immune-responsive state to an intrinsically hyperexcitable state. Such a shift could explain why chronic itch persists even after immune activation subsides, as sensory neurons may remain in a sensitized state through Ebf1-mediated transcriptional reprogramming.

Our analysis also identified several key intracellular pathways enriched in Inf-specific neurons. For example, Inf-specific NP3 neurons exhibited strong Lifr-Stat3 interactions, reinforcing their dependence on Osm/Lif signaling. Additionally, Inf-specific CGRP-alpha and CGRP-epsilon neurons were enriched for Nrxn1-Stat3 and Cadm1-Crebbp interactions, suggesting potential roles for synaptic remodeling and chromatin regulation in itch-associated plasticity.

The emergence of Inf-specific neurons as a transcriptionally distinct subset has broader implications for understanding pruriceptive coding. Unlike classical NP1-NP3 subsets, which display high diversity in their transcriptional responses, Inf-specific neurons exhibit a more uniform expression profile, consistent with a specialized functional state. This supports the notion that neuronal plasticity in chronic itch involves not only transcriptional activation but also a narrowing of gene expression variability, potentially reinforcing a persistent itch-encoding phenotype.

Limitations

While this study provides novel insights into the epigenomic regulation of sensory neuron plasticity in chronic itch, several limitations warrant consideration. First, our ATAC-seq and CUT&RUN analyses were conducted on isolated neurons rather than at a single-cell resolution. Since bulk-based epigenomic profiling captures aggregate signals from all

neurons within a sample, the proportional representation of neuronal subtypes may vary across batches, potentially influencing the relative enrichment of regulatory elements. This limitation is evident in the differing results for *Ebf1* and *Stat3*: while *Ebf1* showed consistent patterns between epigenomic analysis and scRNA-seq, *Stat3* exhibited opposing trends, highlighting the challenges of interpreting bulk-based epigenomic data without single-cell resolution. To overcome this limitation, future studies should incorporate single-cell or nucleus-based epigenomic assays to resolve chromatin accessibility and histone modifications at the level of individual neurons.

Second, our cell-cell interaction analyses relied on reference datasets, which inherently constrain the identification of neuroimmune interactions to those previously characterized. As a result, novel or underrepresented ligand-receptor interactions specific to chronic pruritus may not have been captured. Future approaches integrating spatial transcriptomics or proteomic validation would enable a more comprehensive mapping of sensory neuron-immune cell communication in chronic itch.

Third, while our in vivo functional studies demonstrated that *Ebf1* deletion reduces spontaneous pruritus, the potential role of *Ebf1* in epigenomic priming and pruritic memory formation remains unexplored. Given that chronic neuronal plasticity often extends beyond the resolution of acute inflammation, additional behavioral studies are needed to assess whether *Ebf1* contributes to long-term itch sensitization. Investigating whether *Ebf1*-dependent enhancer remodeling affects neuronal memory of pruritic stimuli could provide crucial insights into the persistence of chronic itch. Furthermore, defining the direct genomic targets of *Ebf1* through ChIP-seq would be essential to elucidate its precise binding regions and regulatory influence in sensory neurons.

Finally, our analysis revealed an apparent discrepancy in *Ebf1* regulation between AD and psoriasis models. While *Ebf1* was enriched in AD mouse model DRG neurons at both the transcriptomic and epigenomic levels, it was absent from ATAC-seq datasets in psoriasis

models despite its presence in scRNA-seq data. This discrepancy may stem from differential neuronal abundance, as our differential abundance analysis indicated that Inf-specific neuron clusters, except for Inf-specific-NP1, were more abundant in AD conditions compared to psoriasis model. However, alternative explanations, such as differences in chromatin accessibility regulation or technical biases in data acquisition, cannot be excluded and warrant further investigation.

5. CONCLUSION

In summary, we identified distinct neuronal subtypes exhibiting transcriptional adaptations under inflammatory conditions, revealing pathways linked to neuronal excitability, synaptic plasticity, and neuroimmune interactions. By integrating single-cell transcriptomics and chromatin accessibility profiling, we determined that Ebf1 functions as a key transcription factor driving chronic itch-associated sensory plasticity. Functional validation using Ebf1-deficient mice demonstrated a marked reduction in spontaneous scratching behavior, epidermal thickening, and pruritus-associated gene expression, supporting its essential role in itch persistence. Further analysis uncovered ligand-receptor interactions between inflamed skin and sensory neurons, suggesting that inflammatory signals sustain chronic neuronal hyperexcitability through Ebf1 activation. This mechanism establishes a neuroimmune feedback loop, maintaining prolonged pruritic states through transcriptional reprogramming. Additionally, comparative analysis across multiple inflammatory models revealed both shared and disease-specific neuronal responses, underscoring the complexity of sensory adaptation in chronic itch conditions. These findings define a novel epigenetic regulatory network that orchestrates sensory neuron adaptation in chronic pruritus. By providing a comprehensive single-cell perspective on neuroimmune crosstalk, this study offers mechanistic insights into itch persistence and presents Ebf1 as a potential therapeutic target for modulating sensory plasticity in chronic pruritic disorders.

References

1. Aibar, S., González-Blas, C. B., Moerman, T., Huynh-Thu, V. A., Imrichova, H., Hulselmans, G.,⋯Aerts, S. (2017). SCENIC: single-cell regulatory network inference and clustering. *Nat Methods*, *14*(11), 1083-1086. https://doi.org/10.1038/nmeth.4463
2. Ajoolabady, A., Lindholm, D., Ren, J., & Pratico, D. (2022). ER stress and UPR in Alzheimer's disease: mechanisms, pathogenesis, treatments. *Cell Death Dis*, *13*(8), 706. https://doi.org/10.1038/s41419-022-05153-5
3. Akinyemi, D. E., Chevre, R., & Soehnlein, O. (2024). Neuro-immune crosstalk in hematopoiesis, inflammation, and repair. *Trends Immunol*, *45*(8), 597-608. https://doi.org/10.1016/j.it.2024.06.005
4. Andersson, R., & Sandelin, A. (2020). Determinants of enhancer and promoter activities of regulatory elements. *Nat Rev Genet*, *21*(2), 71-87. https://doi.org/10.1038/s41576-019-0173-8
5. Badia, I. M. P., Vélez Santiago, J., Braunger, J., Geiss, C., Dimitrov, D., Müller-Dott, S., ⋯Saez-Rodriguez, J. (2022). decoupleR: ensemble of computational methods to infer biological activities from omics data. *Bioinform Adv*, *2*(1), vbac016. https://doi.org/10.1093/bioadv/vbac016
6. Barragán-Iglesias, P., Franco-Enzástiga, Ú., Jeevakumar, V., Shiers, S., Wangzhou, A., Granados-Soto, V.,⋯Price, T. J. (2020). Type I Interferons Act Directly on Nociceptors to Produce Pain Sensitization: Implications for Viral Infection-Induced Pain. *J Neurosci*, *40*(18), 3517-3532. https://doi.org/10.1523/jneurosci.3055-19.2020
7. Barrette, B., Calvo, E., Vallières, N., & Lacroix, S. (2010). Transcriptional profiling of the injured sciatic nerve of mice carrying the Wld(S) mutant gene: identification of genes involved in neuroprotection, neuroinflammation, and nerve regeneration. *Brain Behav Immun*, *24*(8), 1254-1267. https://doi.org/10.1016/j.bbi.2010.07.249
8. Bentsen, M., Goymann, P., Schultheis, H., Klee, K., Petrova, A., Wiegandt, R.,⋯Looso, M. (2020). ATAC-seq footprinting unravels kinetics of transcription factor binding during zygotic genome activation. *Nat Commun*, *11*(1), 4267. https://doi.org/10.1038/s41467-020-18035-1
9. Berest, I., Arnold, C., Reyes-Palomares, A., Palla, G., Rasmussen, K. D., Giles, H.,⋯

Zaugg, J. B. (2019). Quantification of Differential Transcription Factor Activity and Multiomics-Based Classification into Activators and Repressors: diffTF. *Cell Rep*, *29*(10), 3147-3159.e3112. https://doi.org/10.1016/j.celrep.2019.10.106

10. Boller, S., Ramamoorthy, S., Akbas, D., Nechanitzky, R., Burger, L., Murr, R.,⋯ Grosschedl, R. (2016). Pioneering Activity of the C-Terminal Domain of EBF1 Shapes the Chromatin Landscape for B Cell Programming. *Immunity*, *44*(3), 527-541. https://doi.org/10.1016/j.immuni.2016.02.021
11. Butler, D. C., Berger, T., Elmariah, S., Kim, B., Chisolm, S., Kwatra, S. G.,⋯Yosipovitch, G. (2024). Chronic Pruritus: A Review. *Jama*, *331*(24), 2114-2124. https://doi.org/10.1001/jama.2024.4899
12. Cai, X., Han, M., Lou, F., Sun, Y., Yin, Q., Sun, L.,⋯Wang, H. (2023). Tenascin C(+) papillary fibroblasts facilitate neuro-immune interaction in a mouse model of psoriasis. *Nat Commun*, *14*(1), 2004. https://doi.org/10.1038/s41467-023-37798-x
13. Carullo, N. V. N., Phillips Iii, R. A., Simon, R. C., Soto, S. A. R., Hinds, J. E., Salisbury, A. J.,⋯Day, J. J. (2020). Enhancer RNAs predict enhancer-gene regulatory links and are critical for enhancer function in neuronal systems. *Nucleic Acids Res*, *48*(17), 9550-9570. https://doi.org/10.1093/nar/gkaa671
14. Castanza, A. S., Recla, J. M., Eby, D., Thorvaldsdóttir, H., Bult, C. J., & Mesirov, J. P. (2023). Extending support for mouse data in the Molecular Signatures Database (MSigDB). *Nat Methods*, *20*(11), 1619-1620. https://doi.org/10.1038/s41592-023-02014-7
15. Castro-Mondragon, J. A., Riudavets-Puig, R., Rauluseviciute, I., Lemma, R. B., Turchi, L., Blanc-Mathieu, R.,⋯Mathelier, A. (2022). JASPAR 2022: the 9th release of the open-access database of transcription factor binding profiles. *Nucleic Acids Res*, *50*(D1), D165-d173. https://doi.org/10.1093/nar/gkab1113
16. Cavanaugh, D. J., Lee, H., Lo, L., Shields, S. D., Zylka, M. J., Basbaum, A. I., & Anderson, D. J. (2009). Distinct subsets of unmyelinated primary sensory fibers mediate behavioral responses to noxious thermal and mechanical stimuli. *Proc Natl Acad Sci U S A*, *106*(22), 9075-9080. https://doi.org/10.1073/pnas.0901507106
17. Chandran, V., Coppola, G., Nawabi, H., Omura, T., Versano, R., Huebner, E. A.,⋯

Geschwind, D. H. (2016). A Systems-Level Analysis of the Peripheral Nerve Intrinsic Axonal Growth Program. *Neuron*, *89*(5), 956-970. https://doi.org/10.1016/j.neuron.2016.01.034

18. Chen, G., Gu, P., Wu, W., Yin, Y., Pan, L., Huang, S.,⋯Deng, M. (2024). SETD2 deficiency in peripheral sensory neurons induces allodynia by promoting NMDA receptor expression through NFAT5 in rodent models. *Int J Biol Macromol*, *282*(Pt 5), 136767. https://doi.org/10.1016/j.ijbiomac.2024.136767
19. Chen, Y., Wang, Z. L., Yeo, M., Zhang, Q. J., López-Romero, A. E., Ding, H. P.,⋯Liedtke, W. (2021). Epithelia-Sensory Neuron Cross Talk Underlies Cholestatic Itch Induced by Lysophosphatidylcholine. *Gastroenterology*, *161*(1), 301-317.e316. https://doi.org/10.1053/j.gastro.2021.03.049
20. Cheng, X. T., Huang, N., & Sheng, Z. H. (2022). Programming axonal mitochondrial maintenance and bioenergetics in neurodegeneration and regeneration. *Neuron*, *110*(12), 1899-1923. https://doi.org/10.1016/j.neuron.2022.03.015
21. Cherry, C., Maestas, D. R., Han, J., Andorko, J. I., Cahan, P., Fertig, E. J.,⋯Elisseeff, J. H. (2021). Computational reconstruction of the signalling networks surrounding implanted biomaterials from single-cell transcriptomics. *Nat Biomed Eng*, *5*(10), 1228-1238. https://doi.org/10.1038/s41551-021-00770-5
22. Chiu, I. M., Barrett, L. B., Williams, E. K., Strochlic, D. E., Lee, S., Weyer, A. D.,⋯ Woolf, C. J. (2014). Transcriptional profiling at whole population and single cell levels reveals somatosensory neuron molecular diversity. *Elife*, *3*. https://doi.org/10.7554/eLife.04660
23. Choi, W., Choe, M. S., Kim, S. M., Kim, S. J., Lee, J., Lee, Y.,⋯Kim, L. K. (2024). RFX4 is an intrinsic factor for neuronal differentiation through induction of proneural genes POU3F2 and NEUROD1. *Cell Mol Life Sci*, *81*(1), 99. https://doi.org/10.1007/s00018-024-05129-y
24. Corces, M. R., Granja, J. M., Shams, S., Louie, B. H., Seoane, J. A., Zhou, W.,⋯Chang, H. Y. (2018). The chromatin accessibility landscape of primary human cancers. *Science*, *362*(6413). https://doi.org/10.1126/science.aav1898
25. Corces, M. R., Trevino, A. E., Hamilton, E. G., Greenside, P. G., Sinnott-Armstrong, N.

A., Vesuna, S.,⋯Chang, H. Y. (2017). An improved ATAC-seq protocol reduces background and enables interrogation of frozen tissues. *Nat Methods*, *14*(10), 959-962. https://doi.org/10.1038/nmeth.4396

26. Costigan, M., Befort, K., Karchewski, L., Griffin, R. S., D'Urso, D., Allchorne, A.,⋯ Woolf, C. J. (2002). Replicate high-density rat genome oligonucleotide microarrays reveal hundreds of regulated genes in the dorsal root ganglion after peripheral nerve injury. *BMC Neurosci*, *3*, 16. https://doi.org/10.1186/1471-2202-3-16
27. Dann, E., Henderson, N. C., Teichmann, S. A., Morgan, M. D., & Marioni, J. C. (2022). Differential abundance testing on single-cell data using k-nearest neighbor graphs. *Nat Biotechnol*, *40*(2), 245-253. https://doi.org/10.1038/s41587-021-01033-z
28. Datsi, A., Steinhoff, M., Ahmad, F., Alam, M., & Buddenkotte, J. (2021). Interleukin-31: The "itchy" cytokine in inflammation and therapy. *Allergy*, *76*(10), 2982-2997. https://doi.org/10.1111/all.14791
29. Deng, L., Costa, F., Blake, K. J., Choi, S., Chandrabalan, A., Yousuf, M. S.,⋯Chiu, I. M. (2023). S. aureus drives itch and scratch-induced skin damage through a V8 protease-PAR1 axis. *Cell*, *186*(24), 5375-5393.e5325. https://doi.org/10.1016/j.cell.2023.10.019
30. Donnelly, C. R., Chen, O., & Ji, R. R. (2020). How Do Sensory Neurons Sense Danger Signals? *Trends Neurosci*, *43*(10), 822-838. https://doi.org/10.1016/j.tins.2020.07.008
31. Efremova, M., Vento-Tormo, M., Teichmann, S. A., & Vento-Tormo, R. (2020). CellPhoneDB: inferring cell-cell communication from combined expression of multi-subunit ligand-receptor complexes. *Nat Protoc*, *15*(4), 1484-1506. https://doi.org/10.1038/s41596-020-0292-x
32. Elser, B., Lohoff, M., Kock, S., Giaisi, M., Kirchhoff, S., Krammer, P. H., & Li-Weber, M. (2002). IFN-gamma represses IL-4 expression via IRF-1 and IRF-2. *Immunity*, *17*(6), 703-712. https://doi.org/10.1016/s1074-7613(02)00471-5
33. Ewels, P. A., Peltzer, A., Fillinger, S., Patel, H., Alneberg, J., Wilm, A.,⋯Nahnsen, S. (2020). The nf-core framework for community-curated bioinformatics pipelines. *Nat Biotechnol*, *38*(3), 276-278. https://doi.org/10.1038/s41587-020-0439-x
34. Fang, D., Kong, L. Y., Cai, J., Li, S., Liu, X. D., Han, J. S., & Xing, G. G. (2015). Interleukin-6-mediated functional upregulation of TRPV1 receptors in dorsal root ganglion neurons through the activation of JAK/PI3K signaling pathway: roles in the

development of bone cancer pain in a rat model. *Pain*, *156*(6), 1124-1144. https://doi.org/10.1097/j.pain.0000000000000158

35. Flayer, C. H., Kernin, I. J., Matatia, P. R., Zeng, X., Yarmolinsky, D. A., Han, C.,⋯Sokol, C. L. (2024). A γδ T cell-IL-3 axis controls allergic responses through sensory neurons. *Nature*, *634*(8033), 440-446. https://doi.org/10.1038/s41586-024-07869-0
36. Flutter, B., & Nestle, F. O. (2013). TLRs to cytokines: mechanistic insights from the imiquimod mouse model of psoriasis. *Eur J Immunol*, *43*(12), 3138-3146. https://doi.org/10.1002/eji.201343801
37. Fulco, C. P., Nasser, J., Jones, T. R., Munson, G., Bergman, D. T., Subramanian, V.,⋯ Engreitz, J. M. (2019). Activity-by-contact model of enhancer-promoter regulation from thousands of CRISPR perturbations. *Nat Genet*, *51*(12), 1664-1669. https://doi.org/10.1038/s41588-019-0538-0
38. Gao, P. S., Leung, D. Y., Rafaels, N. M., Boguniewicz, M., Hand, T., Gao, L.,⋯Barnes, K. C. (2012). Genetic variants in interferon regulatory factor 2 (IRF2) are associated with atopic dermatitis and eczema herpeticum. *J Invest Dermatol*, *132*(3 Pt 1), 650-657. https://doi.org/10.1038/jid.2011.374
39. Garel, S., Marín, F., Grosschedl, R., & Charnay, P. (1999). Ebf1 controls early cell differentiation in the embryonic striatum. *Development*, *126*(23), 5285-5294. https://doi.org/10.1242/dev.126.23.5285
40. Grandi, F. C., Modi, H., Kampman, L., & Corces, M. R. (2022). Chromatin accessibility profiling by ATAC-seq. *Nat Protoc*, *17*(6), 1518-1552. https://doi.org/10.1038/s41596-022-00692-9
41. Gray, L. T., Yao, Z., Nguyen, T. N., Kim, T. K., Zeng, H., & Tasic, B. (2017). Layer-specific chromatin accessibility landscapes reveal regulatory networks in adult mouse visual cortex. *Elife*, *6*. https://doi.org/10.7554/eLife.21883
42. He, H., Suryawanshi, H., Morozov, P., Gay-Mimbrera, J., Del Duca, E., Kim, H. J.,⋯ Guttman-Yassky, E. (2020). Single-cell transcriptome analysis of human skin identifies novel fibroblast subpopulation and enrichment of immune subsets in atopic dermatitis. *J Allergy Clin Immunol*, *145*(6), 1615-1628. https://doi.org/10.1016/j.jaci.2020.01.042
43. Hong, S., Zheng, G., & Wiley, J. W. (2015). Epigenetic regulation of genes that modulate chronic stress-induced visceral pain in the peripheral nervous system. *Gastroenterology*,

148(1), 148-157.e147. https://doi.org/10.1053/j.gastro.2014.09.032

44. Hou, W., & Ji, Z. (2024). Assessing GPT-4 for cell type annotation in single-cell RNA-seq analysis. *Nat Methods*, *21*(8), 1462-1465. https://doi.org/10.1038/s41592-024-02235-4
45. Huang, Y., Chen, S. R., & Pan, H. L. (2022). Calcineurin Regulates Synaptic Plasticity and Nociceptive Transmission at the Spinal Cord Level. *Neuroscientist*, *28*(6), 628-638. https://doi.org/10.1177/10738584211046888
46. Huynh-Thu, V. A., Irrthum, A., Wehenkel, L., & Geurts, P. (2010). Inferring regulatory networks from expression data using tree-based methods. *PLoS One*, *5*(9). https://doi.org/10.1371/journal.pone.0012776
47. Jain, A., Gyori, B. M., Hakim, S., Jain, A., Sun, L., Petrova, V.,⋯Woolf, C. J. (2024). Nociceptor-immune interactomes reveal insult-specific immune signatures of pain. *Nat Immunol*, *25*(7), 1296-1305. https://doi.org/10.1038/s41590-024-01857-2
48. Jung, M., Dourado, M., Maksymetz, J., Jacobson, A., Laufer, B. I., Baca, M.,⋯Kaminker, J. S. (2023). Cross-species transcriptomic atlas of dorsal root ganglia reveals species-specific programs for sensory function. *Nat Commun*, *14*(1), 366. https://doi.org/10.1038/s41467-023-36014-0
49. Kheradpour, P., & Kellis, M. (2014). Systematic discovery and characterization of regulatory motifs in ENCODE TF binding experiments. *Nucleic Acids Res*, *42*(5), 2976-2987. https://doi.org/10.1093/nar/gkt1249
50. Kim, B., Rothenberg, M. E., Sun, X., Bachert, C., Artis, D., Zaheer, R.,⋯Cyr, S. (2024). Neuroimmune interplay during type 2 inflammation: Symptoms, mechanisms, and therapeutic targets in atopic diseases. *J Allergy Clin Immunol*, *153*(4), 879-893. https://doi.org/10.1016/j.jaci.2023.08.017
51. Kim, S., Kim, H., & Um, J. W. (2018). Synapse development organized by neuronal activity-regulated immediate-early genes. *Exp Mol Med*, *50*(4), 1-7. https://doi.org/10.1038/s12276-018-0025-1
52. Kourrich, S., Calu, D. J., & Bonci, A. (2015). Intrinsic plasticity: an emerging player in addiction. *Nat Rev Neurosci*, *16*(3), 173-184. https://doi.org/10.1038/nrn3877
53. Kulakovskiy, I. V., Vorontsov, I. E., Yevshin, I. S., Sharipov, R. N., Fedorova, A. D., Rumynskiy, E. I.,⋯Makeev, V. J. (2018). HOCOMOCO: towards a complete collection

of transcription factor binding models for human and mouse via large-scale ChIP-Seq analysis. *Nucleic Acids Res*, *46*(D1), D252-d259. https://doi.org/10.1093/nar/gkx1106

54. Kundaje, A., Meuleman, W., Ernst, J., Bilenky, M., Yen, A., Heravi-Moussavi, A.,⋯ Kellis, M. (2015). Integrative analysis of 111 reference human epigenomes. *Nature*, *518*(7539), 317-330. https://doi.org/10.1038/nature14248
55. Kupari, J., & Ernfors, P. (2023). Molecular taxonomy of nociceptors and pruriceptors. *Pain*, *164*(6), 1245-1257. https://doi.org/10.1097/j.pain.0000000000002831
56. La Manno, G., Soldatov, R., Zeisel, A., Braun, E., Hochgerner, H., Petukhov, V.,⋯ Kharchenko, P. V. (2018). RNA velocity of single cells. *Nature*, *560*(7719), 494-498. https://doi.org/10.1038/s41586-018-0414-6
57. Labib, A., Ju, T., & Yosipovitch, G. (2023). Emerging treatments for itch in atopic dermatitis: A review. *J Am Acad Dermatol*, *89*(2), 338-344. https://doi.org/10.1016/j.jaad.2023.04.057
58. LaCroix-Fralish, M. L., Austin, J. S., Zheng, F. Y., Levitin, D. J., & Mogil, J. S. (2011). Patterns of pain: meta-analysis of microarray studies of pain. *Pain*, *152*(8), 1888-1898. https://doi.org/10.1016/j.pain.2011.04.014
59. Lemeille, S., Paschaki, M., Baas, D., Morlé, L., Duteyrat, J. L., Ait-Lounis, A.,⋯Durand, B. (2020). Interplay of RFX transcription factors 1, 2 and 3 in motile ciliogenesis. *Nucleic Acids Res*, *48*(16), 9019-9036. https://doi.org/10.1093/nar/gkaa625
60. Lenaerts, A., Kucinski, I., Deboutte, W., Derecka, M., Cauchy, P., Manke, T.,⋯ Grosschedl, R. (2022). EBF1 primes B-lymphoid enhancers and limits the myeloid bias in murine multipotent progenitors. *J Exp Med*, *219*(11). https://doi.org/10.1084/jem.20212437
61. Li, M., Hener, P., Zhang, Z., Kato, S., Metzger, D., & Chambon, P. (2006). Topical vitamin D3 and low-calcemic analogs induce thymic stromal lymphopoietin in mouse keratinocytes and trigger an atopic dermatitis. *Proc Natl Acad Sci U S A*, *103*(31), 11736-11741. https://doi.org/10.1073/pnas.0604575103
62. Li, Y. Y., Li, H., Liu, Z. L., Li, Q., Qiu, H. W., Zeng, L. J.,⋯Li, Z. Y. (2017). Activation of STAT3-mediated CXCL12 up-regulation in the dorsal root ganglion contributes to oxaliplatin-induced chronic pain. *Mol Pain*, *13*, 1744806917747425. https://doi.org/10.1177/1744806917747425

63. Liang, Y., Sharma, D., Wang, B., Wang, H., Feng, X., Ma, R.,⋯Tao, Y. X. (2024). Transcription factor EBF1 mitigates neuropathic pain by rescuing Kv1.2 expression in primary sensory neurons. *Transl Res*, *263*, 15-27. https://doi.org/10.1016/j.trsl.2023.08.002

64. Liu, B., Li, C., Li, Z., Wang, D., Ren, X., & Zhang, Z. (2020). An entropy-based metric for assessing the purity of single cell populations. *Nat Commun*, *11*(1), 3155. https://doi.org/10.1038/s41467-020-16904-3

65. Liu, B., Tai, Y., Achanta, S., Kaelberer, M. M., Caceres, A. I., Shao, X.,⋯Jordt, S. E. (2016). IL-33/ST2 signaling excites sensory neurons and mediates itch response in a mouse model of poison ivy contact allergy. *Proc Natl Acad Sci U S A*, *113*(47), E7572-e7579. https://doi.org/10.1073/pnas.1606608113

66. Lu, P., Zhao, Y., Xie, Z., Zhou, H., Dong, X., Wu, G. F.,⋯Hu, H. (2023). MrgprA3-expressing pruriceptors drive pruritogen-induced alloknesis through mechanosensitive Piezo2 channel. *Cell Rep*, *42*(4), 112283. https://doi.org/10.1016/j.celrep.2023.112283

67. Lummertz da Rocha, E., Kubaczka, C., Sugden, W. W., Najia, M. A., Jing, R., Markel, A.,⋯Daley, G. Q. (2022). CellComm infers cellular crosstalk that drives haematopoietic stem and progenitor cell development. *Nat Cell Biol*, *24*(4), 579-589. https://doi.org/10.1038/s41556-022-00884-1

68. Ma, C. H., Omura, T., Cobos, E. J., Latrémolière, A., Ghasemlou, N., Brenner, G. J.,⋯ Woolf, C. J. (2011). Accelerating axonal growth promotes motor recovery after peripheral nerve injury in mice. *J Clin Invest*, *121*(11), 4332-4347. https://doi.org/10.1172/jci58675

69. Malik, A. N., Vierbuchen, T., Hemberg, M., Rubin, A. A., Ling, E., Couch, C. H.,⋯ Greenberg, M. E. (2014). Genome-wide identification and characterization of functional neuronal activity-dependent enhancers. *Nat Neurosci*, *17*(10), 1330-1339. https://doi.org/10.1038/nn.3808

70. Marco, A., Meharena, H. S., Dileep, V., Raju, R. M., Davila-Velderrain, J., Zhang, A. L., ⋯Tsai, L. H. (2020). Mapping the epigenomic and transcriptomic interplay during memory formation and recall in the hippocampal engram ensemble. *Nat Neurosci*, *23*(12), 1606-1617. https://doi.org/10.1038/s41593-020-00717-0

71. Misery, L., Pierre, O., Le Gall-Ianotto, C., Lebonvallet, N., Chernyshov, P. V., Le Garrec,

R., & Talagas, M. (2023). Basic mechanisms of itch. *J Allergy Clin Immunol*, *152*(1), 11-23. https://doi.org/10.1016/j.jaci.2023.05.004

72. Mitamura, Y., Reiger, M., Kim, J., Xiao, Y., Zhakparov, D., Tan, G.,⋯Akdis, C. A. (2023). Spatial transcriptomics combined with single-cell RNA-sequencing unravels the complex inflammatory cell network in atopic dermatitis. *Allergy*, *78*(8), 2215-2231. https://doi.org/10.1111/all.15781
73. Moore, J. E., Purcaro, M. J., Pratt, H. E., Epstein, C. B., Shoresh, N., Adrian, J.,⋯Weng, Z. (2020). Expanded encyclopaedias of DNA elements in the human and mouse genomes. *Nature*, *583*(7818), 699-710. https://doi.org/10.1038/s41586-020-2493-4
74. Nattkemper, L. A., Tey, H. L., Valdes-Rodriguez, R., Lee, H., Mollanazar, N. K., Albornoz, C.,⋯Yosipovitch, G. (2018). The Genetics of Chronic Itch: Gene Expression in the Skin of Patients with Atopic Dermatitis and Psoriasis with Severe Itch. *J Invest Dermatol*, *138*(6), 1311-1317. https://doi.org/10.1016/j.jid.2017.12.029
75. Nguyen, M. Q., von Buchholtz, L. J., Reker, A. N., Ryba, N. J., & Davidson, S. (2021). Single-nucleus transcriptomic analysis of human dorsal root ganglion neurons. *Elife*, *10*. https://doi.org/10.7554/eLife.71752
76. Nguyen, M. Q., Wu, Y., Bonilla, L. S., von Buchholtz, L. J., & Ryba, N. J. P. (2017). Diversity amongst trigeminal neurons revealed by high throughput single cell sequencing. *PLoS One*, *12*(9), e0185543. https://doi.org/10.1371/journal.pone.0185543
77. Nicolas, C. S., Peineau, S., Amici, M., Csaba, Z., Fafouri, A., Javalet, C.,⋯Collingridge, G. L. (2012). The Jak/STAT pathway is involved in synaptic plasticity. *Neuron*, *73*(2), 374-390. https://doi.org/10.1016/j.neuron.2011.11.024
78. Oetjen, L. K., Mack, M. R., Feng, J., Whelan, T. M., Niu, H., Guo, C. J.,⋯Kim, B. S. (2017). Sensory Neurons Co-opt Classical Immune Signaling Pathways to Mediate Chronic Itch. *Cell*, *171*(1), 217-228.e213. https://doi.org/10.1016/j.cell.2017.08.006
79. Palmisano, I., Danzi, M. C., Hutson, T. H., Zhou, L., McLachlan, E., Serger, E.,⋯Di Giovanni, S. (2019). Epigenomic signatures underpin the axonal regenerative ability of dorsal root ganglia sensory neurons. *Nat Neurosci*, *22*(11), 1913-1924. https://doi.org/10.1038/s41593-019-0490-4
80. Pang, Z., Sakamoto, T., Tiwari, V., Kim, Y. S., Yang, F., Dong, X.,⋯Caterina, M. J.

(2015). Selective keratinocyte stimulation is sufficient to evoke nociception in mice. *Pain*, *156*(4), 656-665. https://doi.org/10.1097/j.pain.0000000000000092

81. Perkins, J. R., Antunes-Martins, A., Calvo, M., Grist, J., Rust, W., Schmid, R.,⋯Bennett, D. L. (2014). A comparison of RNA-seq and exon arrays for whole genome transcription profiling of the L5 spinal nerve transection model of neuropathic pain in the rat. *Mol Pain*, *10*, 7. https://doi.org/10.1186/1744-8069-10-7
82. Perry, R. B., Hezroni, H., Goldrich, M. J., & Ulitsky, I. (2018). Regulation of Neuroregeneration by Long Noncoding RNAs. *Mol Cell*, *72*(3), 553-567.e555. https://doi.org/10.1016/j.molcel.2018.09.021
83. Powell, R., Young, V. A., Pryce, K. D., Sheehan, G. D., Bonsu, K., Ahmed, A., & Bhattacharjee, A. (2021). Inhibiting endocytosis in CGRP(+) nociceptors attenuates inflammatory pain-like behavior. *Nat Commun*, *12*(1), 5812. https://doi.org/10.1038/s41467-021-26100-6
84. Qi, L., Iskols, M., Shi, D., Reddy, P., Walker, C., Lezgiyeva, K.,⋯Sharma, N. (2024). A mouse DRG genetic toolkit reveals morphological and physiological diversity of somatosensory neuron subtypes. *Cell*, *187*(6), 1508-1526.e1516. https://doi.org/10.1016/j.cell.2024.02.006
85. Qin, S., Zou, Y., & Zhang, C. L. (2013). Cross-talk between KLF4 and STAT3 regulates axon regeneration. *Nat Commun*, *4*, 2633. https://doi.org/10.1038/ncomms3633
86. Ray, P. R., Shiers, S., Caruso, J. P., Tavares-Ferreira, D., Sankaranarayanan, I., Uhelski, M. L.,⋯Price, T. J. (2023). RNA profiling of human dorsal root ganglia reveals sex differences in mechanisms promoting neuropathic pain. *Brain*, *146*(2), 749-766. https://doi.org/10.1093/brain/awac266
87. Razick, S., Magklaras, G., & Donaldson, I. M. (2008). iRefIndex: a consolidated protein interaction database with provenance. *BMC Bioinformatics*, *9*, 405. https://doi.org/10.1186/1471-2105-9-405
88. Renthal, W., Tochitsky, I., Yang, L., Cheng, Y. C., Li, E., Kawaguchi, R.,⋯Woolf, C. J. (2020). Transcriptional Reprogramming of Distinct Peripheral Sensory Neuron Subtypes after Axonal Injury. *Neuron*, *108*(1), 128-144.e129. https://doi.org/10.1016/j.neuron.2020.07.026
89. Sahu, M. R., & Mondal, A. C. (2021). Neuronal Hippo signaling: From development to

diseases. *Dev Neurobiol*, *81*(2), 92-109. https://doi.org/10.1002/dneu.22796

90. Sakai, K., Sanders, K. M., Youssef, M. R., Yanushefski, K. M., Jensen, L., Yosipovitch, G., & Akiyama, T. (2016). Mouse model of imiquimod-induced psoriatic itch. *Pain*, *157*(11), 2536-2543. https://doi.org/10.1097/j.pain.0000000000000674
91. Schep, A. N., Wu, B., Buenrostro, J. D., & Greenleaf, W. J. (2017). chromVAR: inferring transcription-factor-associated accessibility from single-cell epigenomic data. *Nat Methods*, *14*(10), 975-978. https://doi.org/10.1038/nmeth.4401
92. Seijffers, R., Mills, C. D., & Woolf, C. J. (2007). ATF3 increases the intrinsic growth state of DRG neurons to enhance peripheral nerve regeneration. *J Neurosci*, *27*(30), 7911-7920. https://doi.org/10.1523/jneurosci.5313-06.2007
93. Shao, X., Liao, J., Li, C., Lu, X., Cheng, J., & Fan, X. (2021). CellTalkDB: a manually curated database of ligand-receptor interactions in humans and mice. *Brief Bioinform*, *22*(4). https://doi.org/10.1093/bib/bbaa269
94. Sharma, N., Flaherty, K., Lezgiyeva, K., Wagner, D. E., Klein, A. M., & Ginty, D. D. (2020). The emergence of transcriptional identity in somatosensory neurons. *Nature*, *577*(7790), 392-398. https://doi.org/10.1038/s41586-019-1900-1
95. Shin, G. J., Pero, M. E., Hammond, L. A., Burgos, A., Kumar, A., Galindo, S. E.,⋯ Grueber, W. B. (2021). Integrins protect sensory neurons in models of paclitaxel-induced peripheral sensory neuropathy. *Proc Natl Acad Sci U S A*, *118*(15). https://doi.org/10.1073/pnas.2006050118
96. Shiratori-Hayashi, M., Hasegawa, A., Toyonaga, H., Andoh, T., Nakahara, T., Kido-Nakahara, M.,⋯Tsuda, M. (2019). Role of P2X3 receptors in scratching behavior in mouse models. *J Allergy Clin Immunol*, *143*(3), 1252-1254.e1258. https://doi.org/10.1016/j.jaci.2018.10.053
97. Shiratori-Hayashi, M., Koga, K., Tozaki-Saitoh, H., Kohro, Y., Toyonaga, H., Yamaguchi, C.,⋯Tsuda, M. (2015). STAT3-dependent reactive astrogliosis in the spinal dorsal horn underlies chronic itch. *Nat Med*, *21*(8), 927-931. https://doi.org/10.1038/nm.3912
98. Simmons, J., & Gallo, R. L. (2024). The Central Roles of Keratinocytes in Coordinating Skin Immunity. *J Invest Dermatol*, *144*(11), 2377-2398. https://doi.org/10.1016/j.jid.2024.06.1280
99. Skene, P. J., Henikoff, J. G., & Henikoff, S. (2018). Targeted in situ genome-wide

profiling with high efficiency for low cell numbers. *Nat Protoc*, *13*(5), 1006-1019. https://doi.org/10.1038/nprot.2018.015

100. Smith, J. P., Corces, M. R., Xu, J., Reuter, V. P., Chang, H. Y., & Sheffield, N. C. (2021). PEPATAC: an optimized pipeline for ATAC-seq data analysis with serial alignments. *NAR Genom Bioinform*, *3*(4), lqab101. https://doi.org/10.1093/nargab/lqab101
101. Soliman, N., Okuse, K., & Rice, A. S. C. (2019). VGF: a biomarker and potential target for the treatment of neuropathic pain? *Pain Rep*, *4*(5), e786. https://doi.org/10.1097/pr9.0000000000000786
102. Steinhoff, M., Ahmad, F., Pandey, A., Datsi, A., AlHammadi, A., Al-Khawaga, S.,⋯ Buddenkotte, J. (2022). Neuroimmune communication regulating pruritus in atopic dermatitis. *J Allergy Clin Immunol*, *149*(6), 1875-1898. https://doi.org/10.1016/j.jaci.2022.03.010
103. Takahashi, S., Ishida, A., Kubo, A., Kawasaki, H., Ochiai, S., Nakayama, M.,⋯Okada, T. (2019). Homeostatic pruning and activity of epidermal nerves are dysregulated in barrier-impaired skin during chronic itch development. *Sci Rep*, *9*(1), 8625. https://doi.org/10.1038/s41598-019-44866-0
104. Takahashi, S., Ochiai, S., Jin, J., Takahashi, N., Toshima, S., Ishigame, H.,⋯Okada, T. (2023). Sensory neuronal STAT3 is critical for IL-31 receptor expression and inflammatory itch. *Cell Rep*, *42*(12), 113433. https://doi.org/10.1016/j.celrep.2023.113433
105. Talagas, M., Lebonvallet, N., Leschiera, R., Sinquin, G., Elies, P., Haftek, M.,⋯Misery, L. (2020). Keratinocytes Communicate with Sensory Neurons via Synaptic-like Contacts. *Ann Neurol*, *88*(6), 1205-1219. https://doi.org/10.1002/ana.25912
106. Trier, A. M., Mack, M. R., Fredman, A., Tamari, M., Ver Heul, A. M., Zhao, Y.,⋯Kim, B. S. (2022). IL-33 signaling in sensory neurons promotes dry skin itch. *J Allergy Clin Immunol*, *149*(4), 1473-1480.e1476. https://doi.org/10.1016/j.jaci.2021.09.014
107. Trier, A. M., Ver Heul, A. M., Fredman, A., Le, V., Wang, Z., Auyeung, K.,⋯Kim, B. S. (2024). IL-33 potentiates histaminergic itch. *J Allergy Clin Immunol*, *153*(3), 852-859.e853. https://doi.org/10.1016/j.jaci.2023.08.038
108. Tsantoulas, C., & McMahon, S. B. (2014). Opening paths to novel analgesics: the role of

potassium channels in chronic pain. *Trends Neurosci*, *37*(3), 146-158. https://doi.org/10.1016/j.tins.2013.12.002

109. Tseng, P. Y., & Hoon, M. A. (2021). Oncostatin M can sensitize sensory neurons in inflammatory pruritus. *Sci Transl Med*, *13*(619), eabe3037. https://doi.org/10.1126/scitranslmed.abe3037
110. Usoskin, D., Furlan, A., Islam, S., Abdo, H., Lönnerberg, P., Lou, D.,⋯Ernfors, P. (2015). Unbiased classification of sensory neuron types by large-scale single-cell RNA sequencing. *Nat Neurosci*, *18*(1), 145-153. https://doi.org/10.1038/nn.3881
111. Van de Sande, B., Flerin, C., Davie, K., De Waegeneer, M., Hulselmans, G., Aibar, S.,⋯ Aerts, S. (2020). A scalable SCENIC workflow for single-cell gene regulatory network analysis. *Nat Protoc*, *15*(7), 2247-2276. https://doi.org/10.1038/s41596-020-0336-2
112. Vander Heiden, M. G., Cantley, L. C., & Thompson, C. B. (2009). Understanding the Warburg effect: the metabolic requirements of cell proliferation. *Science*, *324*(5930), 1029-1033. https://doi.org/10.1126/science.1160809
113. Voisin, T., Perner, C., Messou, M. A., Shiers, S., Ualiyeva, S., Kanaoka, Y.,⋯Chiu, I. M. (2021). The CysLT(2)R receptor mediates leukotriene C(4)-driven acute and chronic itch. *Proc Natl Acad Sci U S A*, *118*(13). https://doi.org/10.1073/pnas.2022087118
114. Vorontsov, I. E., Eliseeva, I. A., Zinkevich, A., Nikonov, M., Abramov, S., Boytsov, A., ⋯Kulakovskiy, I. V. (2024). HOCOMOCO in 2024: a rebuild of the curated collection of binding models for human and mouse transcription factors. *Nucleic Acids Res*, *52*(D1), D154-d163. https://doi.org/10.1093/nar/gkad1077
115. Wang, F., & Kim, B. S. (2020). Itch: A Paradigm of Neuroimmune Crosstalk. *Immunity*, *52*(5), 753-766. https://doi.org/10.1016/j.immuni.2020.04.008
116. Wang, F., Trier, A. M., Li, F., Kim, S., Chen, Z., Chai, J. N.,⋯Kim, B. S. (2021). A basophil-neuronal axis promotes itch. *Cell*, *184*(2), 422-440.e417. https://doi.org/10.1016/j.cell.2020.12.033
117. Wang, K., Wang, S., Chen, Y., Wu, D., Hu, X., Lu, Y.,⋯Zhang, X. (2021). Single-cell transcriptomic analysis of somatosensory neurons uncovers temporal development of neuropathic pain. *Cell Res*, *31*(8), 904-918. https://doi.org/10.1038/s41422-021-00479-9
118. Wang, L., Zhu, Y., Zhang, N., Xian, Y., Tang, Y., Ye, J.,⋯Jiang, X. (2024). The multiple

roles of interferon regulatory factor family in health and disease. *Signal Transduct Target Ther*, *9*(1), 282. https://doi.org/10.1038/s41392-024-01980-4

119. Wang, S. S., Tsai, R. Y., & Reed, R. R. (1997). The characterization of the Olf-1/EBF-like HLH transcription factor family: implications in olfactory gene regulation and neuronal development. *J Neurosci*, *17*(11), 4149-4158. https://doi.org/10.1523/jneurosci.17-11-04149.1997
120. Wang, Y., Zolotarev, N., Yang, C. Y., Rambold, A., Mittler, G., & Grosschedl, R. (2020). A Prion-like Domain in Transcription Factor EBF1 Promotes Phase Separation and Enables B Cell Programming of Progenitor Chromatin. *Immunity*, *53*(6), 1151-1167.e1156. https://doi.org/10.1016/j.immuni.2020.10.009
121. Willemen, H., Santos Ribeiro, P. S., Broeks, M., Meijer, N., Versteeg, S., Tiggeler, A.,⋯ Eijkelkamp, N. (2023). Inflammation-induced mitochondrial and metabolic disturbances in sensory neurons control the switch from acute to chronic pain. *Cell Rep Med*, *4*(11), 101265. https://doi.org/10.1016/j.xcrm.2023.101265
122. Wilson, S. R., Thé, L., Batia, L. M., Beattie, K., Katibah, G. E., McClain, S. P.,⋯Bautista, D. M. (2013). The epithelial cell-derived atopic dermatitis cytokine TSLP activates neurons to induce itch. *Cell*, *155*(2), 285-295. https://doi.org/10.1016/j.cell.2013.08.057
123. Xiao, H. S., Huang, Q. H., Zhang, F. X., Bao, L., Lu, Y. J., Guo, C.,⋯Zhang, X. (2002). Identification of gene expression profile of dorsal root ganglion in the rat peripheral axotomy model of neuropathic pain. *Proc Natl Acad Sci U S A*, *99*(12), 8360-8365. https://doi.org/10.1073/pnas.122231899
124. Xie, Z., Feng, J., Cai, T., McCarthy, R., Eschbach, M. D., 2nd, Wang, Y.,⋯Hu, H. (2022). Estrogen metabolites increase nociceptor hyperactivity in a mouse model of uterine pain. *JCI Insight*, *7*(10). https://doi.org/10.1172/jci.insight.149107
125. Xing, Y., Chen, J., Hilley, H., Steele, H., Yang, J., & Han, L. (2020). Molecular Signature of Pruriceptive MrgprA3(+) Neurons. *J Invest Dermatol*, *140*(10), 2041-2050. https://doi.org/10.1016/j.jid.2020.03.935
126. Xu, Y., Qiu, Z., Gu, C., Yu, S., Wang, S., Li, C.,⋯Li, W. (2024). Propionate alleviates itch in murine models of atopic dermatitis by modulating sensory TRP channels of dorsal root ganglion. *Allergy*, *79*(5), 1271-1290. https://doi.org/10.1111/all.15998

127. Yamamura, K., Uruno, T., Shiraishi, A., Tanaka, Y., Ushijima, M., Nakahara, T.,⋯Fukui, Y. (2017). The transcription factor EPAS1 links DOCK8 deficiency to atopic skin inflammation via IL-31 induction. *Nat Commun*, *8*, 13946. https://doi.org/10.1038/ncomms13946

128. Yang, J. H., & Hansen, A. S. (2024). Enhancer selectivity in space and time: from enhancer-promoter interactions to promoter activation. *Nat Rev Mol Cell Biol*, *25*(7), 574-591. https://doi.org/10.1038/s41580-024-00710-6

129. Yang, L., Xu, M., Bhuiyan, S. A., Li, J., Zhao, J., Cohrs, R. J.,⋯Renthal, W. (2022). Human and mouse trigeminal ganglia cell atlas implicates multiple cell types in migraine. *Neuron*, *110*(11), 1806-1821.e1808. https://doi.org/10.1016/j.neuron.2022.03.003

130. Yee, C., Xiao, Y., Chen, H., Reddy, A. R., Xu, B., Medwig-Kinney, T. N.,⋯Shen, K. (2024). An activity-regulated transcriptional program directly drives synaptogenesis. *Nat Neurosci*, *27*(9), 1695-1707. https://doi.org/10.1038/s41593-024-01728-x

131. Yu, H., Nagi, S. S., Usoskin, D., Hu, Y., Kupari, J., Bouchatta, O.,⋯Luo, W. (2024). Leveraging deep single-soma RNA sequencing to explore the neural basis of human somatosensation. *Nat Neurosci*, *27*(12), 2326-2340. https://doi.org/10.1038/s41593-024-01794-1

132. Yu, X., Liu, H., Hamel, K. A., Morvan, M. G., Yu, S., Leff, J.,⋯Basbaum, A. I. (2020). Dorsal root ganglion macrophages contribute to both the initiation and persistence of neuropathic pain. *Nat Commun*, *11*(1), 264. https://doi.org/10.1038/s41467-019-13839-2

133. Zeidler, C., Raap, U., Witte, F., & Ständer, S. (2023). Clinical aspects and management of chronic itch. *J Allergy Clin Immunol*, *152*(1), 1-10. https://doi.org/10.1016/j.jaci.2023.04.018

134. Zeisel, A., Hochgerner, H., Lönnerberg, P., Johnsson, A., Memic, F., van der Zwan, J.,⋯ Linnarsson, S. (2018). Molecular Architecture of the Mouse Nervous System. *Cell*, *174*(4), 999-1014.e1022. https://doi.org/10.1016/j.cell.2018.06.021

135. Zhao, M., Wu, X., Zhang, Q., Luo, S., Liang, G., Su, Y.,⋯Lu, Q. (2010). RFX1 regulates CD70 and CD11a expression in lupus T cells by recruiting the histone methyltransferase SUV39H1. *Arthritis Res Ther*, *12*(6), R227. https://doi.org/10.1186/ar3214

136. Zheng, Y., Liu, P., Bai, L., Trimmer, J. S., Bean, B. P., & Ginty, D. D. (2019). Deep

Sequencing of Somatosensory Neurons Reveals Molecular Determinants of Intrinsic Physiological Properties. *Neuron*, *103*(4), 598-616.e597. https://doi.org/10.1016/j.neuron.2019.05.039

137. Zolotarev, N., Bayer, M., & Grosschedl, R. (2022). EBF1 is continuously required for stabilizing local chromatin accessibility in pro-B cells. *Proc Natl Acad Sci U S A*, *119*(48), e2210595119. https://doi.org/10.1073/pnas.2210595119

Abstract in Korean

아토피피부염 만성 가려움증 민감화의 후성유전학적 기전 규명

만성 가려움증은 삶의 질을 심각하게 저하시킬 수 있는 만성적인 질환으로, 아토피피부염을 포함한 다양한 피부질환에서 주요한 임상적 특징으로 나타난다. 그러나, 아토피피부염의 면역병리학적 기전에 대한 이해에 비해서, 만성 가려움증을 지속시키는 신경면역 상호작용의 기전과 등쪽뿌리신경절 내에서 발생하는 장기적인 후성유전체 및 전사체의 변화에 대해서는 여전히 명확히 연구되어 있지 않다. 본 연구는 이러한 지식적 공백을 해결하기 위해, 단일세포 RNA 시퀀싱(scRNA-seq), ATAC-seq 및 CUT&RUN 기반 다중오믹스 분석을 활용하여 만성 가려움 자극에 대한 감각 신경의 분자적 변화를 규명하고자 하였다.

아토피피부염 및 건선 마우스 모델을 이용하여 등쪽뿌리신경절의 감각신경세포 및 피부 조직의 단일세포 전사체 분석을 수행한 결과, 염증 조건에 따라 특정한 전사적 특성을 지닌 신경세포 아형이 존재함을 확인하였다. 이러한 아형들은 신경흥분성 조절, 시냅스 가소성 및 신경-면역 상호작용과 관련된 경로가 활성화된 특징을 보였으며, 이는 만성 가려움 자극이 감각 신경의 적응적 변화를 유도하여 지속적인 가려움증을 유발할 가능성을 시사하였다. 또한, 다양한 염증 모델 간 비교 분석을 통해 공통적이면서도 질환 특이적인 신경세포 전사적 변화를 확인하였다.

후성유전체적 분석을 위해 ATAC-seq 및 CUT&RUN 기반 크로마틴 접근성 분석을 수행한 결과, 만성 가려움증과 관련된 유전자 조절인자의 활성화가 확인되었다. 특히, 감각신경 기능, 시냅스 조절 및 만성 염증과 연관된 유전자들을 조절할 것으로 생각되는 핵심적 후성유전 인자를 발굴하였다. 단일세포전사체와 후성유전체를 통합적으로 분석한 결과, RFX, IRF, STAT 등의 염증과 신경발달에서 중요한 역할을 담당하는 전사인자를 발굴하였고, 특히 Ebf1 이라는 전사인자가 만성 가려움증에 핵심적인 역할을 수행할 것으로 예측되었다. 이를 Ebf1 결손 마우스모델

유래 단일세포전사체 및 가려움증 행동 측정을 진행한 결과, 해당 조절 경로를 감각신경에서 선택적으로 억제할 경우, 자발적 긁기 행동이 현저히 감소하고, 만성 가려움증 마우스 모델에서 표피 비후가 완화됨을 확인하였으며, 단일세포전사체에서 만성 가려움증에 핵심적 역할을 수행하는 유전자가 유의하게 감소하는 것을 확인하였다.

추가적으로, Ebf1 의 상위에 존재할 것으로 생각되는 신경-면역 상호작용 리간드-수용체 쌍을 발굴하였다 아토피피부염 상태에서 증가된 리간드가 감각신경에 발현된 수용체에 결합하여, 주변 염증과 감각 신경의 지속적 가소성을 연결하는 피드백 루프를 형성하는 것으로 나타났다. 이러한 염증 신호가 지속적인 신경 과흥분성을 유도하고 장기적인 유전자 조절 네트워크 변화를 촉진함으로써 가려움증의 만성화를 유지하는 핵심 기전임을 규명하였다.

종합적으로, 본 연구는 만성 가려움증을 조절하는 새로운 후성유전학적 조절 네트워크를 규명함으로써, 감각신경 내 염증 자극에 의해 유도되는 전사체의 변화를 단일세포 수준에서 상세히 분석하였다. 단일세포 전사체 및 후성유전체 분석을 통합한 본 연구 결과는 만성 가려움증에서 신경-면역 상호작용의 분자적 이해를 확장하며, 이러한 경로를 표적으로 하는 치료 전략 개발의 새로운 가능성을 제시할 것이다.

핵심되는 말 : 만성 가려움증, 아토피피부염, 후성유전체, 단일세포오믹스, 등쪽뿌리신경절